Functional analysis of maltose phosphorylase MalE from *Bacillus* sp. AHU2001 and synthesis of oligosaccharides and sugar phosphates with the enzyme

（*Bacillus* sp. AHU 2001 由来マルトースホスホリラーゼ MalE の機能ならびに本酵素を用いたオリゴ糖および糖リン酸の合成に関する研究）

北海道大学　大学院農学院

共生基盤学専攻 博士後期課程

高　宇

CONTENTS

ABBREVIATIONS

ABC, ATP-binding cassette

All, D-allose

Alt, D-altrose

Ara, L-arabinose

BR, Britton-Robinson

BSA, bovine serum albumin

CAZy, carbohydrate active enzymes database

CBB, Coomassie Brilliant Blue

COSY, correlated spectroscopy

EDTA, 2,2′,2″,2‴-(ethane-1,2-diyldinitrilo)tetraacetic acid

ESI-MS, electrospray ionization mass spectrometry

FOS, fructooligosaccharide

Fru, D-fructose

Gal, D-galactose

GGP, 1,2-α-glucosylglycerol phosphorylase

GH, glycoside hydrolase

GlcA, D-gluconic acid

Glc, D-glucose

GlcN, D-glucosamine

GlcNAc, *N*-acetyl-D-glucosamine

Glc6*P*, D-glucose 6-phosphate

GP, glycoside phosphorylase

GT, glycosyltransferase

G6PDH, glucose-6-phosphate dehydrogenase

HEPES, 2-[4-(2-hydroxyethyl)piperazin-1-yl]ethanesulfonic acid

HMBC, heteronuclear multiple bond correlation

HSQC, heteronuclear single quantum coherence

H2BC, heteronuclear two bond correlation spectroscopy

Isomal, isomaltose

IPTG, Isopropyl β-D-1-thiogalactopyranoside

Koj, kojibiose

KojP, kojibiose phosphorylase

LB, Luria-Bertani

LbMP, maltose phosphorylase from *Lactobacillus brevis*

Lyx, D-lyxose

MES, 2-morpholin-4-ylethanesulfonic acid

Mal, maltose

Man, D-mannose

MP, maltose phosphorylase

$NADP^+$, nicotinamide adenine dinucleotide phosphate

NCBI, National Center for Biotechnology Information

Nig, nigerose

NMR, nuclear magnetic resonance

NP, nigerose phosphorylase

PCR, polymerase chain reaction

Rha, L-rhamnose

SDS-PAGE, sodium dodecyl sulfate-polyacrylamide gel electrophoresis

Sor, L-sorbose

Tag, D-tagatose

Tal, D-talose

TP, trehalose phosphorylase

Tre, trehalose

Thio-NAD^+, thionicotinamide-adenine dinucleotide

TOCSY, total correlation spectroscopy

Tris, 2-amino-2-hydroxymethyl-propane-1,3-diol

T6PP, trehalose 6-phosphate phosphorylase

Xul, D-xylulose

Xyl, D-xylose

α-MG, methyl α-D-glucoside

β-Glc1*P*, β-D-glucose 1-phosphate

β-MG, methyl β-D-glucoside

β-PGM, β-phosphoglucomutase

1,5-AG, 1,5-anhydro-D-glucitol

2-deoxyGlc, 2-deoxy-D-glucose

3-deoxyGlc, 3-deoxy-D-glucose

4-deoxyGlc, 4-deoxy-D-glucose

6-deoxyGlc, 6-deoxy-D-glucose

CHAPTER I. General introduction

I.1 Glycoside phosphorylase

Glycoside phosphorylases (GPs) are a group of carbohydrate-active enzymes that transfer a glycosyl moiety from the non-reducing end of a polysaccharide or oligosaccharide sugar donor to inorganic phosphate (Pi), to generate a glycosyl phosphate [1, 2]. Their phosphorolytic reaction is reversible and of practical importance because they are able to synthesize new glycosidic bond from appropriate glycosyl phosphate and an acceptor [3]. Such a synthetic reaction has much potential to produce various oligosaccharides. Theoretically, there could be categorized into two types of GPs in regard to anomeric configuration of the glycosyl donor and the resulting glycosyl phosphate. Retaining GPs do not change the anomeric configuration between the substrate and the phosphorylated product. Action of inverting phosphorylases changes the anomeric configuration in the product yielding α-glycosyl phosphate from β-glycoside or β-glycosyl phosphate from α-glycoside (Fig. 1) [4]. All GPs are classified in eight families of carbohydrate active enzymes database (CAZy) [5]. Retaining enzymes are grouped to two glycosyltransferases (GT) families, GT35 and GT4, and two glycoside hydrolases (GH) family, GH3 and GH13. Inverting enzymes are found solely in GH families, namely GH65, GH94, GH112, GH130, and GH149. Within the GT and GH families, that are based on amino acid sequence similarity of the members, the following properties of the enzymes are conserved: retaining or inverting character of the family members, anomeric configuration of the substrate (and the product) and in most cases also its glycosidic nature. Substrates for GP-catalyzed glycosylations are more readily

available, in comparison to those for GT-catalyzed reactions; this makes GPs attractive biocatalysts for carbohydrate syntheses to be applied as food additives and cosmetic ingredients [3, 6]. GPs that are currently known to date are summarized in Table 1. According to the third digit of their EC numbers all entries in the table with one exception are hexosyltransferases transferring single hexopyranosyl (aldohexose) residue to Pi. The last entry is maltosyltransferase that transfers aldobiose moiety and generates α-maltosyl phosphate.

The use of GP biocatalysts has been demonstrated in academic research, such as in the synthesis of homogeneous crystalline cellulose [7], self-assembled structures of alkylated cellulose [8], cellulose nanoribbons with primary amino groups [9], and the formation of oligo (ethylene glycol)-bearing cellulose hydrogels [10], and more widely at an industrial scale, such as for the synthesis of 2-*O*-(α-D-glucopyranosyl)-*sn*-glycerol, a cosmetic ingredient, by sucrose phosphorylase [11]; kilogram-scale synthesis of lacto-*N*-biose, a prebiotic made with lacto-*N*-biose phosphorylase [12]; and the synthesis of disaccharide sweetener kojibiose (Koj), produced with a sucrose phosphorylase variant from *Bifidobacterium adolescentis* [13].

I.2 GH65 enzymes

GH65 is a family of inverting phosphorylases acting on α-glucosides to produce β-D-glucose 1-phosphate (β-Glc1*P*). With exception of isomaltose (Isomal), all other α-linked glucobioses are phosphorolytically processed by the corresponding inverting GPs in GH65. It contains maltose phosphorylase (MP, EC 2.4.1.8), trehalose phosphorylase (TP, EC 2.4.1.64), trehalose 6-phosphate phosphorylase (T6PP, EC 2.4.1.216), kojibiose phosphorylase (KP, EC 2.4.1.230), nigerose phosphorylase (NP, EC 2.4.1.279), 1,3-α-glucosyl-L-rhamnose phosphorylase (EC 2.4.1.282), 1,2-α-glucosylglycerol phosphorylase (GGP, EC 2.4.1.332), and 1,3-α-oligoglucan phosphorylase (EC 2.4.1.334), as well as acid trehalose hydrolase (EC 3.2.1.28) from

eukaryotes [14, 15]. Among them, the novel enzyme, α-1,3-oligo-D-glucan phosphorylase with a preference for α-1,3-glucooligosaccharides has just been discovered and so far it is the only GH65 phosphorylase known to be active on the substrates larger than disaccharides [15]. All of the bacterial enzymes characterized in this family are phosphorylases, while all of the eukaryotic enzymes are trehalases. This fact suggests evolutionary relationship of GH65 members with some other GHs operating on α-glucosidic linkages [4]. Structures of GH65 enzymes were solved in *L. brevis* MP [16], *C. saccharolyticus* KP [17], *B. selenitireducens* GGP [18], and *Thermoanaerobacter* sp. TP [19], which enhanced understanding of substrate recognition in this family. The GH65 enzymes have an $(\alpha/\alpha)_6$-barrel catalytic domain similar to those of GH15 inverting glycosidases, including glucoamylase (EC 3.2.1.3) and glucodextranase (EC 3.2.1.70) [16, 20, 21]. They form the clan GH-L. In GH65 phosphorylases, Pi is located in the active site at the position, corresponding to the general base catalyst Glu residue of GH15 glycosidases [16-18]. The Glu residue on the loop connecting the fifth and sixth α-helices of the catalytic domain serves as the general acid catalyst and conserved in the enzymes of GH65 and GH15 [16-18, 20, 21].

I.3 Maltose phosphorylase

MP catalyzes the reversible phosphorolysis of maltose (Mal) to β-Glc1*P* and D-glucose (Glc). This enzyme cleaves the glucosidic linkage via the single displacement mechanism, in which the general acid catalyst donates a proton to the scissile glucosidic oxygen, and the Pi attacks the anomeric carbon of the Glc residue in subsite -1 [16]. MP has been found in many bacteria, such as *Bacillus selenitireducens* [22], *Bacillus* sp. RK-1 [23, 24], *Bacillus subtilis* [25], *Enterococcus faecalis* [26], *Enterococcus hirae* [27], *Lactobacillus acidophilus* [28], *Lactobacillus brevis* [29], *Lactobacillus sanfranciscensis* [30], *Lactobacillus* sp. [31], *Lactococcus casei* [32], *Lactococcus lactis* [33],

Nessericia meningitides [34], *Nessericia perflava* [35], *Paenibacillus* sp. SH-55 [36], *Propionibacterium freudenreichii* [37], and *Streptococcus bovis* [38]. These bacteria utilize MP for the intracellular metabolism of Mal/maltodextrin. *Bacillus subtilis* and *Lactobacillus acidophilus* utilize MP along with α-glucosidase (EC 3.2.1.20) and neopullulanase (EC 3.2.1.135) for the intracellular metabolism of maltodextrin [25, 28, 39]. In *Lactococcus casei* and *Lactococcus lactis*, Mal is transported to the cytosol by ATP-binding cassette transporter, then degraded by MP [32, 33, 40]. By utilizing the specific phosphorolytic activity of MP to Mal, quantification methods for Mal and Pi were established [41, 42].

Based on the amino acid sequence classification of GH, MP is classified into GH65. The structure of MP from *Lactobacillus brevis* (LbMP) has been solved and was found to fold in a way that resembles glucoamylase belonging to GH15 [16]. MP has an $(\alpha/\alpha)_6$-barrel catalytic domain similar to those of GH65 and GH15 enzymes, and form the clan GH-L. The catalytic acid residue is Glu487 in LbMP, which is situated at the center of the active pocket (Fig. 2). At the exit of the active site, just above Glu487, is a well-exposed tryptophan ring (Trp582) that could be a binding site for the second Glc ring of the Mal substrate (Fig. 2). His416, and Tyr352, all positioned around the rim of the pocket, provide side chains that could interact with substrate (Fig. 2). The pocket is further filled with well-defined water molecules. Asp359 is sitting at the very bottom of the active site pocket and is surrounded by a cluster of well-conserved hydrophobic residues (Pro344, Trp358, Phe363, and Leu629) that would be good candidates for interaction with the hydrophobic parts of a glucopyranosyl ring (Fig. 2). Although the structure of MP in complex with Mal is not available, structural comparison between *L. acidophilus* MP and *Thermoanaerobacterium thermosaccharolyticum* glucoamylase suggested that His413 and Glu415 on loop 3, that connects the third and fourth α-helices of the $(\alpha/\alpha)_6$–catalytic domain, are involved in the binding to the reducing end Glc residue of Mal in subsite +1 [43].

I.4 Enzymatic synthesis of oligosaccharides using MPs

Like other GP, the reaction catalyzed by MP is reversible. The reverse phosphorolysis is an efficient reaction to synthesize the oligosaccharides, and several non-naturally occurring α-(1→4)-glucosides have been synthesized by MPs [22, 35, 44]. Vigsnaes *et al.* reported that the α-(1→4)-glucosides enhanced the growth of *Bifidobacteria animalis* subsp. *lactis* and *Bifidobacterium longum* [45]. It has also been reported that β-Glc fluoride can be an alternative of the Glc donor β-Glc1*P* in the reverse phosphorolysis. Tsumuraya *et al.* showed that *Lactobacillus brevis* MP transferred Glc residue from β-Glc fluoride to α-Glc to produce α-Mal and hydrogen fluoride [46]. Several MPs show relatively high activity of reverse phosphorolysis to acceptor of Glc derivatives at the 2-C and 6-C positions, including D-glucosamine (GlcN), *N*-acetyl-D-glucosamine (GlcNAc), and D-xylose (Xyl), and form α-(1→4)-glucosides. MP can synthesize β-Glc1*P* from Mal, which can be easily produced from abundant starch. By coupling the reactions of MP and other α-GPs, several oligosaccharides are produced from Mal. Trehalose (Tre) or nigerose (Nig) were produced by the coupling reactions of MP and TP [47], or MP and NP [48], respectively.

I.5 Purpose of this study

The gene *malE* that encodes a GH65 enzyme is found a neighboring gene of the GH31 α-glucosidase gene in *Bacillus* sp. AHU2001 (formerly known as *Bacillus* sp. SW20) [49]. The gene is downstream of five open reading frames *malA*, *malB, BspAG31A*, *malC*, and *malD*. The nucleotide sequence of *malA*, *malB, BspAG31A*, *malC*, *malD*, and *malE* were deposited in the DDBJ database under accession numbers AB971787, AB971798, AB971789, AB971790, AB971791, and AB971792, respectively. The GH31 α-glucosidase was characterized to be BspAG31A [49]. The amino acid sequence of MalA was 56%

identical with *Brachybacterium faecium* permeases of the ATP-binding cassette (ABC)-type sugar transport system [National Center for Biotechnology Information (NCBI) code, YP_003153876.1], and that of MalB was 54% identical with the *B. faecium* ABC-type sugar transport system permease component (NCBI code, YP_003793713.1). Thus, these proteins are predicted to be involved in the uptake of maltooligosaccharides. *malC* and *malD* showed the sequence identity of 78% with the *Bacillus cereus* Mal operon transcriptional repressor (NCBI code, YP_003793713.1), and that of 53% with the *B. cereus* Mal operon transcriptional repressor (NCBI code, NP_980355.1), respectively. The deduced amino acid sequence of MalE share 52–60% identity with that of characterized MPs: *B. selenitireducens* MP (GenBank number, ADH99560.1) [14], *Bacillus* sp. RK-1 MP (GenBank number, BAC54904.1) [24], *E. faecalis* MP (GenBank number, AAO80764.1) [50], *L. acidophilus* MP (GenBank number, AAV43670.1) [28], *L. brevis* MP (Uniprot number, Q7SIE1) [16], *L. sanfranciscensis* MP (GenBank number, ADH99560.1) [30], and *Paenibacillus* sp. SH-55 MP (GenBank number, BAD97810.1) [39]. It is speculated that although short maltooligosaccharides can be hydrolyzed completely to Glc by BspAG31A solely, the presence of MalE indicates that a part of Mal, resulting from the hydrolysis of maltooligosaccharides catalyzed by BspAG31A, is metabolized thorough phosphorolysis. In this work, the *malE*-gene product, putative GH65 MP, was characterized to address the predicted involvement in maltooligosaccharides metabolism in *Bacillus* sp. AHU2001. Through the detailed acceptor specificity analysis, the hidden ability of this GH65 enzyme was classified, together with the possible binding mode on this protein structure. The ability was applied for the enzymatic synthesis of oligosaccharides including novel compounds and sugar phosphates using MalE.

A

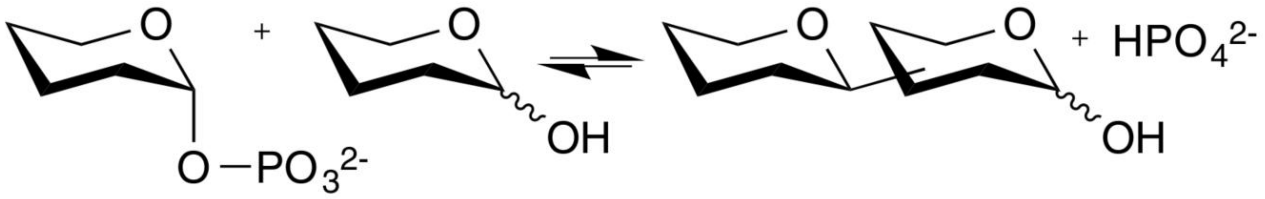

B

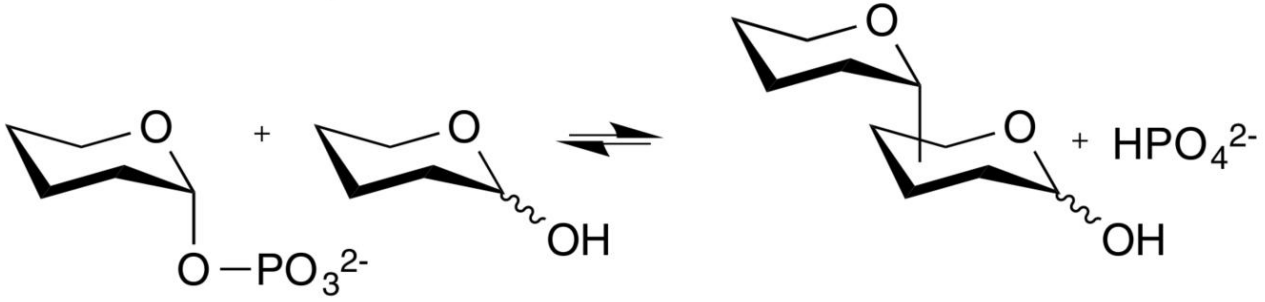

Fig. 1. General scheme for phosphorylase actions.

(A) The reaction of inverting phosphorylases. (B) The reaction of retaining phosphorylases.

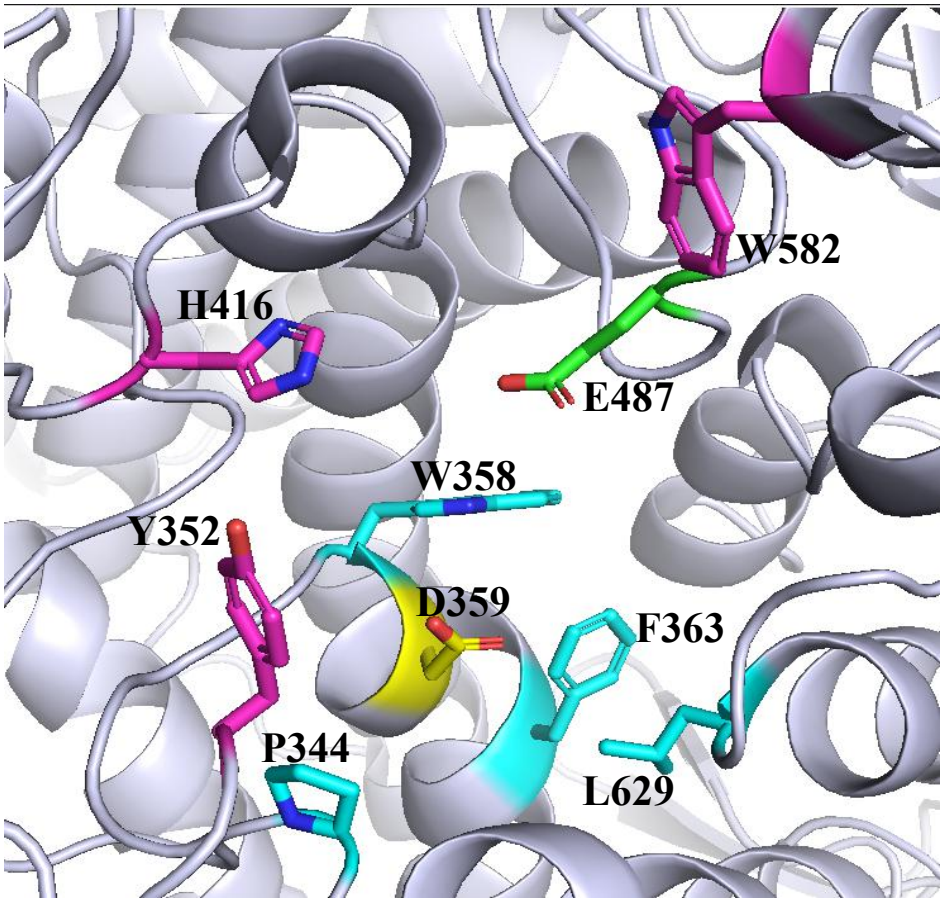

Fig. 2. Active site residues of LbMP.

The residues lining the active site pocket were shown. Glu487 (green) is general catalytic acid which is situated at the center of the pocket. Asp359 (yellow) is sitting at the bottom of the active site pocket and is surrounded by hydrophobic residues (Pro344, Trp358, Phe363, and Leu629, cyan). Trp582, His416, and Tyr352 (magenta) could interact with hydroxyl groups of the substrate.

Table. 1. Phosphorylases acting on carbohydrates.

Enzyme	EC	Family	Carbohydrate substrate	Reaction mechanism
Glycogen (starch) phosphorylase	2.4.1.1	GT35	D-Glc-(α1,4-D-Glc)$_n$	Retention
Sucrose phosphorylase	2.4.1.7	GH13	D-Glc-α1,β2-D-Fru	Retention
Maltose phosphorylase	2.4.1.8	GH65	D-Glc-α1,4-D-Glc	Inversion
Cellobiose phosphorylase	2.4.1.20	GH94	D-Glc-β1,4-D-Glc	Inversion
Laminaridextrin phosphorylase	2.4.1.30	GH94	D-Glc-(β1,3-D-Glc)$_n$	Inversion
Laminaribiose phosphorylase	2.4.1.31	GH94	D-Glc-β1,3-D-Glc	Inversion
Cellodextrin phosphorylase	2.4.1.49	GH94	D-Glc-(β1,4-D-Glc)$_n$	Inversion
Trehalose phosphorylase	2.4.1.64	GH65	D-Glc-α1,α1-D-Glc	Inversion
β-1,3-Glucan phosphorylase	2.4.1.97	GH149	D-Glc-(β1,3-D-Glc)$_n$	Inversion
Galacto-*N*-biose/Lacto-*N*-biose phosphorylase	2.4.1.211	GH112	D-Glc-β1,3-D-Gal/Glc	Inversion
Trehalose 6-phosphate phosphorylase	2.4.1.216	GH65	D-Glc-α1,4-D-Glc-6*P*	Inversion
Kojibiose phosphorylase	2.4.1.230	GH65	D-Glc-(α1,2-D-Glc)$_n$	Inversion
Trehalose phosphorylase	2.4.1.231	GT4	D-Glc-α1,α1-D-Glc	Retention
D-Galactosyl-β-1,4-L-rhamnose phosphorylase	2.4.1.247	GH112	D-Glc-β1,4-L-Rha	Inversion
N-Acetylglucosaminidase	2.4.1.255	GH3	*p*NPGlcNAc	Retention

Table. 1. Continued.

Enzyme	EC	Family	Carbohydrate substrate	Reaction mechanism
Nigerose phosphorylase	2.4.1.279	GH65	D-Glc-α1,3-D-Glc	Inversion
Chitinbiose phosphorylase	2.4.1.280	GH94	D-GlcNAc-β1,4-D-GlcNAc	Inversion
D-Mannosyl-β-1,4-D-glucose phosphorylase	2.4.1.281	GH130	D-Man-β1,4-D-Glc	Inversion
3-*O*-α-D-Glucosyl-L-rhamnose phosphorylase	2.4.1.282	GH65	D-Glc-α1,3-L-Rha	Inversion
β-1,4-Mannooligosaccharide phosphorylase	2.4.1.319	GH130	D-Man-(α1,4-D-Glc)$_n$	Inversion
1,4-β-Mannosyl-*N*-acetylglucosamine phosphorylase	2.4.1.320	GH130	D-Man-β1,4-D-GlcNAc	Inversion
Cellobionic acid phosphorylase	2.4.1.321	GH94	D-Glc-β1,4-D-GlcA	Inversion
Sucrose 6-phosphate phosphorylase	2.4.1.329	GH13	D-Glc-α1,β2-D-Fru6*P*	Retention
1,2-α-Glucosylglycorel phosphorylase	2.4.1.332	GH65	D-Glc-α1,2-Glycerol	Inversion
1,2-β-Oligoglucan phosphorylase	2.4.1.333	GH94	D-Glc-(β1,2-D-Glc)$_n$	Inversion
1,3-α- Oligoglucan phosphorylase	2.4.1.334	GH65	D-Glc-(α1,3-D-Glc)$_n$	Inversion
β-1,2-Mannobiose phosphorylase	2.4.1.339	GH130	D-Man-β1,2-D-Man	Inversion
1,2-β-Oligomannan phosphorylase	2.4.1.340	GH130	D-Man-(β1,2-D-Man)$_n$	Inversion
Glucosylglycerate phosphorylase	2.4.1.352	GH13	D-Glc-α1,2-glycerate	Retention
α-1,4-Glucan:maltose-1-*P* maltosyltransferase	2.4.99.16	GH13	D-Glc-(α1,4-D-Glc)$_n$	Retention

CHAPTER II. Biochemical characterization of maltose phosphorylase MalE

II.1 Introduction

The bacterial strain *Bacillus* sp. AHU2001 was isolated from soil sample near a hot spring in Hokkaido, Japan. The partial sequence of the 16S rDNA (1389 bp) was 96.3% identical with that of *Bacillus cytotoxicus* NVH391-98, and thus it was designated as a *Bacillus* sp. This bacterial strain AHU2001 is deposited at Laboratory of Culture Collection of Microorganisms, Faculty of Agriculture, Hokkaido University (Sapporo, Japan). The cloning of gene coding a GH31 α-glucosidase and exploring its neighboring region of the genomic DNA revealed that *malE* encoding a putative MP is located downstream the gene coding GH31 α-glucosidase, BspAG31A (Fig. 3) [49]. The deduced amino acid sequence of MalE is 52-60% identical to those of GH65 MPs, and MalE falls in the cluster of MP in the phylogenetic tree of GH65 proteins (Fig. 4). Although MPs and possible MP proteins in various bacterial origins are found in sequence database, analysis of enzymatic properties such as the precise substrate specificity is limited. In particular, acceptor specificity of MPs in the reverse phosphorolysis was analyzed only on a few MPs [22, 28, 37]. In this chapter, the biochemical characteristics of the deduced GH65 MP, MalE in *Bacillus* sp. AHU2001 will be described. The kinetic analysis of the reverse phosphorolysis is described in detail. Various acceptor substrates including poor acceptors are all mentioned, and the kinetic model for the reverse phosphorolysis reaction with concomitant hydrolysis of β-Glc1*P* was proposed based on the reaction velocities.

II.2 Materials and methods

II.2.1 Chemicals

The following sugars were used as substrate: Glc, 1,5-anhydro-D-glucitol (1,5-AG), methyl α-D-glucoside (α-MG), methyl β-D-glucoside (β-MG), D-mannose (Man), Koj, D-allose (All), nigerose (Nig), D-gluconic acid (GlcA), D-tagatose (Tag), Xyl (Wako Pure Chemical Industries; Osaka, Japan); 2-deoxy-D-glucose (2-deoxyGlc), Isomal, GlcN (Tokyo Chemical; Tokyo, Japan); 3-deoxy-D-glucose (3-deoxyGlc), 4-deoxy-D-glucose (4-deoxyGlc) (Carbosynth, Berkshire, UK); 6-deoxy-D-glucose (6-deoxyGlc), L-fucose (Fuc), D-talose (Tal), L-rhamnose (Rha), D-altrose (Alt), D-xylulose (Xul) (Sigma, St. Louis, USA); D-galactose (Gal), L-sorbose (Sor), D-fructose (Fru), maltotriose, GlcNAc (Nacalai Tesque; Kyoto, Japan); D-lyxose (Lyx, Alfa Aesar, Lancashire, UK); L-arabinose (Ara, Kanto Chemical, Tokyo, Japan); Tre (Hayashibara, Okayama, Japan); and Mal (Nihon Shokuhin Kako, Tokyo, Japan).

II.2.2 Preparation of the expression plasmid of MalE

The expression plasmid derived from pET-23a (Novagene, Darmstadt, Germany) was prepared for production a recombinant MalE protein (GenBank accession number: BAQ19546.1) with 8 extra-amino acid residues (Leu-Glu-His-His-His-His-His-His), attached to its C-terminal. The *Nde*I and *Xho*I restriction sites were introduced to the 5′- and 3′-terminals of *malE*, respectively. An internal *Nde*I site was mutated by the overlap extension polymerase chain reaction (PCR) method [51]. In the first PCR, the 5′- and 3′- regions of *malE* were amplified from the genomic DNA of *Bacillus* sp. AHU2001 using the following two sets of primers: for the 5′-region, 5′-AAGGTGATAACATATGAAAAGATTAT-3′ (primer A, sense orientation, *Nde*I site underlined) and 5′-CGCATCCCCATGTGACCGTTTCC-3′ (antisense

orientation, substituted nucleotide in boldface); for the 3′-region, 5′-GGAAACGGTCA**C**ATGGGGATGCG-3′ (sense orientation, substituted nucleotide in boldface) and 5′- AGCTTCATATCTCGAGGCCGGAATTGCTTG-3′ (primer B, antisense, *Xho*I site underlined). The second PCR was performed using the amplified DNA fragments as template and primers A and B. The amplified DNA fragment and pET-23a were subjected to the restriction digestion using *Nde*I and *Xho*I (Takara Bio, Kusatsu, Japan). The resulting DNA fragments were ligated using DNA Ligation Kit Mighty Mix (Takara Bio). The DNA sequence of the insert and the flanking regions was analyzed using BigDye Terminator Kit (Thermo Fisher Scientific, San Jose, USA) for the reactions, and an Applied Biosystems 3130 Genetic Analyzer (Life Technologies, Carlsbad, USA) for their analysis.

II.2.3 Production and purification of MalE

Recombinant MalE was produced in the transformant of *E. coli* BL21 (DE3), harboring the expression plasmid. The transformant was incubated in 2 L Luria-Bertani (LB) medium, containing 100 μg/mL ampicillin, at 37°C with vigorous shaking until the absorbance at A_{600} reached 0.5. The recombinant protein production was induced by adding 2 mL of 100 mM isopropyl β-D-1-thiogalactopyranoside (IPTG) to the culture medium (final concentration, 0.1 mM), and the cells were further incubated at 18°C for 22 h. The bacterial cells were collected by centrifugation (8,000 ×g, 4°C, 10 min), and disrupted by sonication in 100 mL of 30 mM imidazole-HCl buffer (pH 6.5) containing 500 mM NaCl. The cell debris was removed by centrifugation (12,000 ×g, 4°C, 10 min), and the cell-free extract was obtained as the starting material for MalE purification. The proteins were applied to a Ni^{2+}-immobilized Chelating Sepharose chromatography column (2.8 cm i.d. × 5.0 cm; resin, Sepharose Fast Flow, GE Healthcare, Uppsala, Sweden; pre-equilibrant with the starting buffer 30 mM imidazole with 0.5 M NaCl, pH 6.5). The column was washed with the

starting buffer and the adsorbed protein was eluted with a linear gradient of imidazole from 30 to 500 mM in the starting buffer (total elution volume, 400 mL). The collected fractions, containing highly purified MalE judged by UV method (detail described in section II.2.4) and sodium dodecyl sulfate-polyacrylamide gel electrophoresis (SDS-PAGE, detail described in section II.2.6), were pooled and dialyzed against 10 mM 2-morpholin-4-ylethanesulfonic acid (MES)-NaOH buffer (pH 6.5). The purified protein was concentrated using Vivaspin concentrators (Vivaspin 20, 30,000 MWCO PES, Sartorius, Göttingen, Germany).

II.2.4 Protein quantification

The protein concentration of the cell-free extract was measured by the Bradford method [52], in which bovine serum albumin (BSA; Nacalai Tesque) was used as the standard. During the purification process, the protein concentration was determined by the UV method at A_{280} [53]. The protein concentration of a protein solution showing A_{280} equals 1 was regarded as 1 mg/mL. The concentration of purified protein was determined by the amino acid analysis using JLC-500/V (JEOL, Tokyo, Japan) after hydrolysis of the purified protein in 6 M HCl at 110°C for 24 h [54]. Protein concentration was calculated from amino acid contents (nmol) and their calculated contents (mol) per enzyme (1 mol).

II.2.5 Measurement of molecular mass by gel filtration column chromatography

Two hundred μL of 0.46 mg/mL MalE in the native state was subjected to gel filtration column chromatography under following conditions: column, Superdex 200 10/300 GL (1.0 cm i.d. × 30 cm, 24 mL, GE Healthcare); mobile phase, 10 mM 2-[4-(2-hydroxyethyl)piperazin-1-yl]ethanesulfonic acid

(HEPES)-NaOH buffer (pH 6.5) containing 0.2 M NaCl; flow rate, 0.5 mL/min; detection, A_{280}. A set of gel filtration standards (vitamin B12, 1.35 kDa; myoglobin, 17 kDa; ovalbumin 44 kDa; γ-globulin 158 kDa; thyroglobulin 670 kDa; Gel Filtration Standard, Bio-Rad, Hercules, USA) were used to calibrate the molecular mass. The molecular mass determination is made by comparing the value of the equilibrium distribution coefficient K_d for the measured protein to the K_d of protein standards of known molecular mass, according to plot the logarithms of the standard molecular masses versus their respective K_d values produces a linear calibration curve. K_d is calculated for the ratio of elution volume (V_e) minuses void volume (V_0) and total geometric volume of the column (V_c) minuses void volume (V_0). The V_0 is based on the volume of effluent required for the elution of blue dextran (molecular mass of 2,000 kDa, Wako Pure Chemical Industries).

II.2.6 SDS-PAGE

SDS-PAGE was carried out according to the method of Laemmli [55]. Protein sample (2 μg) or 10 μL of cell-free extract of *E. coli* transformant was mixed with the equal volume of 2× sample loading buffer, that is 0.1 M 2-amino-2-hydroxymethyl-propane-1,3-diol (Tris)-HCl (pH 6.8), 4% β-mercaptoethanol, 4% sodium dodecyl sulfate, and 20% glycerol, then heated at 100°C for 5 min. The sample was applied for separation in the 10% polyacrylamide separation gel. Electrophoresis was carried out at constant voltage, 200 V. The gel was visualized with Rapid CBB Kanto (Kanto Chemical). Precision Plus Protein Dual Color Standards (Bio-Rad) were used as protein size marker.

II.2.7 Concentration determination of β-Glc1*P*

The concentration of β-Glc1*P* was determined by using the β-phosphoglucomutase (β-PGM)/glucose-6-phosphate dehydrogenase (G6PDH)

method [56]. A reaction mixture (150 μL), containing 0.1 μM Glc 1,6-bisphosphate (Sigma), 0.83 mM thionicotinamide-adenine dinucleotide (Thio NAD^+, Nacalai Tesque), G6PDH (Toyobo, Osaka, Japan), 5 U/mL *Lactococcus lactis* subsp. *lactis* β-PGM (Sigma), and 2 mM $MgAC_2$ (Nacalai Tesque), and 50 mM HEPES-NaOH buffer (pH 7.0), was incubated at 30°C for 10 min. A_{400} was measured after the incubation.

II.2.8 Preparation of β-Glc1*P*

β-Glc1*P* was prepared by the phosphorolysis of Mal using MalE. A reaction mixture (2 L), containing 0.3 M Mal (600 mmol), 0.3 M potassium phosphate buffer (pH 8.0; 600 mmol), and 16.5 mg/L MalE, was incubated at 37°C for 96 h. From the reaction, 178 mmol β-Glc1*P* was obtained. The pH of the reaction mixture was adjusted to pH 4.0 with 6 M HCl. Further, 4 mL glucoamylase (AMG300L; Novozymes, Bagsværd, Denmark) was added, and the mixture was incubated at 60°C for 3 h to digest the remaining Mal. The pH of the mixture was adjusted to pH 6.5 with 5 M KOH. Next, 41 mL of 28% (w/v) ammonium water and 128 g of $MgAc_2$ were added and the mixture was incubated at 4°C for 1 h. The insoluble $NH_4MgPO_4 \cdot 6H_2O$ was removed by filtration using Celite No. 545 (Wako Pure Chemical Industries). The resulting solution was concentrated to 500 mL under reduced pressure. The pH of the solution was adjusted to pH 8.5 with 5 M KOH, and the insoluble $NH_4MgPO_4 \cdot 6H_2O$ generated was removed again as described above. Methanol (2.4 L) was added to the mixture and incubated at 25°C for 2 h. The precipitate was collected by filtration using filter paper, and dissolved in 700 mL water. The yield of β-Glc1*P* was 164 mmol. Five hundred mL of this mixture containing 117 mmol β-Glc1*P* was further subjected to anion exchange column chromatography with Amberjet 4400 (3.6 cm i.d. × 90 cm, 600 mL, acetate form; Organo, Tokyo, Japan) according to the method previously described [57]. The fractions containing β-Glc1*P* were concentrated under reduced pressure, and β-Glc1*P* was precipitated in 80% ethanol. β-Glc1*P*,

collected by filtration, was dried in vacuo, and stored at −20°C. The yield of β-Glc1*P* was 72.8 mmol, determined by the description in section II.2.7.

II.2.9 Standard enzyme activity assay

A reaction mixture (50 μL), containing 2.94−14.7 μg/mL of enzyme, 4 mM Mal, 10 mM sodium phosphate buffer (pH 8.0), 100 mM HEPES-NaOH buffer (pH 8.0), and 0.2 mg/mL BSA, was incubated at 37°C for 10 min. The reaction was stopped by heating at 90°C for 5 min. 100 μL of 2 M Tris-HCl buffer (pH 7.0) was added to the sample, and the released Glc was measured by the Glc oxidase-peroxidase method [58] using Glc CII test (Wako Pure Chemical Industries). One unit of MP activity was defined as the amount of enzyme required to phosphorolyze 1 μmol of Mal in 1 min under these conditions.

II.2.10 Substrate specificity of MalE in the phosphorolysis

The phosphorolytic activity of the recombinant protein was measured using 4 mM Tre, Koj, Nig, Mal, Isomal, and maltotriose under the standard assay conditions.

II.2.11 Evaluation of the effect of pH and temperature on enzyme activity and stability

The optimal pH for enzyme activity was measured under the standard assay conditions but 100 mM HEPES-NaOH buffer (pH 8.0) was replaced with 100 mM various buffers: sodium citrate buffer (pH 4.1–6.1), MES-NaOH buffer (pH 6.1–7.1), HEPES-NaOH buffer (pH 7.1–8.5), and glycine-NaOH buffer (pH 8.6–9.6). The optimal temperature for the enzyme activity was determined at various temperatures. The pH stability was evaluated by determining the residual enzyme activity after incubating 0.29 mg/mL MalE with 100 mM Britton-Robinson (BR) buffer (pH 3.5–11.3) at 4°C for 24 h. BR buffer was prepared by

mixing of 0.2 M acetic acid (Kanto Chemical), 0.2 M phosphoric acid (Nacalai Tesque), and 0.2 M glycine (Wako Pure Chemical Industries), then adjusted pH with 1 M NaOH. After the incubation of the enzyme, the treated enzyme solution was diluted by 20 times with 10 mM HEPES-NaOH buffer (pH 8.0) containing 1 mg/mL BSA for the activity assay. The stable range for temperature was evaluated by measuring the residual enzyme activity after incubating 15 μg/mL MalE with 100 mM sodium phosphate buffer (pH 8.0) at 30–60°C for 15 min. The pH and temperature, in which the enzyme showed residual activity higher than 80%, were regarded as the stable ranges.

II.2.12 Kinetic analysis of phosphorolytic reaction of maltose

The reaction rate for phosphorolysis of Mal at various concentrations of Mal (0.5–4 mM) and sodium phosphate buffer (1–8 mM) was measured as the standard enzyme assay. The kinetic parameters were calculated by fitting the reaction equation (Eq. 1) for a sequential bi bi mechanism [59] to the reaction rates with Grafit version 7.0.2 (Erithacus Software, East Grinstead, UK).

Eq. 1: $v = k_{cat}[A][B]/(K_{iA}K_{mB} + K_{mB}[A] + K_{mA}[B] + [A][B])$

where, A = Pi, B = Mal.

II.2.13 Acceptor specificity in the reverse phosphorolysis

To investigate the acceptor specificity in the reverse phosphorolysis, Pi−releasing velocity to β-Glc1*P* and acceptors (monosaccharides and disaccharides mentioned in section II.2.1) was measured. A reaction mixture (20 μL), containing 1.47–588 μg/mL MalE, 10 mM β-Glc1*P*, 10 mM acceptor, and 100 mM HEPES-NaOH buffer (pH 8.0), was incubated at 37°C for 10 min. The sample was heated at 90°C for 5 min to stop the reaction, and the released Pi was measured following the methods of Lowry and Lopez [60].

II.2.14 Kinetic analysis of reaction with β-Glc1*P* and acceptor

To determine the kinetic parameters for the reaction to β-Glc1*P* and acceptor, the reaction scheme that involves both the hydrolysis of β-Glc1*P* and the reverse phosphorolysis (Fig. 5) was used. The rate equation (Eq. 2) obtained from the scheme is as follows:

Eq. 2: $v = (k_{cat1}K_{mQ}[P] + k_{cat2}[P][Q])/(K_sK_{mQ} + K_{mP}[Q] + K_{mQ}[P] + [P][Q])$

where, [P] and [Q] are molar concentration of β-Glc1*P* and acceptor, respectively.

Kinetic parameters, K_{mP}, K_{mQ}, and K_s, were defined as follows by the rate constants shown in Fig. 5:

$$K_{mP} = k_{cat2}/k_1$$

$$K_{mQ} = (k_{-2} + k_{cat2})/k_2$$

$$K_s = (k_{-1} + k_{cat1})/k_1$$

At a constant [P], the rate equation is shown as Eq. 3.

Eq. 3: $v = (k_{cat(app)}[Q] + v_0K_{m(app)})/(K_{m(app)} + [Q])$

v_0 is the hydrolytic velocity of β-Glc1*P* without the acceptor (measured from Glc-releasing velocity):

Eq. 4: $v_0 = k_{cat1}[P]/(K_s + [P])$

The apparent kinetic parameters, $k_{cat(app)}$ and $K_{m(app)}$, are given by the following equations:

$$k_{cat(app)} = k_{cat2}[P]/(K_{mP} + [P])$$

$$K_{m(app)} = K_{mQ}(K_s + [P])/(K_{mP} + [P])$$

The apparent kinetic parameters for Glc, 1,5-AG, α-MG, 2-deoxyGlc, Man, GlcN, GlcNAc, Koj, 3-deoxyGlc, All, 6-deoxyGlc, Xyl, Lyx, Fuc, and Sor were

determined by fitting the reaction equation Eq. 3 to reaction rates at 0.75–25 mM of the acceptor and 10 mM β-Glc1*P*.

k_{cat1} and K_s, which are the kinetic parameters for the hydrolysis of β-Glc1*P*, were determined by fitting Eq. 4 to the hydrolytic velocity to various concentrations of β-Glc1*P* in the absence of acceptor.

II.3 Results

II.3.1 Purification of the recombinant MalE

The recombinant MalE protein was successfully produced in *E. coli* BL21 (DE3) transformant. From *E. coli* cells proliferated in 2 L of culture broth, cell-free extract was prepared by sonication. The cell-free extract (34 mL, 2660 mg of protein) included 717 U of activity (specific activity was 0.27 U/mg). Recombinant MalE was purified by Ni^{2+}–affinity column chromatography (Fig. 6A and B). The yield of the purified enzyme was 13.6 mg. The specific activity of purified enzyme was 15.9 U/mg. The molecular mass of MalE was 90 kDa as determined by SDS-PAGE (theoretical molecular mass is 89.6 kDa; Fig. 7A), and 193 kDa as determined by gel-filtration column chromatography (Fig, 7B). This indicated that MalE exists as homodimer under nondenaturing conditions similar to other MPs [22, 28].

II.3.2 Specificity of MalE in the phosphorolysis

MalE phosphorolyzed Mal with a Glc-releasing velocity of 15.9 μmol/min/mg for 4 mM Mal in pH 8.0 at 37°C (Table. 2). Unlike the reaction to Mal, phosphorolytic activity of MalE to Tre, Koj, Nig, Isomal, and maltotriose were not detectable (less than 0.089 μmol/min/mg, which is 0.56% of that to

Mal).

II.3.3 Effects of pH and temperature on enzyme activity and stability

MalE exhibited the highest phosphorolytic activity at pH 8.1 on 4 mM Mal and 10 mM Pi (Fig. 8A). The optimal pH of MalE is higher than many MPs from other origins, which showed optimal pH at ≤7.0 [22, 28, 39, 42] (Tab. 3). The enzyme showed the highest activity at 45°C (Fig. 8B). The residual activity was higher than 80% of the original activity in a pH range of 4.5–10.4 after the pH treatment at 4°C for 24 h (Fig. 8C) and at ≤40°C after the heat treatment at pH 8.0 for 15 min (Fig. 8D).

II.3.4 Kinetic analysis of the phosphorolysis of MalE

In the phosphorolysis of Mal, the curves obtained by plotting 1/[Pi] versus 1/v at various Mal concentrations were linear and intersected at a point on the second quadrant (Fig. 9). This result indicates that MalE catalyzed the phosphorolytic reaction of Mal through a sequential bi bi mechanism, involving the formation of a ternary complex as observed [22, 46], similar to the reactions of other inverting disaccharide phosphorylases [61, 62]. The Glc donor is the second substrate in the direction of phospholysis of Mal. Binary-complex formation, in which the interaction between the enzyme and the phosphate group evidently plays the key role, appears to drive the arrangement of the correct active-site conformation and is, therefore, required for enzyme–substrate recognition. The calculated kinetic parameters were as follows: k_{cat}, 30.9 ± 0.6 s^{-1}; K_{mA}, 0.295 ± 0.059 mM; K_{mB}, 0.835 ± 0.123 mM; and K_{iA}, 9.07 ± 1.74 mM (A, Pi; B, Mal).

II.3.5 Acceptor specificity of MalE in reverse phosphorolysis

Acceptor specificity of the reverse phosphorolysis was determined by

measuring initial reaction rates to 10 mM β-Glc1*P* and 10 mM various acceptors. As the result shown in Table. 4, compared to the reaction without acceptor, which β-Glc1*P* was the only substrate, the production velocity of Pi was increased by the addition of Glc, Man, All, 2-deoxyGlc, 3-deoxyGlc, 6-deoxyGlc, Fuc, Sor, Lyx, Xyl, Koj, α-MG, GlcN, GlcNAc, and 1,5-AG as acceptors. Such enhancement was not observed in the reactions with Gal, Tal, Alt, Ara, 4-deoxyGlc, Rha, Fru, Tag, and Xul, Tre, Nig, Mal, Isomal, β-MG, and GlcA, indicating that these sugars were possible poor acceptors.

The apparent kinetic parameters for the reverse phosphorolysis with Glc, Man, All, 2-deoxyGlc, 3-deoxyGlc, 6-deoxyGlc, Fuc, Sor, Lyx, Xyl, Koj, α-MG, GlcN, GlcNAc, and 1,5-AG were determined based on the Pi-releasing velocity in the presence of 10 mM β-Glc1*P* (Table. 5). In the reverse phosphorolysis with Glc, Man, 2-deoxyGlc, 3-deoxyGlc, 6-deoxyGlc, Xyl, Koj, GlcN, and GlcNAc, the hydrolysis of β-Glc1*P* can be neglected, and the apparent kinetic parameters for acceptor were determined by fitting the Michaelis-Menten equation to the reaction velocity at various concentrations of acceptor. On the other hand, the hydrolytic activity of β-Glc1*P* was not negligible in the reactions to All, Fuc, Sor, Lyx, α-MG, and 1,5-AG due to low activity of reverse phosphorolysis (Fig. 10). Thus, the reaction equation (Eq. 3), obtained from the reaction scheme, in which both hydrolysis of β-Glc1*P* and the reverse phosphorolysis occur, was employed to determine the apparent kinetic parameters. The reaction velocity for 10 mM β-Glc1*P* (v_0) was measured to be 0.088 s^{-1} from the kinetic parameters of β-Glc1*P* hydrolysis in the absence of acceptors: k_{cat1}, 0.983 ± 0.029 s^{-1}; and K_s, 28.9 ± 1.1 mM (Fig. 11). Velocities for all the tested acceptors followed well Eq. 3 (Fig. 5). The apparent kinetic parameters were determined as shown in Table. 5. MalE exhibited high $k_{cat(app)}/K_{m(app)}$ for Glc, GlcN, and 6-deoxyGlc (12.8, 15.2, and 12.2$s^{-1}mM^{-1}$, respectively). GlcN was the most favorable substrate than Glc in reverse phosphorolysis due to its higher $k_{cat(app)}/K_{m(app)}$ value than that of Glc.

Even at high acceptor concentration, GlcN shows higher $k_{cat(app)}$. Furthermore, 6-deoxyGlc possessed almost similar affinity to Glc. The $k_{cat(app)}/K_{m(app)}$ value for the other tested acceptors was 0.23–12% of that to Glc, because of lower $k_{cat(app)}$ and higher $K_{m(app)}$ values.

II.4 Discussion

In the phosphorolysis, MalE did not exhibit any detectable activity to maltotriose, Tre, Koj, Nig, and Isomal, indicating that MalE is specific to the α-(1→4)-glucobiose, Mal, similar to other MPs. To understand the substrate binding mechanism, the binding mode of Glc in subsite +1 of MalE was predicted through structural comparison between a model structure of MalE and the crystal structure of *Caldicellulosiruptor saccharolyticus* KP [17]. Model structure of MalE was constructed through a homology modeling with Phyre2 program [63]. In the model structure of MalE, the orientation of the amino acid residues in the substrate binding site was consistent well with that of the template protein (*L. brevis* MP [16]; amino acid sequence of MalE is 52% identical with that of *L. brevis* MP). The superimposition showed that the amino acid residues in subsite −1 of MalE, including the general acid catalyst Glu486, were located at similar position to the corresponding residues of *C. saccharolyticus* KP (Fig. 12A). This suggests that MalE and the KP share the binding mode of non-reducing end Glc residue, meaning that the glucosidic oxygen (4-O and 2-O of the reducing end Glc residue of Mal and Koj, respectively) is situated at the same position in these enzymes. To predict the binding mode of Mal, α-Glc, which is utilized as acceptor of MP in the reverse phosphorolysis [46], was superimposed onto the reducing end Glc residue of Koj in subsite +1 (Fig. 12B). His415, Glu417, and Lys595 of MalE were predicted to form hydrogen bonds with 5-O, 1-O, and 3-O of the superimposed Glc in subsite +1, respectively (Fig. 12C). The

hydrogen bonds formed by Glu417 and Lys595 are consistent with the prediction using *L. acidophilus* MP [43]. In addition to these residues, Tyr351 is predicted to form a hydrogen bond with 3-O of Glc. As the residues of MalE, predicted to be involved in the formation of subsite +1, are conserved in MPs (Fig. 13), the substrate binding mode is presumably common to MPs.

For the acceptor screening, 30 carbohydrates were used as candidates. Among them, Glc derivatives at the 4-C position (4-deoxyGlc and Gal) were not used as acceptors, suggesting that that equatorial hydroxy group at 4-C position of Glc was essential for acceptor.

The $k_{cat(app)}/K_{m(app)}$ for reverse phosphorolysis of GlcN by MalE was as high as that of Glc (15.2 and 12.8 $s^{-1}mM^{-1}$, respectively), although the $k_{cat(app)}/K_{m(app)}$ values for 2-deoxyGlc and Man were 16- and 61-fold lower than that for Glc. This indicated that the equatorial 2-hydroxy group or amino group are required for good acceptors. MalE utilized GlcNAc harboring equatorial bulky chemical group at the 2-C position as acceptor, although its $k_{cat(app)}/K_{m(app)}$ value was as low as 2-deoxyGlc and Man. Other MPs of *Neisseria perflava* [35], *L. acidophilus* [44], and *Bacillus selenitireducens* [22] are also reported to utilize GlcNAc as acceptor in phosphorolytic reaction. Furthermore, MalE acted on Koj [α-D-Glc*p*-(1→2)-Glc*p*] as an acceptor with low $k_{cat(app)}/K_{m(app)}$. The reducing end of Glc, 2-O of which is glucosylated, was thought to serve as acceptor, as *B. selenitireducens* MP, glucosylates the reducing end Glc residue of Koj through the reverse phosphorolysis [22]. The model structure of MalE suggests no interaction with 2-O of Glc in subsite +1, and has open space near the 2-O of this Glc (Fig. 12C). This space could account for the activity of reverse phosphorolysis to the derivatives of Glc with bulky chemical group at the 2-C position. The subsite +1 of MalE presumably has enough space to accommodate the acceptor with an equatorial bulky chemical group at the 2-C position. The space opened for the solvent possible requires hydrophobic group in the 2-C

equatorial position.

The $k_{cat(app)}/K_{m(app)}$ of MalE for 6-deoxyGlc (12.2 $s^{-1}mM^{-1}$) was comparable with that of Glc (12.8 s^{-1} mM^{-1}). However, the $k_{cat(app)}/K_{m(app)}$ of MalE for Xyl (1.57 s^{-1} mM^{-1}) was considerably lower. This suggests that 6-C, not 6-OH, of Glc is involved in binding at subsite +1. In the modeled structure of MalE, Met406 is situated near the hydroxymethylene group of Glc in subsite +1 to have a hydrophobic interaction (Fig. 12A). The requirement of 6-C for the binding of MalE is higher than *B. selenitireducens* MP, which exhibited reverse phosphorolysis activity to Xyl comparable to that to Glc [22].

In contrast to the reaction with the Glc derivatives of 2-C and 6-C positions, MalE exhibited very low synthetic activity to all the 1- and 3-OH Glc derivatives tested: 1,5-AG, α-MG, 3-deoxyGlc, and All. In addition, the tested 4-OH Glc derivatives, 4-deoxyGlc and Gal, were not able to be utilized as acceptor. This indicates that 1-, 3- and 4-hydroxy groups of Glc are important for the subtract binding. Tyr351, Glu417, Glu486 and Lys595, predicted to interact with these hydroxy groups as mentioned above, are thought to be essential for the substrate binding. Judging from Glu417 forming a hydrogen bond with the 1-O hydroxyl of the α-anomer at subsite +1, MalE might act only on the α-anomeric configuration of Mal but not on β-Mal. Furthermore, the docking model suggested that Trp357, Gln358, Glu486, Lys595, and Gln596, which are strictly conserved in GH65 disaccharide phosphorylases, form hydrogen bonds with a Glc unit at subsite -1 [28], implying that identical interactions occur with the Glc moiety at subsite -1 in GH65 members. The importance of these hydroxy groups of the acceptor substrate for the reverse phosphorolysis is also reported in MPs from other origins [22, 28, 37].

Table. 2. Glc-releasing velocities to glucooligosaccharides on phosphorolysis.

Substrate [1)]	***v*** [2)] **(μmol/min/mg)**	**Relative *v*** [3)] **(%)**
Tre (Glcα1−1αGlc)	≤ 0.089	≤ 0.56
Koj (Glcα1−2Glc)	≤ 0.089	≤ 0.56
Nig (Glcα1−3Glc)	≤ 0.089	≤ 0.56
Mal (Glcα1−4Glc)	15.9 ± 0.20	100
Isomal (Glcα1−6Glc)	≤ 0.089	≤ 0.56
Maltotriose (Glcα1−4Glcα1−4Glc)	≤ 0.089	≤ 0.56

[1)] 4 mM substrate. [2)] Average and standard deviation from three independent measurements. [3)] The velocity to Mal was regarded as 100%.

Table. 3. The basic properties of phosphorolysis of MalE and comparison with other GH65 MPs

Enzyme	Microbial origin	Optimal pH	Optimal temperature (°C)	pH Stability	Thermostablity (°C)
MalE	*Bacillus* sp. AHU2001	8.1	45	4.5—10.4 [1)]	≤ 40 [4)]
LbMP	*Lactobacillus brevis* ATCC 8287	6.5	36	6.0—7.0 [2)]	≤ 40 [5)]
Bsel2056	*Bacillus selenitireducens*	6.5	55	5.0—10.5 [1)]	≤ 50 [4)]
MapA	*Paenibacillus* sp. SH-55	7.0	50	5.5—7.0 [3)]	≤ 55 [4)]
MalP	*Lactobacillus acidophilus* NCFM	6.2	45	3.0—8.2 [1)]	≤ 45 [4)]

[1)] Determined at 4°C in 24 h. [2)] Determined at 20°C in 24 h. [3)] Determined at 50°C in 15 min. [4)] Determined in 15 min. [5)] Determined in 60 min.

Table 4. Velocity of reverse phosphorolysis on 10 mM β-Glc1*P* and 10 mM various acceptors.

Acceptor	v [1,2] (s^{-1})	Relative v [3] (%)
None	0.088 ± 0.003	0.16
Glc	54.1 ± 1.73	100
Man	1.91 ± 0.16	3.54
All	0.323 ± 0.015	0.60
Gal	≤ 0.088	≤ 0.16
Tal	≤ 0.088	≤ 0.16
Alt	≤ 0.088	≤ 0.16
Ara	≤ 0.088	≤ 0.16
2-DeoxyGlc	8.83 ± 0.56	16.3
3-DeoxyGlc	3.58 ± 0.17	6.63
4-DeoxyGlc	≤ 0.088	≤ 0.16
6-DeoxyGlc	28.6 ± 1.02	52.9
Fuc	0.584 ± 0.041	1.08
Rha	≤ 0.088	≤ 0.16
Fru	≤ 0.088	≤ 0.16
Sor	0.237 ± 0.011	0.44
Tag	≤ 0.088	≤ 0.16
Lyx	0.274 ± 0.008	0.51
Xyl	9.94 ± 0.78	18.4
Xul	≤ 0.088	≤ 0.16
Tre	≤ 0.088	≤ 0.16
Koj	3.34 ± 0.15	6.18
Nig	≤ 0.088	≤ 0.16
Mal	≤ 0.088	≤ 0.16
Isomal	≤ 0.088	≤ 0.16
α-MG	0.548 ± 0.023	1.01
β-MG	≤ 0.088	≤ 0.16
GlcN	87.8 ± 3.59	163
GlcNAc	6.94 ± 0.32	12.8
1,5-AG	0.907 ± 0.041	1.68
GlcA	≤ 0.088	≤ 0.16

[1] Pi-releasing velocity. [2] μmol Pi/sec/μmol protein. [3] Relative velocity to that for Glc.

Table. 5. Apparent kinetic parameters with 10 mM β-Glc1*P* of acceptor substrates in reverse phosphorolysis.

Acceptor	$k_{cat(app)}$ (s^{-1})	$K_{m(app)}$ (mM)	$k_{cat(app)}/K_{m(app)}$ (s^{-1} mM^{-1})
Glc	107 ± 5	8.38 ± 0.43	12.8
1,5-AG	1.12 ± 0.002	14.1 ± 2.1	0.0794
α-MG	0.957 ± 0.116	16.3 ± 3.4	0.0587
2-DeoxyGlc	39.2 ± 2.7	47.8 ± 6.1	0.820
Man	8.55 ± 0.81	40.9 ± 5.0	0.209
GlcN	237 ± 6	15.6 ± 0.1	15.2
GlcNAc	N. D.	N. D.	0.497
Koj	15.8 ± 3.6	36.2 ± 13.1	0.436
3-DeoxyGlc	N. D.	N. D.	0.282
All	0.682 ± 0.034	31.2 ± 1.6	0.0219
6-DeoxyGlc	69.1 ± 3.5	5.68 ± 0.22	12.2
Xyl	29.9 ± 2.4	19.2 ± 2.8	1.57
Lyx	0.436 ± 0.018	15.1 ± 0.3	0.0289
Fuc	1.21 ± 0.01	20.7 ± 1.5	0.0585
Sor	0.568 ± 0.046	28.1 ± 5.7	0.0701

Apparent kinetic parameters for reverse phosphorolysis were determined from reaction rates of Pi liberation in the reaction with 10 mM β-Glc1*P* and various concentrations of compounds as Glc acceptors. The regression curve was fitted with Eq.3. Values are mean ± standard deviation for three independent experiments. N. D., not determined, because of too high $K_{m(app)}$ values.

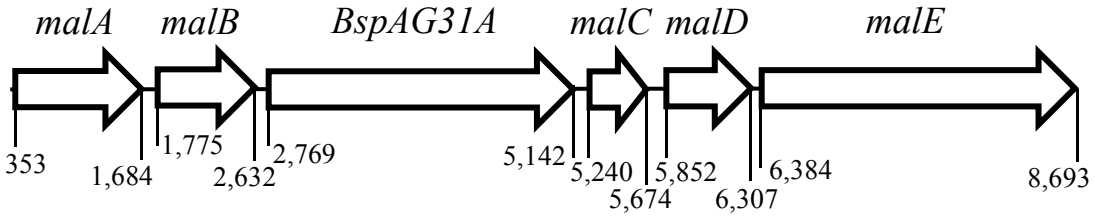

Fig. 3. Gene organization of *malE* and neighboring genes.

The *malE* gene was found downstream of the gene *BspAG31A* coding for GH31 α-glucosidase and the other four genes (*malA*, *malB*, *malC*, and *malD*). The amino acid sequence of MalA and MalB was 56% and 54% identical with *B. faecium* permeases of the ABC-type sugar transport system, respectively. The amino acid sequence identity of MalC and MalD with identity the *B. cereus* Mal operon transcriptional repressor and *B. cereus* Mal operon transcriptional repressor is 78 % and 53 %, respectively.

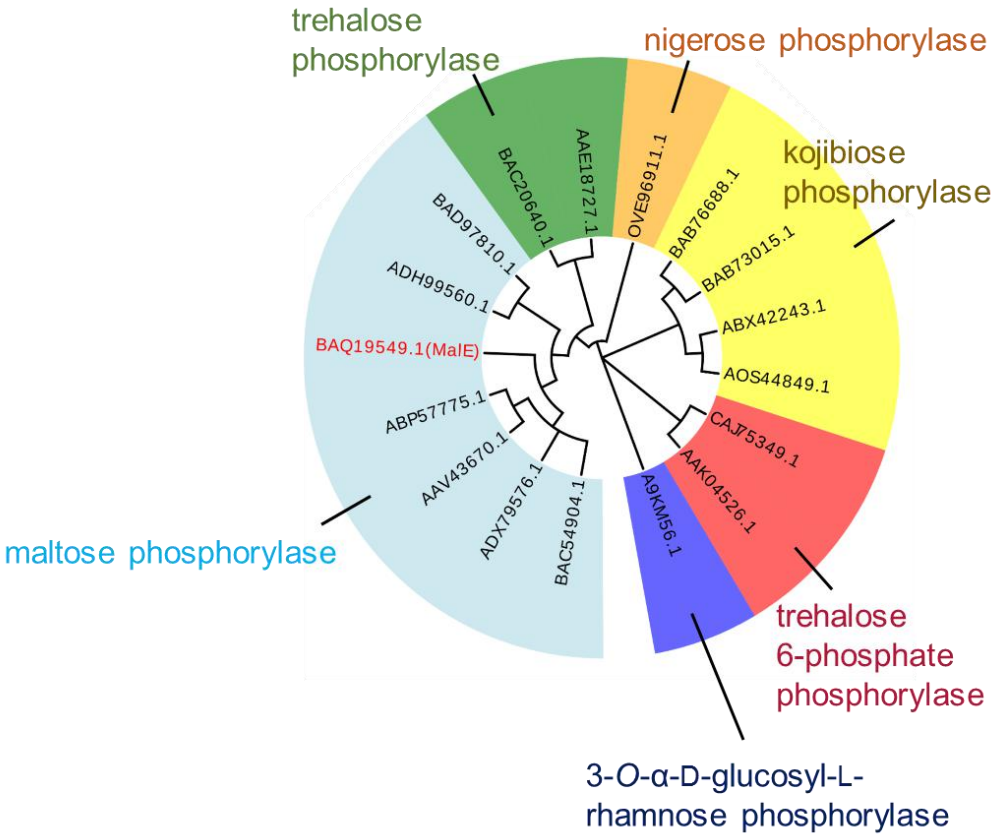

Fig. 4. Phylogenetic tree of GH65 enzymes.

Phylogenetic tree of MP, KP, NP, TP, T6PP and 3-*O*-α-D-glucosyl-L-rhamnose phosphorylase in GH65 was constructed using the Clustal W program [64]. GenBank IDs are shown in the figure. MalE (BAQ19549.1); *Paenibacillus* sp. SH-55 MP (BAD97810.1); *Bacillus selenitireducens* MP (ADH99560.1); *Lactobacillus casei* MP (ABP57775.1); *Lactobacillus acidophilus* MP (AAV43670.1); *Enterococcus faecalis* MP (ADX79576.1); *Bacillus* sp. RK-1 MP (BAC54904.1); *Geobacillus stearothermophilus* TP (BAC20640.1); *Thermoanaerobacter brockii* TP (AAE18727.1); *C.phytofermentans* NP (OVE96911.1); *Nostoc* sp. PCC 7120 KP All1058 (BAB76688.1); *Nostoc* sp. PCC 7120 KP All4989 (BAB76688.1); *C. phytofermentans* KP (ABX42243.1); *C. atypicum* KP AOS44849.1); *Kuenenia stuttgartiensis* T6PP (CAJ75349.1); *Lactococcus lactis* subsp. *lactis* T6PP (AAK04526.1); *Lachnoclostridium phytofermentans* 3-*O*-α-D-glucosyl-L-rhamnose phosphorylase (Uniprot number, A9KM56.1).

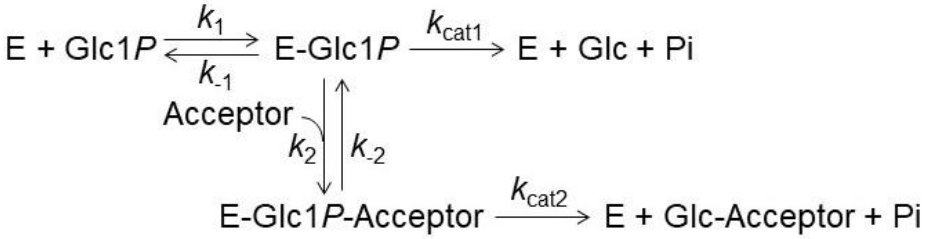

Fig. 5. Kinetic scheme of the reverse phosphorolysis and hydrolysis of β-Glc1*P*.

A

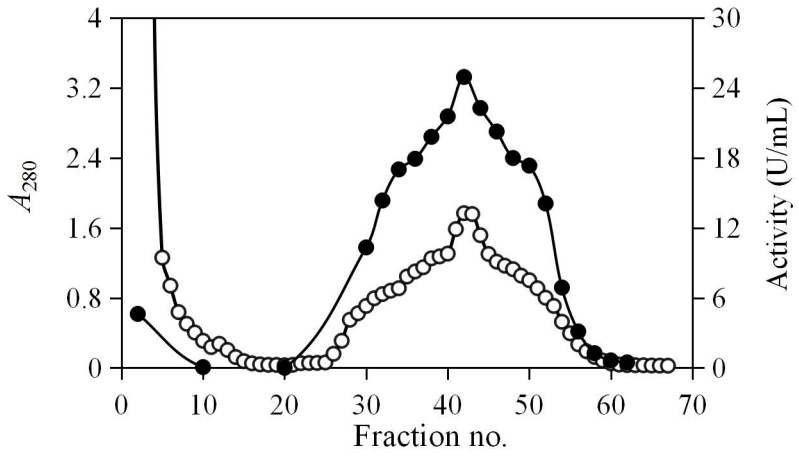

B

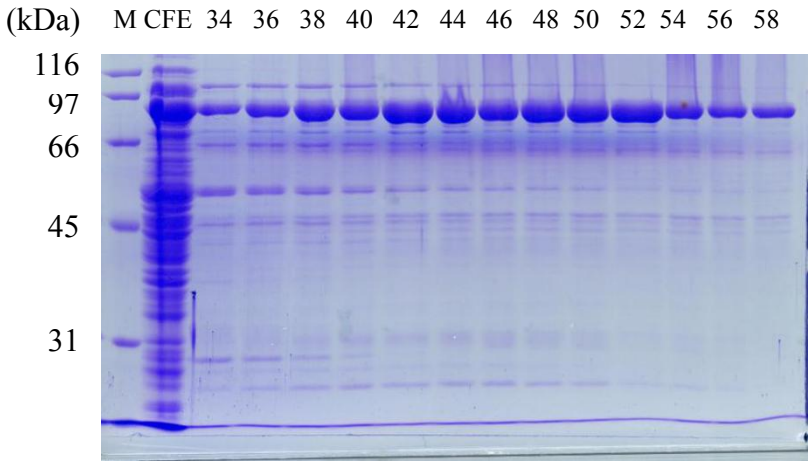

Fig. 6. Ni^{2+}-immobilized Chelating Sepharose Fast Flow column chromatography of MalE and SDS-PAGE analysis.

A, Absorbance at 280 nm (-○-) and enzyme activity (-●-) are shown. Nickle-immobilized Chelating Sepharose Fast Flow column was equilibrated with 30 mM imidazole buffer (pH6.5) containing 0.5 M NaCl. The proteins were eluted by 30−500 mM imidazole buffer (pH6.5) containing 0.5 M NaCl (total elution volume, 400 mL). Fractions 30-54 were collected (5 mL for each fraction, totally 125mL). B, protein samples from cell-free extract and fractions containing MalE were analyzed by SDS-PAGE. Numbers above indicate the fraction numbers. Lane M: molecular size protein marker; Lane CFE: cell-free extract sample.

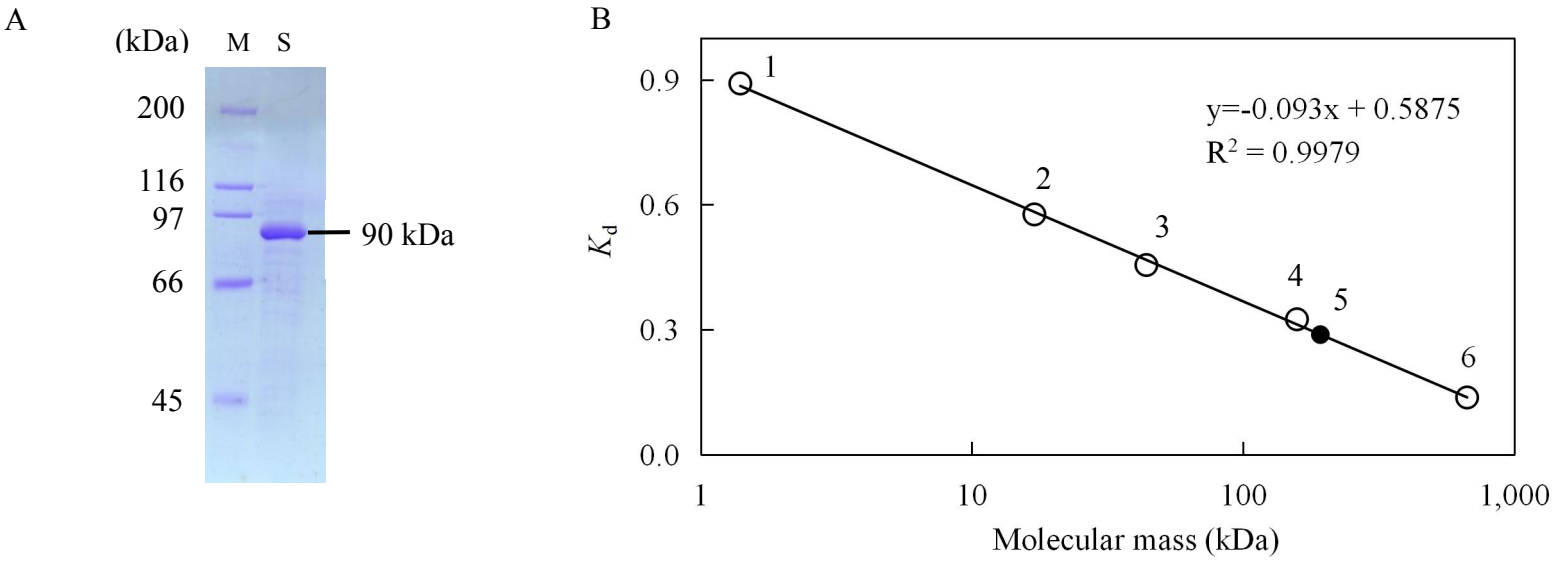

Fig. 7. Molecular mass analysis of recombinant MalE by SDS-PAGE and gel filtration column chromatography.

A, SDS-PAGE of purified recombinant MalE. Lane M: molecular size marker; and lane S: the purified MalE (2 μg). Protein was visualized by the CBB staining. The molecular mass of MalE determined by SDS-PAGE was 90 kDa. B, molecular mass of MalE determined by gel filtration column chromatography. Standard materials (-○-) and MalE (-●-) are shown. Plotting the logarithms of the standard molecular masses versus their respective the equilibrium distribution coefficient values (K_d) produces a linear calibration curve (calculation of K_d is described in section II.2.5 in detail). 1, vitamin B12; 2, myoglobin, 3, ovalbumin; 4, γ-globulin; 5, MalE sample; 6, thyroglobulin.

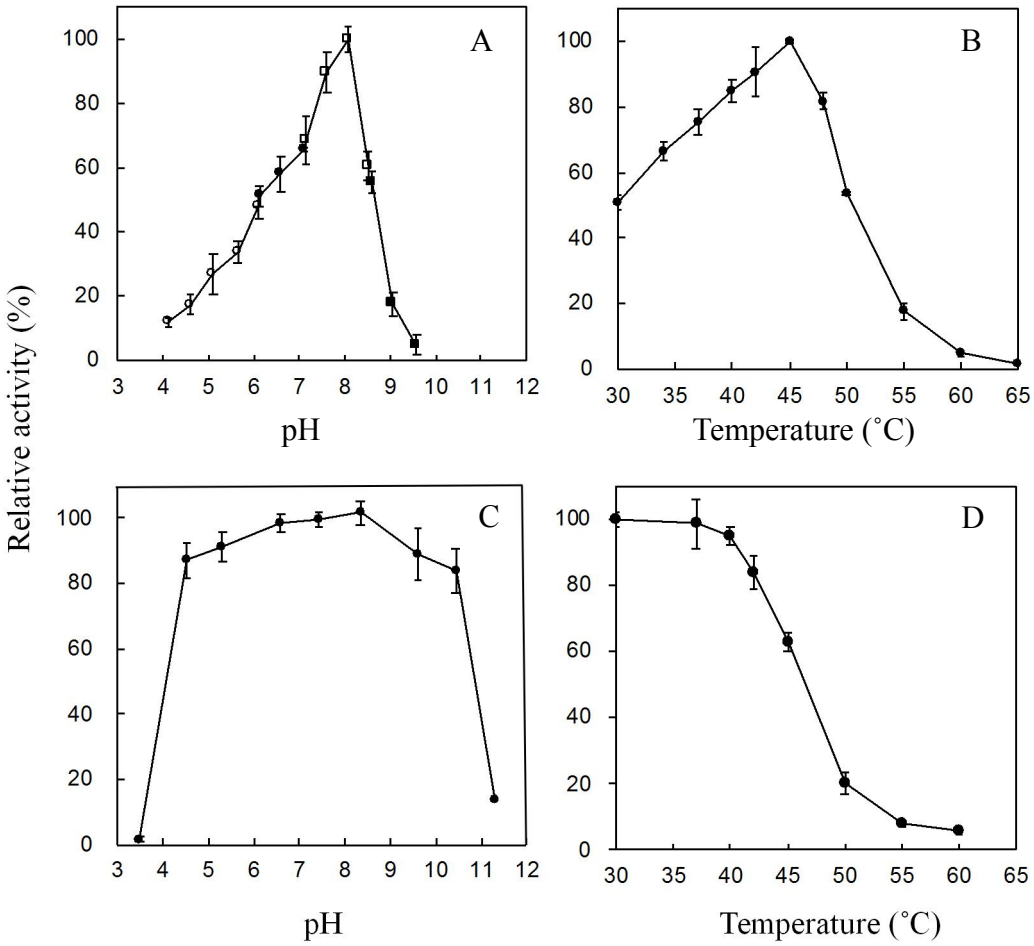

Fig. 8. Effects of pH and temperature on phosphorolysis of Mal.

A, pH activity curve. Reaction buffers are sodium citrate buffer (open circles), MES-NaOH buffer (close circles), HEPES-NaOH buffer (open squares), and glycine-NaOH buffer (close squares). B, temperature activity curve. C, pH stability. Residual activity after the pH treatment at 4˚C for 24 h is shown. D, temperature stability. Residual activity after the heat treatment for 15 min is shown. Values and error bars are average and standard deviation of three independent experiments.

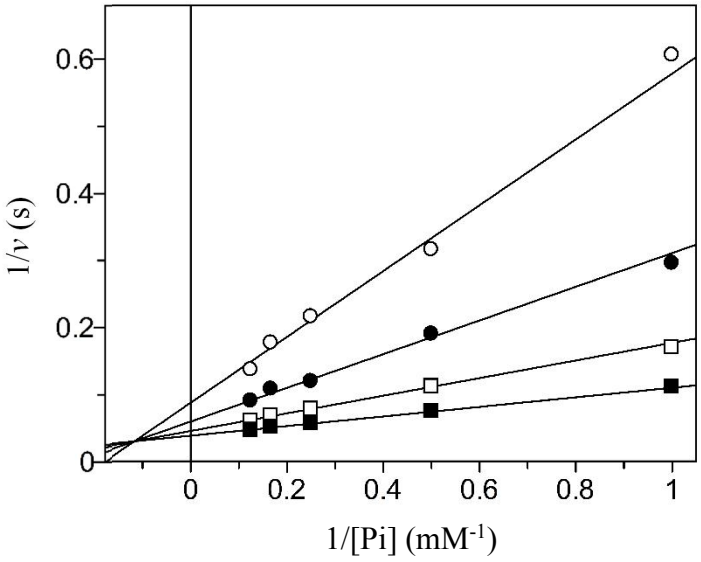

Fig. 9. Double reciprocal plots for phosphorolysis of Mal by MalE

Mal concentrations are 0.5 mM (open circles), 1.0 mM (closed circles), 2.0 mM (open squares), and 4.0 mM (closed squares). Values and error bars are average and standard deviation of three independent experiments.

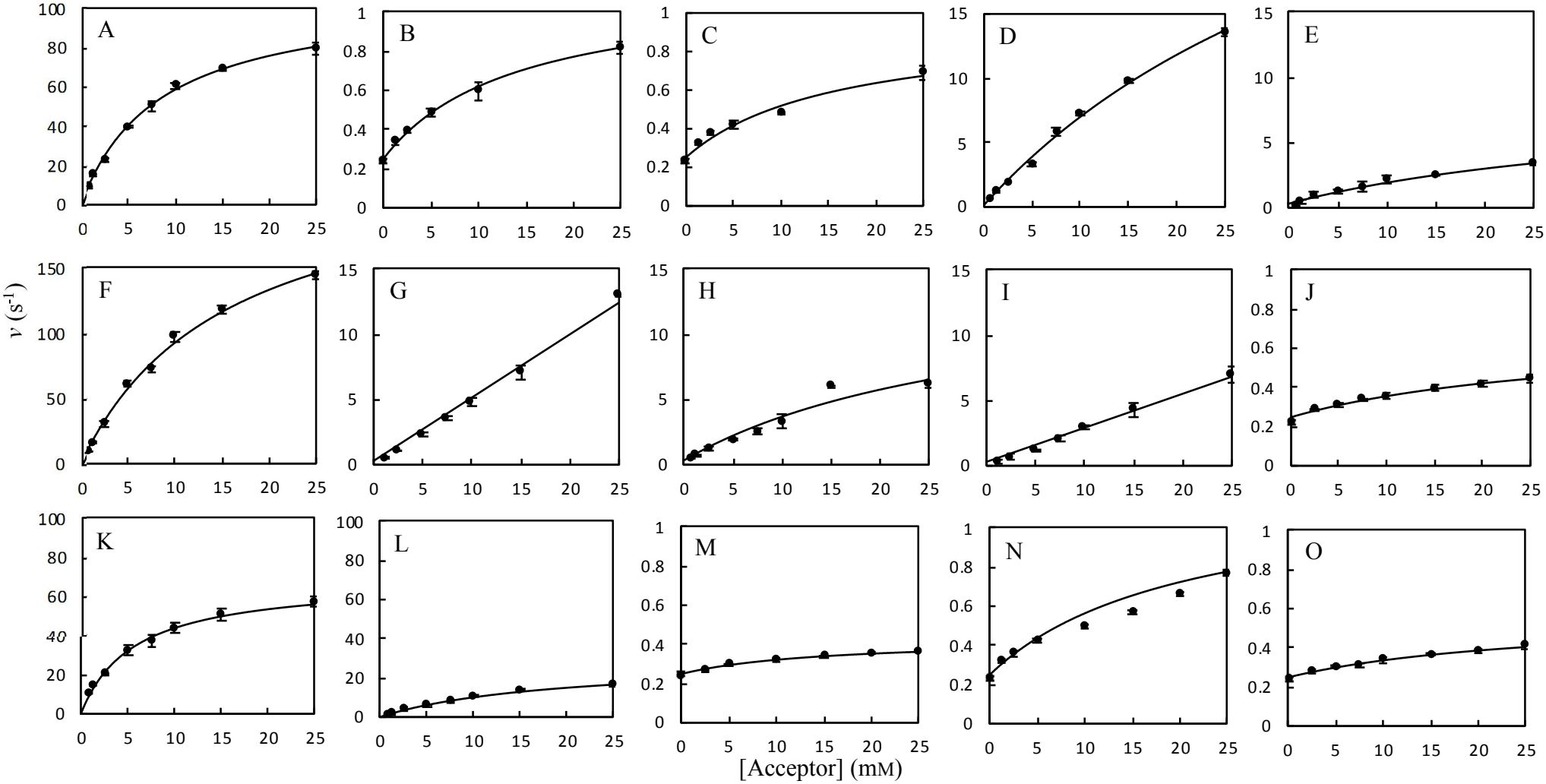

Fig. 10. The s-*v* plots for reverse phosphorolysis catalyzed by MalE.

The s-*v* plots for the reverse phosphorolysis with various concentrations of acceptors are shown: A, Glc; B, 1,5-AG; C, α-MG; D, 2-deoxyGlc; E, Man; F, GlcN; G, GlcNAc; H, Koj; I, 3-deoxyGlc; J, All; K, 6-deoxyGlc; L, Xyl; M, Lyx; N, Fuc; and O, Sor. Regression line was followed Eq. 3. Values and error bars are average and standard deviation of three independent experiments.

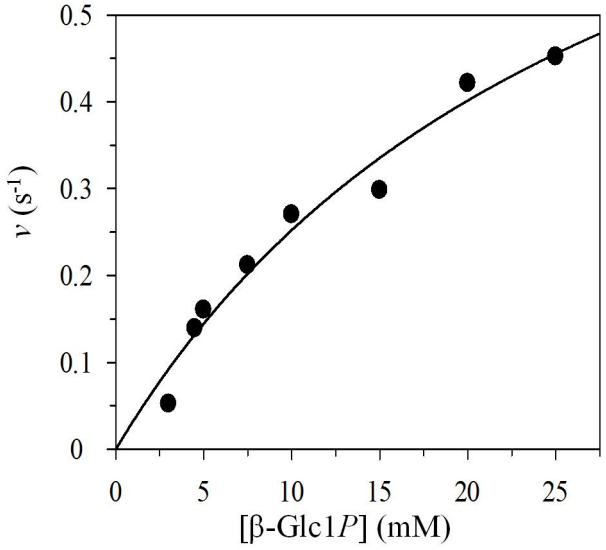

Fig. 11. Kinetic analysis of hydrolysis of β-Glc1*P*.

The s-*v* plots for the hydrolysis of β-Glc1*P* are shown. Values and error bars are average and standard deviation of three independent experiments. Regression line was followed Eq.4.

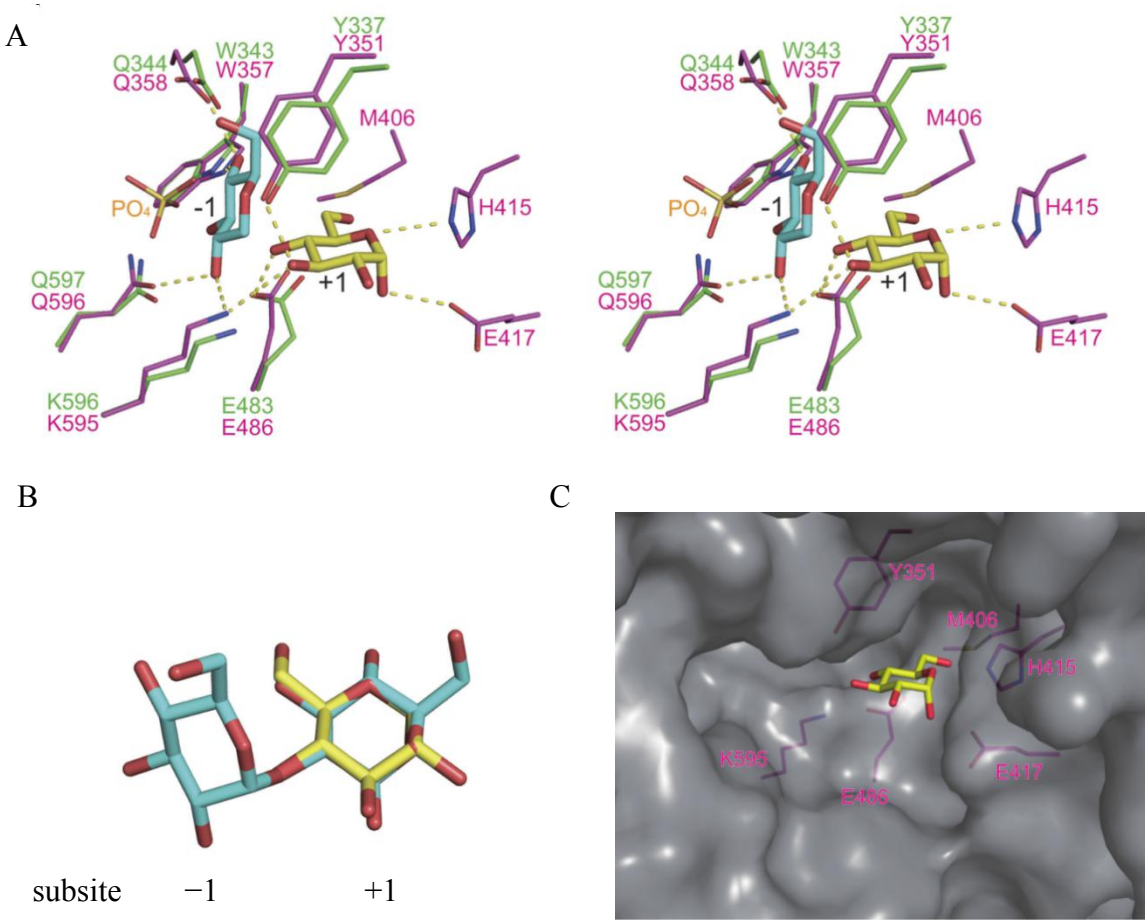

Fig. 12. Predicted substrate binding structure of MalE.

A, Superimposition of model structure of MalE (magenta) and *C. saccharolyticus* KP (PDB entry, 3WIQ; green). The modeled structure of MalE was constructed using structure of LbMP as template. Glc residue bound to subsite -1 of the KP is shown in cyan. α-Glc (PDB entry, AGC), shown in yellow, is superimposed onto Glc residue of Koj in subsite +1 (this Glc residue is not shown in this panel). Dotted line indicates predicted hydrogen bonds. B, Superimposition of α-Glc (yellow) and the reducing end Glc residue of Koj. C, Surface model of MalE. α-Glc bound to subsite +1 is shown in the yellow stick representation. The amino acid residues forming subsite +1 are shown in magenta.

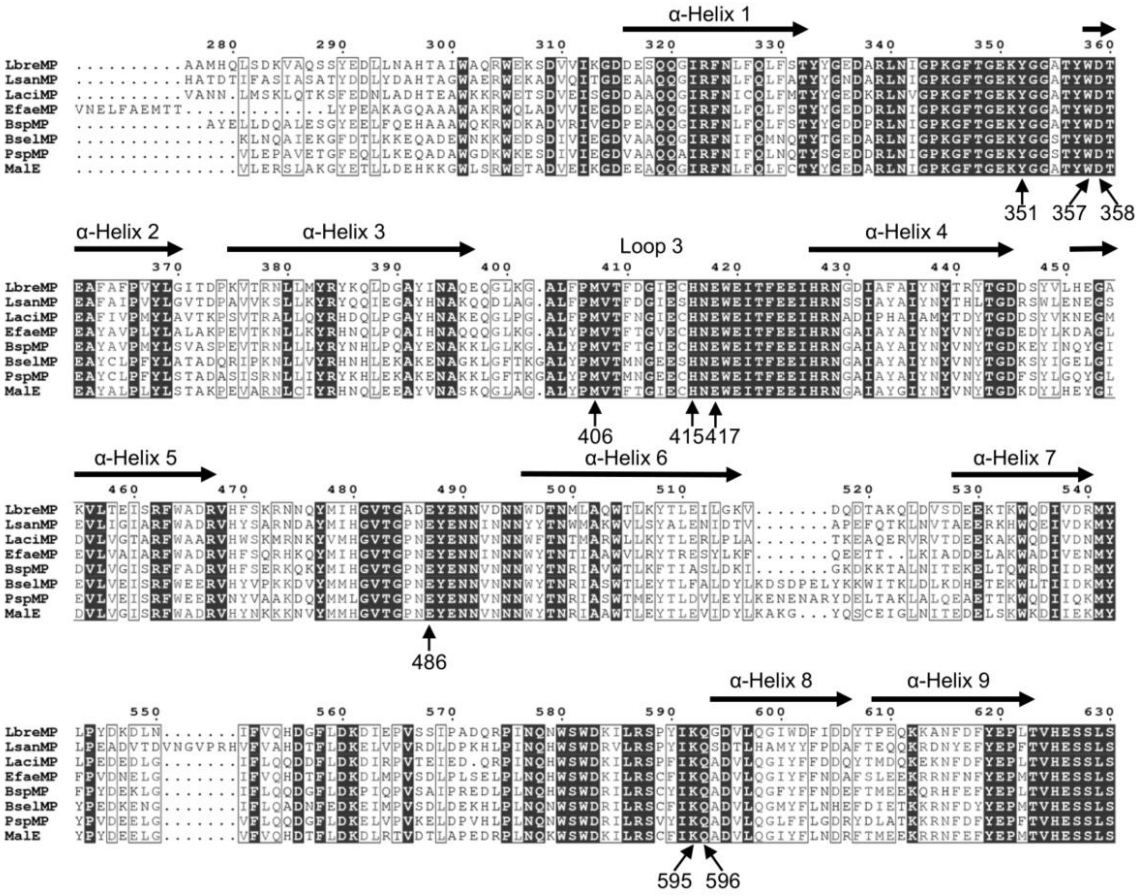

Fig. 13. Comparison of amino acid sequences of MPs.

Multiple-alignment was conducted by Clustal W program [64]. LbreMP, *Lactobacillus brevis* MP (Uniprot number, Q7SIE1); LsanMP, *Lactobacillus sanfranciscensis* MP (GenBank number, CAA11905.1); LaciMP, *Lactobacillus acidophilus* MP (GenBank number, AAV43670.1); EfaeMP, *Enterococcus faecalis* MP (GenBank number, AAO80764.1); BspMP, *Bacillus* sp. RK-1 MP (GenBank number, BAC54904.1); BselMP, *Bacillus selenitireducens* MP (GenBank number, ADH99560.1); PspMP, *Paenibacillus* sp. SH-55 MP (GenBank number, BAD97810.1). Numbers above the figure show the number of amino acid residue of LbreMP. Completely conserved residues are shaded in gray. Highly conserved residues (≥75% conservation) are shown in black letters with boxes. Secondary structures are indicated above the figure. Residues of MalE are shown by arrows.

CHAPTER III. Enzymatic synthesis of oligosaccharides and sugar phosphate by MalE

III.1 Introduction

MP can synthesize oligosaccharides efficiently through reverse phosphorolysis. It was reported that *L. acidophilus* MP efficiently produced several α-(1→4)-glucosides, such as α-D-Glc*p*-(1→4)-GlcN, α-D-Glc*p*-(1→4)-GlcNAc, α-D-Glc*p*-(1→4)-Man, α-D-Glc*p*-(1→4)-L-Fuc, and α-D-Glc*p*-(1→4)-Xyl through the reverse phosphorolysis [28, 44]. In addition, Nihira *et al.* reported that *B. selenitireducens* MP (Bsel2056) which is capable of using Koj and sophorose as acceptors, formed trisaccharides, α-D-Glc*p*-(1→4)[α-D-Glc*p*-(1→2)]-D-Glc and α-D-Glc*p*-(1→4)[β-D-Glc*p*-(1→2)]-D-Glc [22], respectively. In chapter II, the biochemical properties of MalE were described in detail. MalE showed activity of the reverse phosphorolysis with various monosaccharide acceptors. In this chapter, the preparation and chemical structures of the synthesized oligosaccharides from eight acceptors (GlcN, 2-deoxyGlc, Man, GlcNAc, All, Xyl, Lyx, and Sor) through the reverse phosphorolysis of MalE are described. In addition, their digestibility by rat intestinal enzyme investigation is mentioned. Furthermore, sugar phosphates, β-Glc1*P* and glucose 6-phosphate (Glc6*P*), were efficiently synthesized in the presence of yeast.

III.2 Materials and methods

III.2.1 Preparation of oligosaccharides produced by the reverse phosphorolysis of MalE

A reaction mixture (1 or 50 mL), containing 8.81−145 μg/mL MalE, 0.1 M β-Glc1*P*, 0.1 M acceptor (GlcN, 2-deoxyGlc, Man, GlcNAc, All, Xyl, Lyx, or Sor),

and 0.1 M HEPES-NaOH buffer (pH 8.0), was incubated at 37°C for 5−72 h, then the reaction was stopped by heating the samples at 90°C for 5 min. For the reaction with All, 2-deoxyGlc, Lyx, and Sor, 0.1 M $MgAc_2$ (Nacalai Tesque) and 0.1 M NH_4Ac (Wako Pure Chemical Industries) were added, and the insoluble $NH_4MgPO_4 \cdot 6H_2O$ was removed by centrifugation after the reaction. The synthesized oligosaccharides were purified by gel-filtration column chromatography using Bio-Gel P2 [Bio-Rad; 1.6 cm i.d. × (60 cm + 60 cm + 100 cm)], and lyophilized by using vacuum freeze dryer (FDU-1200, EYELA, Tokyo, Japan).

III.2.2 Structural analysis of synthesized products

The molecular mass of the products was measured by electrospray ionization mass spectrometry (ESI-MS) using an Exactive mass spectrometer (Thermo Scientific). The sample was applied to the mass spectrometer by flow injection. Methanol was used as the mobile phase solvent. The positive ion was detected under the following conditions: spray voltage, 3.00 kV; capillary temperature, 300°C. NMR spectra were recorded in D_2O (99.9%, Sigma) at 27°C using a Bruker AMX500 (500 MHz; Bruker Corporation, Billerica, USA). A series of two-dimensional homo- and heteronuclear correlated spectra [correlated spectroscopy, heteronuclear single quantum correlation (HSQC) spectroscopy, HSQC total correlation spectroscopy, heteronuclear 2 bond correlation spectroscopy, and heteronuclear multiple bond correlation spectroscopy (HMBC)] were acquired to determine the chemical structure of the reaction products.

III.2.3 Digestion of the synthesized oligosaccharides using rat intestinal α-glucosidases

The digestion rate of the oligosaccharides obtained from GlcN, 2-deoxyGlc, Man, GlcNAc, All, Xyl, Lyx, and Sor through the reverse phosphorolysis was compared with that of Mal. As the α-glucosidase solution, 13 mg of rat intestine acetone powder (Sigma) was suspended in 0.26 mL of 10 mM sodium phosphate buffer (pH 6.5, 4°C), and the supernatant was collected by centrifugation (13,000 ×g, 4°C, 5 min). A reaction mixture (50 μL), containing α-glucosidase, 10 mM glucoside,

and 40 mM sodium phosphate buffer (pH 6.5), was incubated at 37°C for 10 min. The reaction was terminated by adding 100 μL of 2 M Tris-HCl buffer (pH 7.0), and the released Glc was measured as described in section II.2.8.

III.2.4 Enzymatic synthesis of β-Glc1*P*

Enzymatic synthesis of β-Glc1*P* from Mal by MalE was performed in the presence of yeast, which consumes Glc generated from Mal through the phosphorolysis. A reaction mixture (1 mL), containing 0.1 M Mal, 0.4 M phosphate buffer (pH 7.0), 0.02 U/mL MalE, and 5 mg/mL dried bakery yeast (Nisshin Seifun Group, Tokyo, Japan), was incubated at 30°C for 72 h. Produced β-Glc1*P* was measured as described in section II.2.7. The production amount of β-Glc1*P* was compared with the reaction without yeast.

III.2.5 Enzymatic synthesis of Glc6*P*

Glc6*P* was produced from Mal by the reactions of MalE and β-PGM. A reaction mixture (1 mL), containing 0.1 M Mal, 0.1 M phosphate buffer (pH 7.0), 1.5 U/ml MalE, 5 U/mL β-PGM (Sigma), 2 mM $MgCl_2$ (Wako Pure Chemical Industries), 0.5 μM Glc1,6-bisphosphate (Sigma), and 5 mg/mL bakery yeast was incubated at 30°C for 96 h. Produced Glc6*P* was quantified according to Levy and Daouk [65]. Thio-NAD^+ was used instead of nicotinamide adenine dinucleotide phosphate ($NADP^+$). The production amount of Glc6*P* was compared with the reaction without yeast.

III.3 Results

III.3.1 Synthesis of oligosaccharides through reverse phosphorolysis

In the reaction with Man, GlcN, GlcNAc, and Xyl (starting substrates: 5 mmol of β-Glc1*P* and acceptor), the obtained amount of the oligosaccharides after the purification was 1.3 mmol (26% yield), 0.66 mmol (13% yield), 2.0 mmol (39%

yield), and 2.4 mmol (49% yield), respectively. The yield of oligosaccharides from 100 μmol of β-Glc1*P* and acceptors (All, Lyx, 2-deoxyGlc, and Sor) was 33 μmol (33% yield), 61 μmol (61% yield), 38 μmol (38% yield), and 76 μmol (76% yield), respectively. The chemical structure of the oligosaccharides prepared was analyzed by ESI-MS and NMR. The molecular mass of the reaction products from Man, GlcN, GlcNAc, All, Xyl, Lyx, 2-deoxyGlc, and Sor was 365 *m*/*z* $[M + Na]^+$ (Fig. 14), 380 *m*/*z* $[M + K]^+$ (Fig. 15), 406 *m*/*z* $[M + Na]^+$ (Fig. 16), 365 *m*/*z* $[M + Na]^+$ (Fig. 17), 335 *m*/*z* $[M + Na]^+$ (Fig. 18), 335 *m*/*z* $[M + Na]^+$ (Fig. 19), 349 *m*/*z* $[M + Na]^+$ (Fig. 20), and 381 *m*/*z* $[M + K]^+$ (Fig. 21), respectively, indicating that all the oligosaccharides were disaccharides. HSQC-spectrum of the synthesized products is shown in Figures 22−29 to summarize the chemical shifts of the products. In HMBC-spectrum, correlation peak between C1 of the non-reducing end Glc residue and H4 of Man, GlcN, GlcNAc, All, Xyl, Lyx residue, and between H1 of a Glc residue and C4 of a Man, GlcN, GlcNAc, All, Xyl, Lyx residue, were observed (Fig. 30−35), indicating that the glucosidic linkages was formed between C1 of the Glc and C4 of Man, GlcN, GlcNAc, All, Xyl, and Lyx. The $J_{H1, H2}$ values of Glc residue of the products from Man, GlcN, GlcNAc, All, Xyl, Lyx were 3.90, 3.85, 3.90, 3.50, 3.85, and 4.00 Hz, respectively, indicating the formation of α-glucosidic linkage. Taken together, the reaction products from Man, GlcN, GlcNAc, All, Xyl, and Lyx were determined to be α-D-Glc*p*-(1→4)-D-Man, α-D-Glc*p*-(1→4)-D-GlcN, α-D-Glc*p*-(1→4)-D-GlcNAc, α-D-Glc*p*-(1→4)-D-All, α-D-Glc*p*-(1→4)-D-Xyl, α-D-Glc*p*-(1→4)-D-Lyx, respectively. Correlation peak between C1 of the non-reducing end Glc residue and H3 of 2-deoxyGlc and Sor residue, and between H1 of the Glc residue and C3 of a 2-deoxyGlc and Sor residue, was observed in the HMBC-spectrum (Fig. 36 and 37). The $J_{H1, H2}$ value of Glc residue was 3.70 and 3.85 Hz. These results indicated that MalE produced α-D-Glc*p*-(1→3)-D-2-deoxyGlc and α-D-Glc*p*-(1→3)-L-Sor from 2-deoxyGlc and Sor, respectively. The chemical shifts of ^1H- and ^{13}C- NMR analyses are summarized in Table. 6.

III.3.2 Digestion of the oligosaccharides by rat intestinal α-glucosidase

The disaccharides prepared from 2-deoxyGlc, Man, GlcN, GlcNAc, All, Xyl,

Lyx, and Sor were digested by rat intestinal α-glucosidases. And the Glc-releasing velocity (digestion rate) was compared with that of Mal. The hydrolytic velocities (bond-cleaving velocities) of α-D-Glc*p*-(1→4)-D-Man, α-D-Glc*p*-(1→4)-D-GlcN, α-D-Glc*p*-(1→4)-D-GlcNAc, α-D-Glc*p*-(1→4)-D-All, α-D-Glc*p*-(1→4)-D-Xyl, α-D-Glc*p*-(1→4)-D-Lyx, α-D-Glc*p*-(1→3)-D-2-deoxyGlc, and α-D-Glc*p*-(1→3)-L-Sor were 43.8 ± 2.5%, 39.8 ± 2.0%, 40.4 ± 0.3%, 37.9 ± 0.8%, 45.0 ± 0.3%, 39.3 ± 1.2%, 28.1 ± 0.9%, and 28.0 ± 0.7% of that of Mal, respectively. The tested α-(1→3)-glucosides exhibited even higher tolerance than the others. All compounds showed higher tolerance than Mal, particularly.

III.3.3 Production of β-Glc1*P* and Glc6*P* from maltose

β-Glc1*P* was produced from 0.1 M Mal and 0.4 M Pi in the presence and absence of bakery yeast (Fig. 38). In the reaction without bakery yeast, β-Glc1*P* concentration of the reaction mixture reached plateau at reaction 24 h, and the yield of β-Glc1*P* was 47% at 72 h reaction. The yield is calculated from the ratio of β-Glc1*P* concentration to the starting Mal concentration. Addition of bakery yeast to the reaction mixture reduced the concentration of Glc, which was produced through the phosphorolysis of Mal, and enhanced the production of β-Glc1*P*. Production yield of the reaction with bakery yeast reached 62% at 72 h reaction.

Glc6*P* was produced from 0.1 M Mal and 0.1 M phosphate buffer (pH 7.0) by the coupling reaction of MalE and β-PGM. The production of Glc6*P* in the presence and absence of bakery yeast reached the maximum at 48 h reaction, and the yields of Glc6*P* were 80% (with bakery yeast) and 68% (without bakery yeast). The yield is calculated from the ratio of produced Glc6*P* concentration to the starting Mal concentration. Glc6*P* concentration slightly decreased in the reaction with bakery yeast, whereas the concentration was not changed in the reaction without bakery yeast (Fig. 39).

III.4 Discussion

In this chapter, eight oligosaccharides were synthesized through reverse

phosphorolysis, the chemical structures were analyzed as the α-(1→4)-glucosides from Man, GlcN, GlcNAc, All, Xyl and Lyx. Although some MPs are reported to glucosylate 2-deoxyGlc [22, 35], the structure of the reaction product has not yet been determined. Structural analysis of the product from 2-deoxyGlc revealed that α-(1→3)-glucoside was synthesized. This suggested that 2-deoxyGlc in $^{3}C_{O}$ may bind to subsite +1 upside down, and 3-OH group serves as the nucleophile during the reverse phosphorolysis (Fig. 40). MalE exhibited weak but apparent reverse phosphorolysis activity to a ketose, Sor, and catalyzed the formation of α-(1→3)-glucoside, indicating that 3-O of Sor, acted as the nucleophile in the reverse phosphorolysis. As 1-C, 1-O, 2-C, 3-C, 3-O, 4-C, 4-O, 5-C, 5-O, 6-C and 6-O of α-L-sorbopyranose could be located at positions similar to 6-C, 6-O, 5-C, 4-C, 4-O, 3-C, 3-O, 2-C, 2-O, 1-C, and 5-O of Glc, respectively, α-L-sorbopyranose presumably served as the acceptor in this reaction (Fig. 40).

The digestibility of α-D-Glc*p*-(1→4)-D-Man, α-D-Glc*p*-(1→4)-D-GlcN, α-D-Glc*p*-(1→4)-D-GlcNAc, α-D-Glc*p*-(1→4)-D-All, α-D-Glc*p*-(1→4)-D-Xyl, α-D-Glc*p*-(1→4)-D-Lyx, α-D-Glc*p*-(1→3)-D-2-deoxyGlc, and α-D-Glc*p*-(1→3)-L-Sor by rat intestinal α-glucosidase were less digestible compared to Mal. This indicated that these oligosaccharides could reach large intestine. It has been reported that α-D-Glc*p*-(1→4)-D-GlcN, α-D-Glc*p*-(1→4)-D-GlcNAc, α-D-Glc*p*-(1→4)-D-Xyl promoted the growth of *B. animalis* and *B. longum*, which were involved in enhancing gut health and prevent gastrointestinal infections in humans [45]. The other synthesized α-(1→4)-glucosides: α-D-Glc*p*-(1→4)-D-Man, α-D-Glc*p*-(1→4)-D-All, and α-D-Glc*p*-(1→4)-D-Lyx, may play an important role in prebiotic oligosaccharides. As α-D-Glc*p*-(1→3)-D-2-deoxyGlc and α-D-Glc*p*-(1→3)-L-Sor exhibited higher tolerance against the α-glucosidase than the α-(1→4)-glucosides, they might also act as prebiotic oligosaccharides.

β-Glc1*P* is the donor when synthesizes various of reverse phosphorolysis using inverting α-glucoside phosphorylases including MPs. As an efficient Glc donor, currently β-Glc1*P* is very costly. Previously, Van der Borght *et al.* provided a production method of β-Glc1*P* from Tre and phosphate using the recombinant

thermostable TP from *Theroanaerobacter brockii* at 60°C. They achieved maximum 26% yield of conversion, which is 52 mM β-Glc1*P* from 200 mM Tre and Pi [66]. In order to produce more β-Glc1*P* from phosphorolysis of Mal using MalE, adding bakery yeast to consume Glc generated by the phosphorolysis of Mal into reaction mixture, were performed. In consideration of good condition for fermentation of bakery yeast [67, 68], the reaction mixture was incubated at 30°C at pH 7.0. The yield of β-Glc1*P* reached to 62 % in the presence of bakery yeast at 72 h. After 72 h, since Glc was consumed up by bakery yeast, concentration of β-Glc1*P* was not increased, indicating optimal time was 72 h in the presence of bakery yeast. Meanwhile, β-Glc1*P* concentration was stable at about 46 mM after 48 h without bakery yeast. Obviously, adding bakery yeast to the mixture can promote yield of β-Glc1*P*, but yield only reached to 62% was not high as expected. One reason is that when Glc was consumed by bakery yeast, hydrolysis of β-Glc1*P* might be promoted as well. This makes concentration of β-Glc1*P* decreased, but may be not the main reason due to the velocity of hydrolysis of β-Glc1*P* was very low, which was determined in chapter II. Mal can be fermented by bakery yeast through their inducible system in the membrane, but if the medium contained Glc and Mal, the yeast ferments Glc priorly [69]. In the reaction mixture, bakery yeast grew by utilizing produced Glc firstly. When large amount of bakery yeast grew up and consumed majority of Glc after 48 h, the yeast might start to use Mal. This may lead to the equilibrium of phosphorolysis decreased and prevented converting to β-Glc1*P* and Glc. In the reaction mixture, bakery yeast grows by utilizing produced Glc. In bacteria, β-Glc1*P* generated by MPs cannot be metabolized directly. β-Glc1*P* is converted into Glc6*P* by the action of β-PGM to facilitate entry into the glycolytic pathway [70-72]. The equilibrium constant of reaction from β-Glc1*P* to Glc6*P* by β-PGM, calculated from [Glc6*P*]/[β-Glc1*P*], was 18.5-28.6 [71, 73, 74], indicating that β-PGM can convert almost completely β-Glc1*P* into Glc6*P*. Glc6*P* could be produced efficiently from Mal by coupling reaction using MalE and β-PGM in the presence of yeast. As the Glc6*P* preparation result showed, Glc6*P* was reached to maximum 80% yield (calculated from [Glc6*P*]/[Mal]) at 48h. The yield is higher than that of preparing by hexokinase (EC 2.7.1.1) from Glc [75] and by

phosphoglucose isomerase (EC 5.3.1.9) from fructose 1,6-disphosphate in mild acid [76], which only reached to 65% and 70%, respectively. In view of yield and cost, producing Glc6*P* from Mal using MalE and β-PGM in addition of bakery yeast it is feasible.

Table. 6. Chemical shifts of oligosaccharides produced through the reverse phosphorolysis in the ^{1}H- and ^{13}C- NMR spectra.

Product	Residue	No.	δ_c (ppm)	δ_H (ppm)	$J_{H,H}$ (Hz)	Residue	No.	δ_c (ppm)	δ_H (ppm)	$J_{H,H}$ (Hz)	Residue	No.	δ_c (ppm)	δ_H (ppm)	$J_{H,H}$ (Hz)
Glcα-4Man	α-Glc	1	102.7	5.35	d 3.90	α-Man	1	96.6	5.19	d 1.80	β-Man	1	96.4	4.92	s
		2	74.6	3.60	dd 3.85, 9.85	(Major)	2	73.8	3.94	m	(Minor)	2	76.4		
		3	75.7	3.71	m		3	73.5	4.11	dd 3.40, 9.10		3	N. D.	N. D.	N. D.
		4	72.1	3.43	t 9.65		4	78.1	3.84	m		4	N. D.	N. D.	N. D.
		5	75.5	3.74	m		5	77.5	3.53	m		5	N. D.	N. D.	N. D.
		6	63.3	3.79	m		6	63.8	3.81	m		6	N. D.	N. D.	N. D.
				3.86	m				3.92	m					
Glcα-4GlcN	α-Glc	1	102.4	5.44	d 3.85	α-GlcN	1	91.9	5.46	d 3.55	β-GlcN	1	95.7	4.95	d 8.45
		2	74.4	3.62	dd 3.90, 10.0	(Major)	2	57.0	3.36	dd 3.60, 10.7	(Minor)	2	59.5	3.05	dd 8.45, 10.6
		3	75.6	3.71	m		3	73.0	4.19	dd 9.05, 10.5		3	N. D.	N. D.	N. D.
		4	72.1	3.45	t 9.75		4	79.1	3.76	m		4	N. D.	N. D.	N. D.
		5	75.5	3.71	m		5	72.9	4.03	m		5	N. D.	N. D.	N. D.
		6	63.3	3.80	m		6	63.2	3.80	m		6	N. D.	N. D.	N. D.
				3.88	m				3.88	m					
Glcα-4GlcNAc	α-Glc	1	102.6	5.43	d 3.90	α-GlcNAc	1	97.6	5.21	d 3.50	β-GlcNAc	1	102.3	4.73	d 8.45
		2	74.5	3.59	m	(Major)	2	56.7	3.93	m	(Minor)	2	59.4	3.93	m
		3	75.6	3.69	m		3	74.0	4.03	dd 8.80, 10.8		3	N. D.	N. D.	N. D.
		4	72.1	3.43	t 9.4		4	80.2	3.72	m		4	N. D.	N. D.	N. D.
		5	75.5	3.73	m		5	72.9	3.97	m		5	N. D.	N. D.	N. D.
		6	63.3	3.77	m		6	63.4	3.80	m		6	63.5	3.93	m
				3.86	m				3.85	m				N. D.	N. D.
Glcα-3(2-deoxy-)Glc	α-Glc	1	100.6	5.19	d, 3.70	α-2-deoxy-	1	92.0	5.35	s	β-2-deoxy-	1	94.1	4.92	d, 8.95
		2	72.4	3.52	m	Glc	2	37.2	1.85	m	Glc	2	39.5	1.65	m
						(Major)			2.25	m	(Minor)			2.40	m
		3	73.7	3.72	m		3	77.5	4.00	m		3	79.6	3.80	m
		4	70.4	3.48	m		4	70.8	3.60	m		4	70.5	3.50	m
		5	72.9	3.73	m		5	72.7	3.82	m		5	76.5	3.42	m
		6	61.3	3.75	m		6	61.4	3.75	m		6	61.7	3.75	m
				3.83	m				3.83	m				3.83	m

N.D., not determined.

Table. 6. Continued.

Product	Residue	No.	δ_c (ppm)	δ_H (ppm)	$J_{H,H}$ (Hz)	Residue	No.	δ_c (ppm)	δ_H (ppm)	$J_{H,H}$ (Hz)	Residue	No.	δ_c (ppm)	δ_H (ppm)	$J_{H,H}$ (Hz)
Glcα-4All	α-Glc	1	95.6	5.14	d, 3.5	β-All	1	94.2	4.94	d, 8.25	α-All	1	N. D.	N. D.	N. D.
		2	71.8	3.59	m	(Major)	2	71.9	3.43	m	(Minor)	2	N. D.	N. D.	N. D.
		3	73.6	3.72	m		3	67.5	4.44	s		3	N. D.	N. D.	N. D.
		4	70.1	3.44	m		4	71.3	3.78	m		4	N. D.	N. D.	N. D.
		5	73.5	3.65	m		5	72.9	3.95	m		5	N. D.	N. D.	N. D.
		6	61.1	3.76	m		6	61.7	3.70	m		6	N. D.	N. D.	N. D.
				3.82	m				3.88	m					
Glcα-4Xyl	α-Glc	1	102.8	5.15	d 3.85	β-Xyl	1	99.2	4.57	d 7.90	α-Xyl	1	94.7	5.18	d 3.65
		2	74.3	3.54	m	(Major)	2	76.5	3.26	t 8.05	(Minor)	2	73.9	3.56	m
		3	75.5	3.70	m		3	77.5	3.65	m		3	74.4	3.85	m
		4	72.2	3.39	t 9.50		4	80.9	3.66	m		4	80.9	3.66	m
		5	75.0	3.66	m		5	67.0	3.44	m		5	62.8	3.80	m
									4.14	dd 4.45, 11.4				3.90	dd 5.65, 11.3
		6	63.3	3.74	m										
				3.84	m										
Glcα-4Lyx	α-Glc	1	100.5	5.10	d, 4.00	β-Lyx	1	94.6	4.96	d, 5.05	α-Lyx	1	94.7	4.85	d, 1.4
		2	72.2	3.52	dd, 3.80, 9.90	(Major)	2	70.8	3.78	m	(Minor)	2	N. D.	N. D.	N. D.
		3	73.6	3.70	m		3	69.6	4.07	m		3	N. D.	N. D.	N. D.
		4	70.3	3.37	m		4	76.6	3.83	m		4	N. D.	N. D.	N. D.
		5	73.0	3.71	m		5	63.2	3.84	m		5	N. D.	N. D.	N. D.
									3.95	m					
		6	61.3	3.74	m										
				3.83	m										
Glcα-3Sor	α-Glc	1	101.5	5.32	d, 3.85	Sor	1	64.4	3.50	d, 11.65					
									3.73	m					
		2	72.7	3.57	dd, 3.90, 9.90		2	98.2							
		3	73.6	3.74	m		3	79.5	3.68	m					
		4	70.1	3.40	t, 9.50		4	75.2	3.88	m					
		5	73.5	3.74	m		5	69.9	3.64	m					
		6	61.2	3.77	m		6	62.4	3.64	m					
				3.83	m				3.74	m					

N.D., not determined.

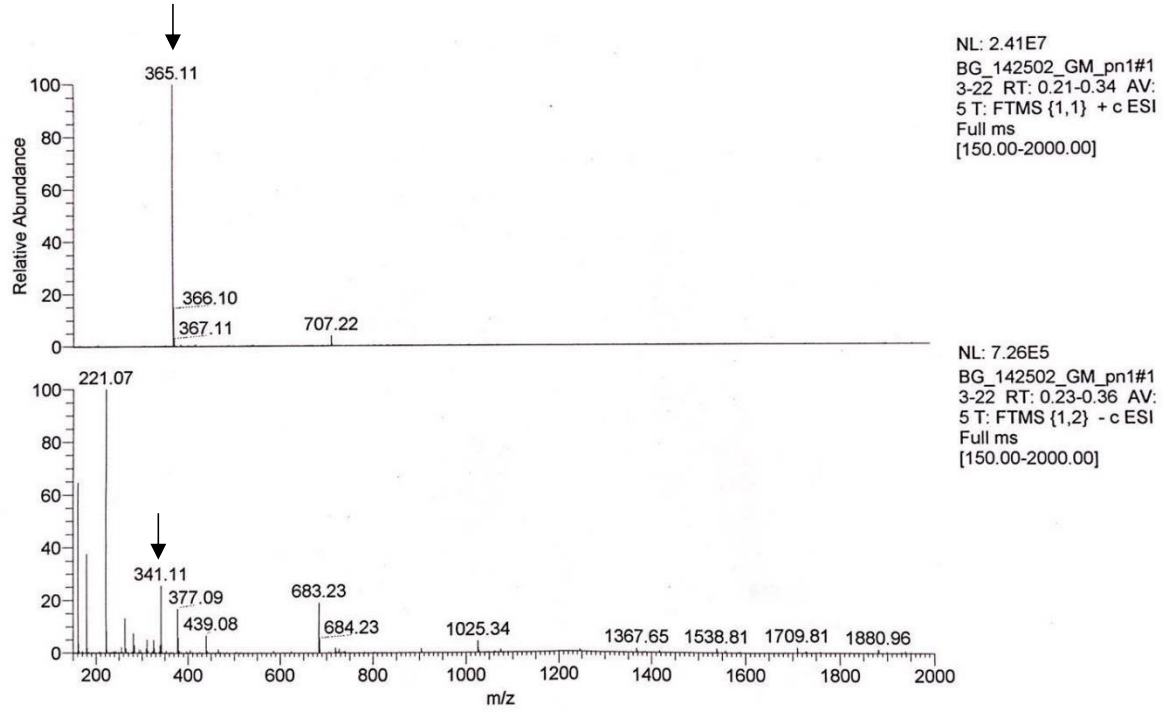

Fig. 14. ESI-MS spectra of synthesized product from Man and β-Glc1*P* by MalE.

The positive and negative mode are shown in upper and lower figures, respectively. The signal ions at 365.11 *m*/*z* $[M + Na]^+$ and 341.11 *m*/*z* $[M - H]^-$ were the positive and negative signal ions of synthesized product, respectively (indicated by arrows).

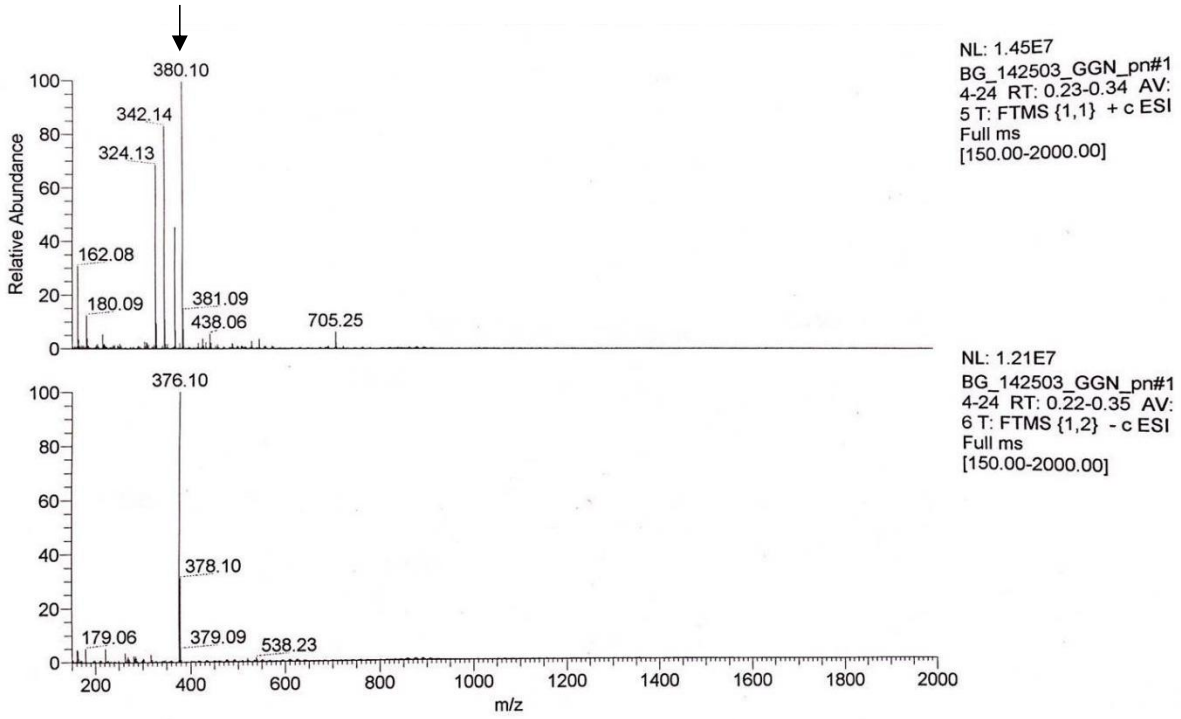

Fig. 15. ESI-MS spectra of synthesized product from GlcN and β-Glc1*P* by MalE.

The positive and negative mode are shown in upper and lower figures, respectively. The signal ions at 380.10 *m/z* $[M + K]^+$ was the positive signal ions of synthesized product (indicated by arrow).

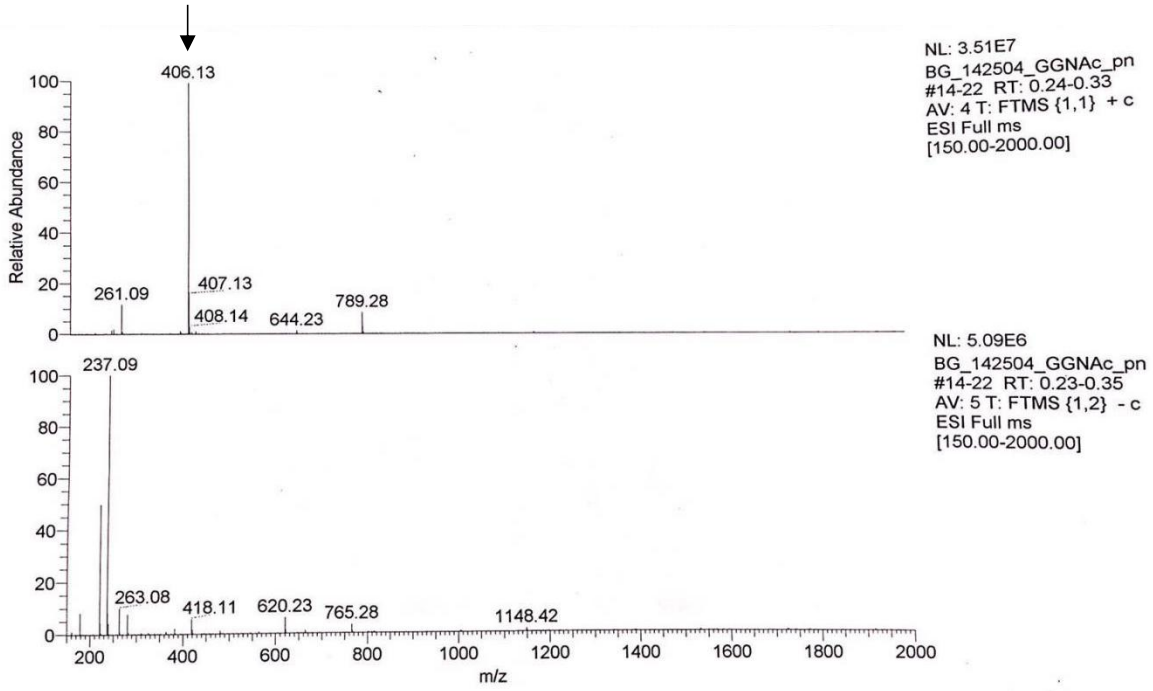

Fig. 16. ESI-MS spectra of synthesized product from GlcNAc and β-Glc1*P* catalyzed by MalE.

The positive and negative mode are shown in upper and lower figures, respectively. The signal ions at 406.13 *m*/*z* $[M + Na]^+$ was the positive signal ions of synthesized product (indicated by arrow).

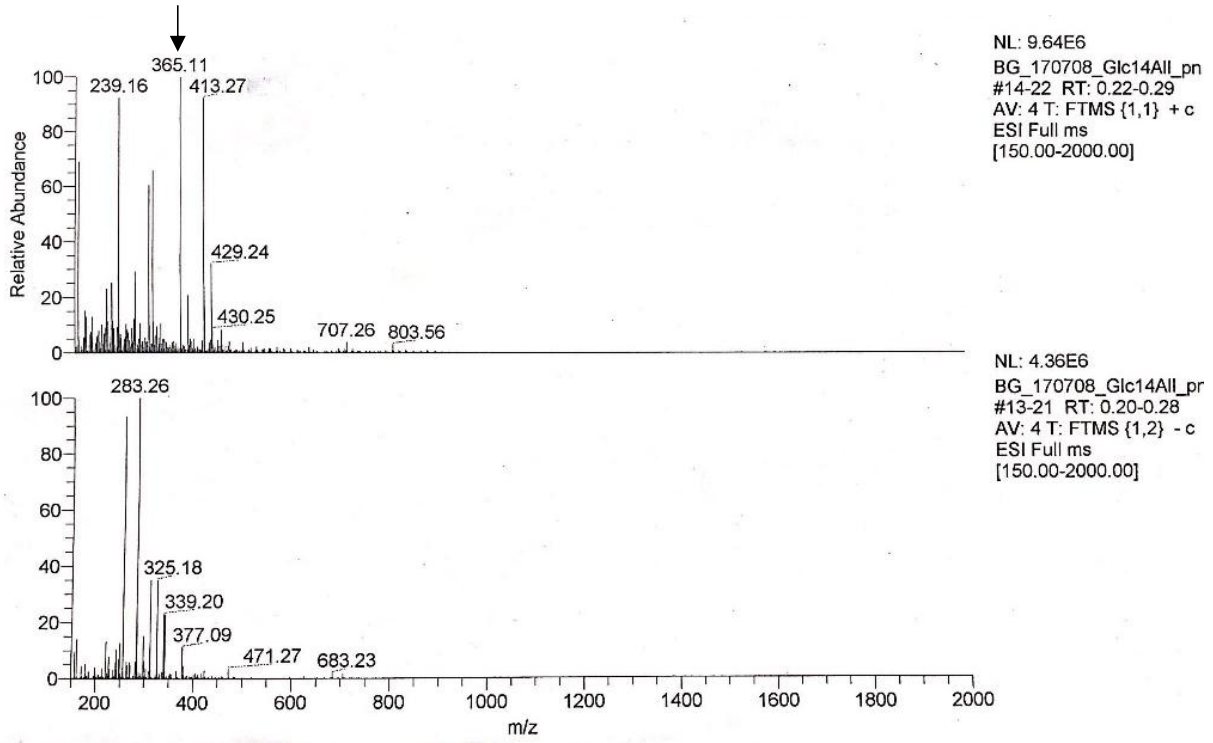

Fig. 17. ESI-MS spectra of synthesized product from All and β-Glc1*P* by MalE.

The positive and negative mode are shown in upper and lower figures, respectively. The signal ions at 365.11 $[M + Na]^+$ *m*/*z* was the positive signal ions of synthesized product (indicated by arrow).

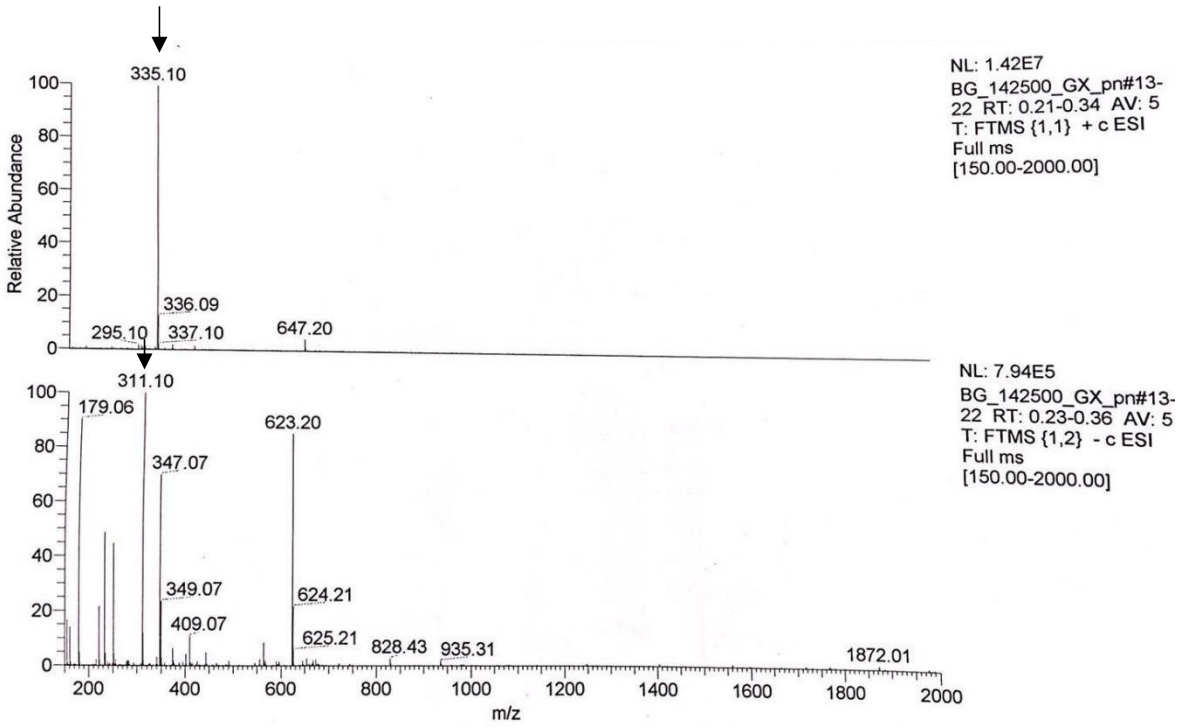

Fig. 18. ESI-MS spectra of synthesized product from Xyl and β-Glc1*P* by MalE.

The positive and negative mode are shown in upper and lower figures, respectively. The signal ions 335.10 *m*/*z* $[M + Na]^+$ and 311.10 *m*/*z* $[M - H]^-$ were the positive and negative signal ions of synthesized product, respectively (indicated by arrows).

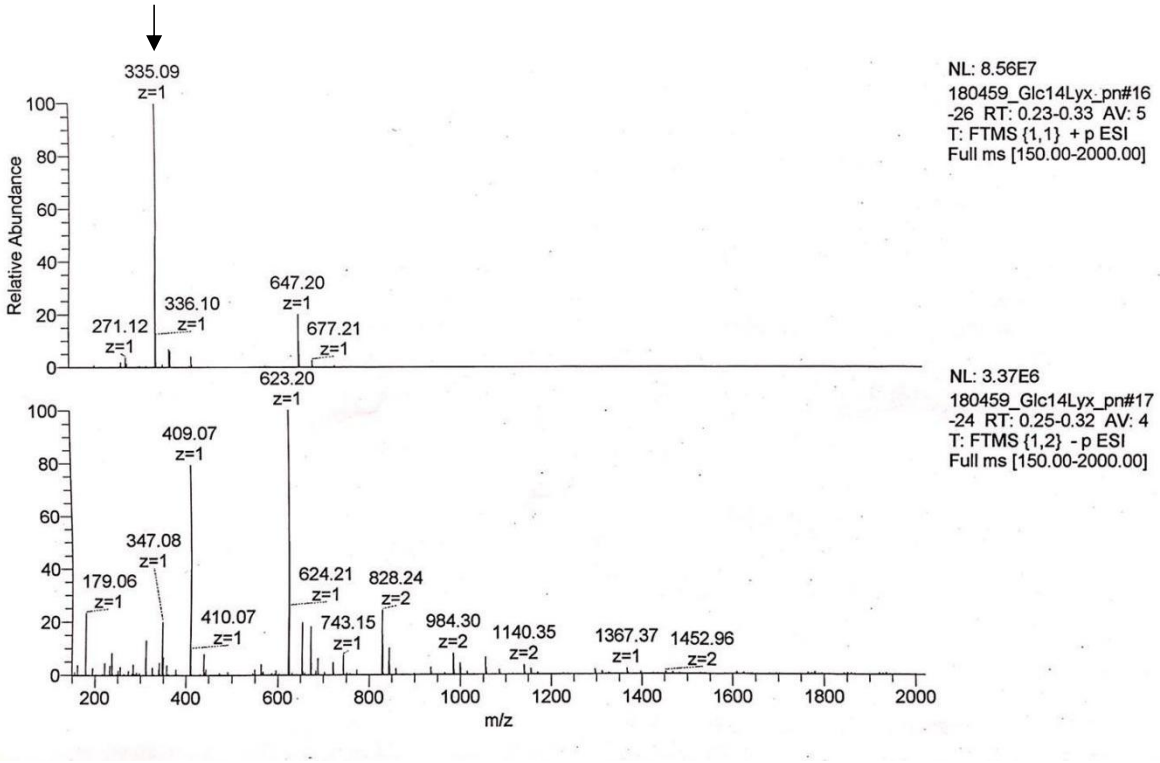

Fig. 19. ESI-MS spectra of synthesized product from Lyx and β-Glc1*P* by MalE.

The positive and negative mode are shown in upper and lower figures, respectively. The signal ions 335.09 $[M + Na]^+$ *m*/*z* was the positive signal ions of synthesized product (indicated by arrow).

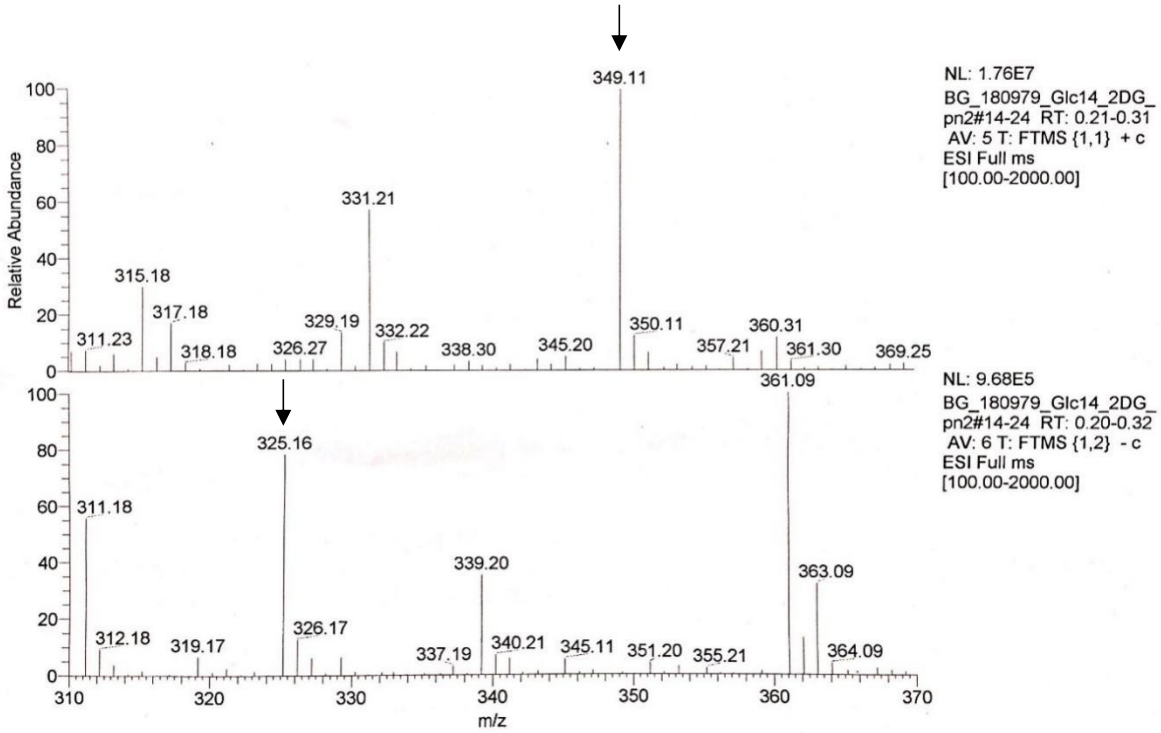

Fig. 20. ESI-MS spectra of synthesized product from 2-deoxyGlc and β-Glc1*P* by MalE.

The positive and negative mode are shown in upper and lower figures, respectively. The signal ions 349.11 *m*/*z* $[M + Na]^+$ and 325.16 *m*/*z* $[M - H]^-$ were the positive and negative signal ions of synthesized product, respectively (indicated by arrows).

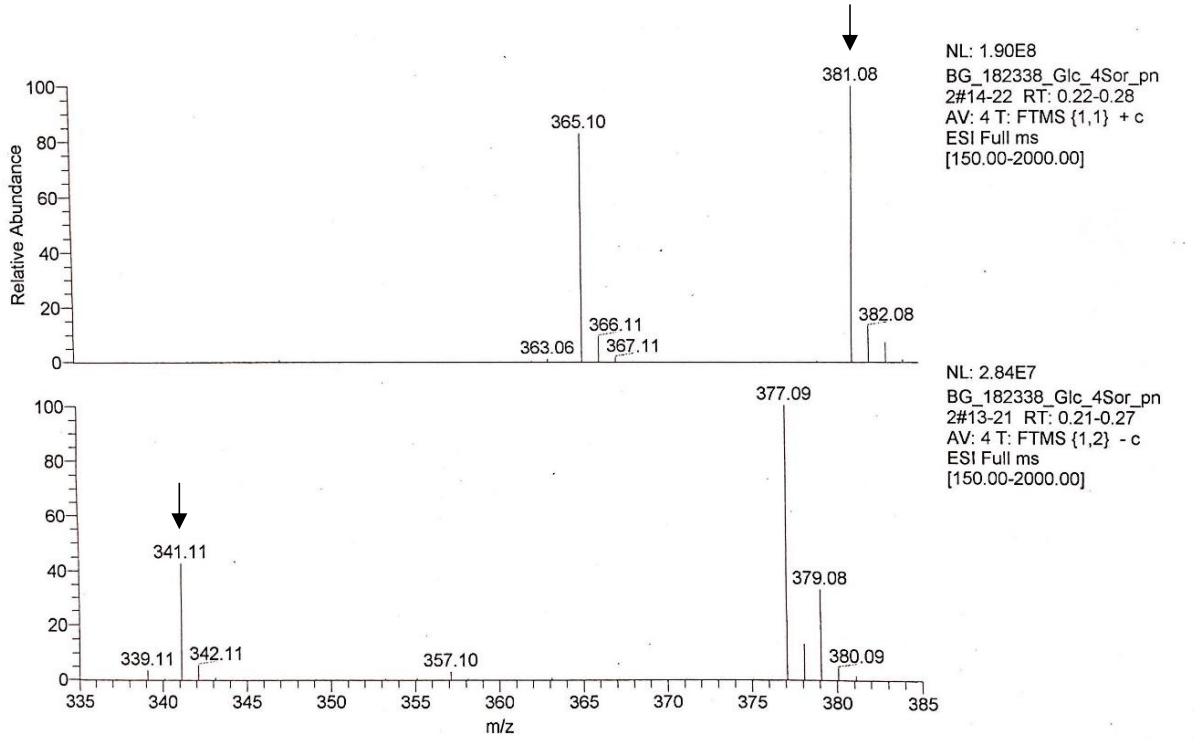

Fig. 21. ESI-MS spectra of synthesized product from Sor and β-Glc1*P* by MalE.

The positive and negative mode are shown in upper and lower figures, respectively. The signal ions 381.08 *m*/*z* $[M + K]^+$ and 341.11 *m*/*z* $[M - H]^-$ were the positive and negative signal ions of synthesized product, respectively (indicated by arrows)..

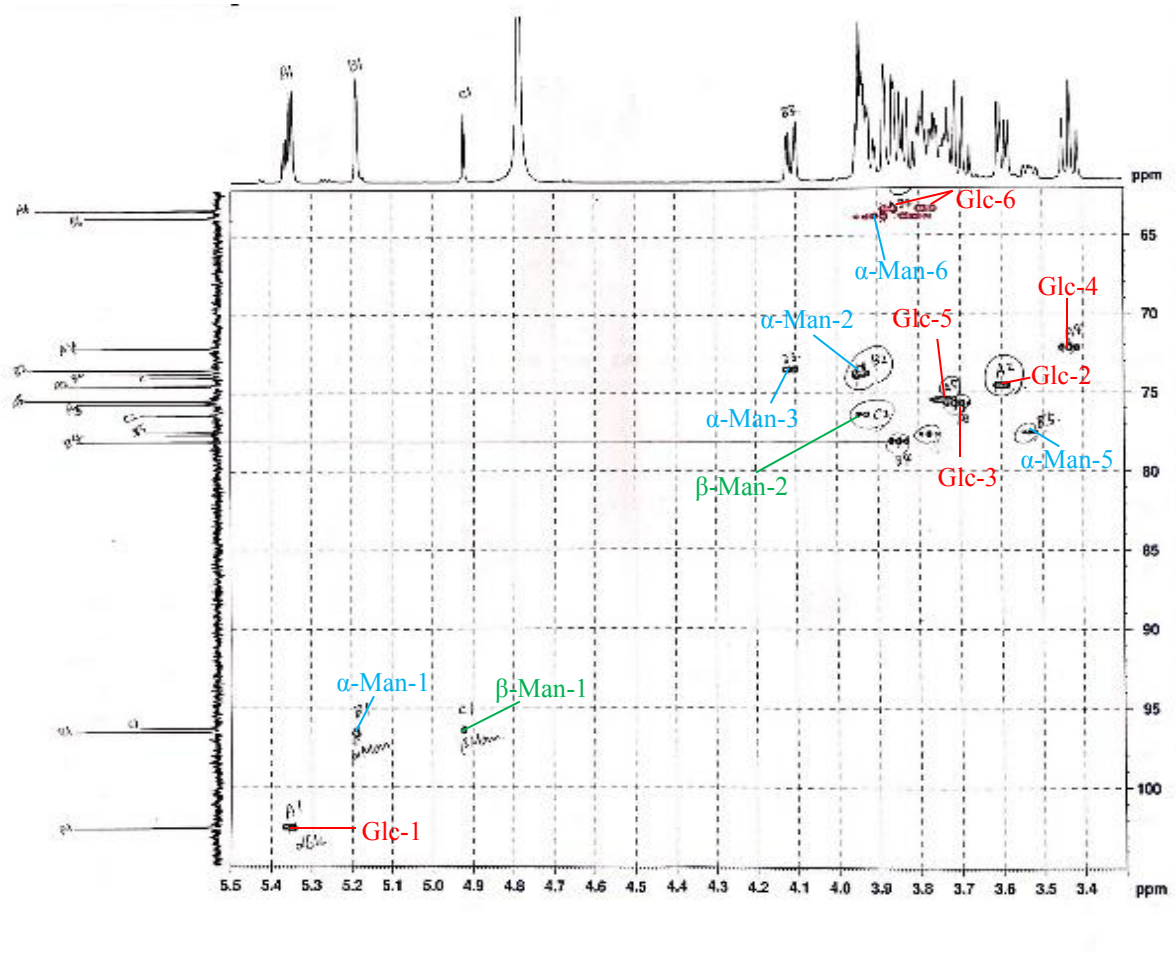

Fig. 22. HSQC-spectrum of synthesized product from Man and β-Glc1*P*.

Each number shown after the residue indicates the number of carbon and proton.

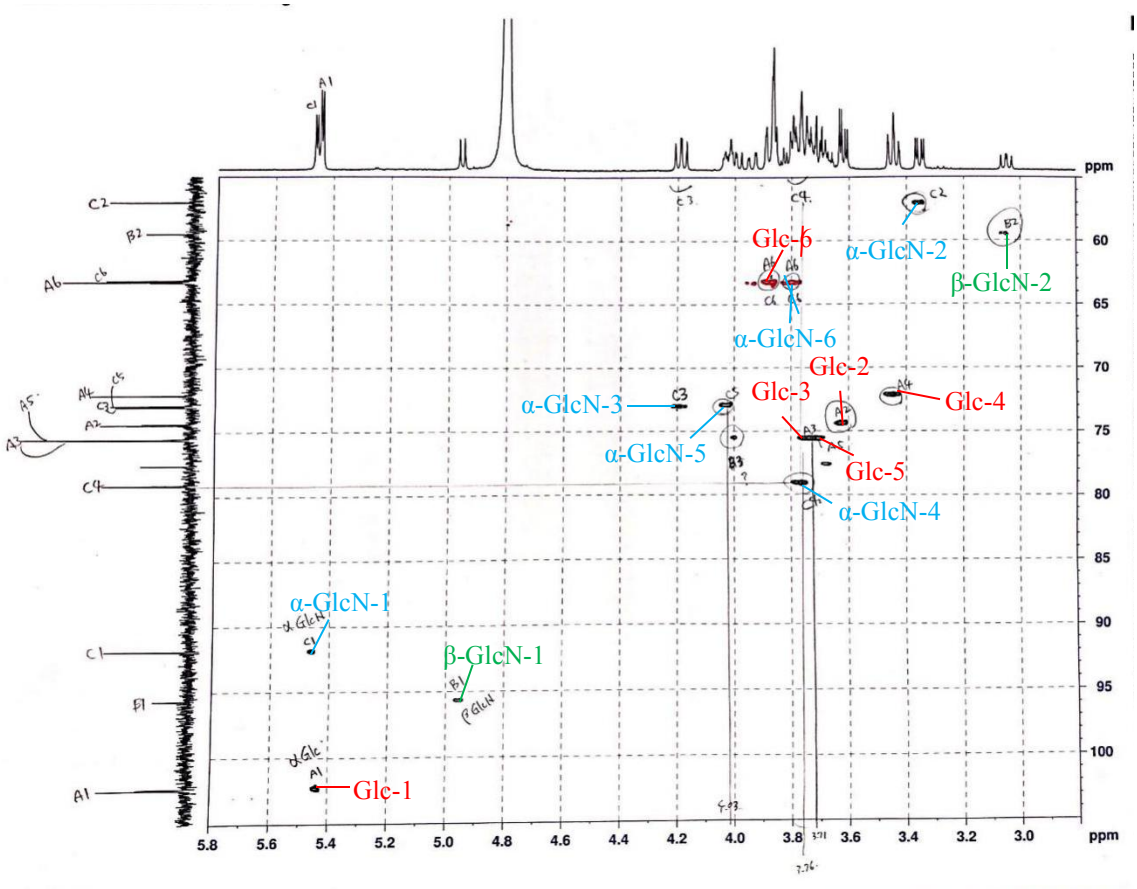

Fig. 23. HSQC-spectrum of synthesized product from GlcN and β-Glc1*P*.

Each number shown after the residue indicates the number of carbon and proton.

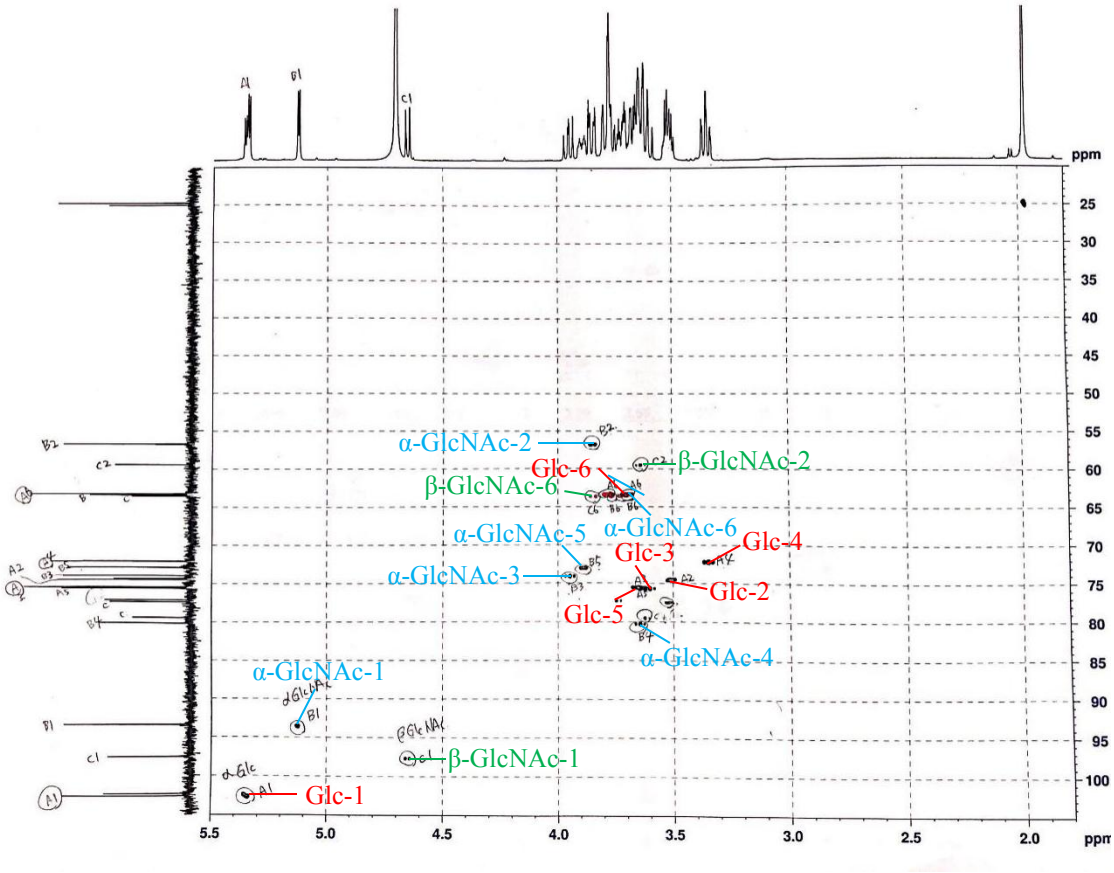

Fig. 24. HSQC-spectrum of synthesized product from GlcNAc and β-Glc1*P*.

Each number shown after the residue indicates the number of carbon and proton.

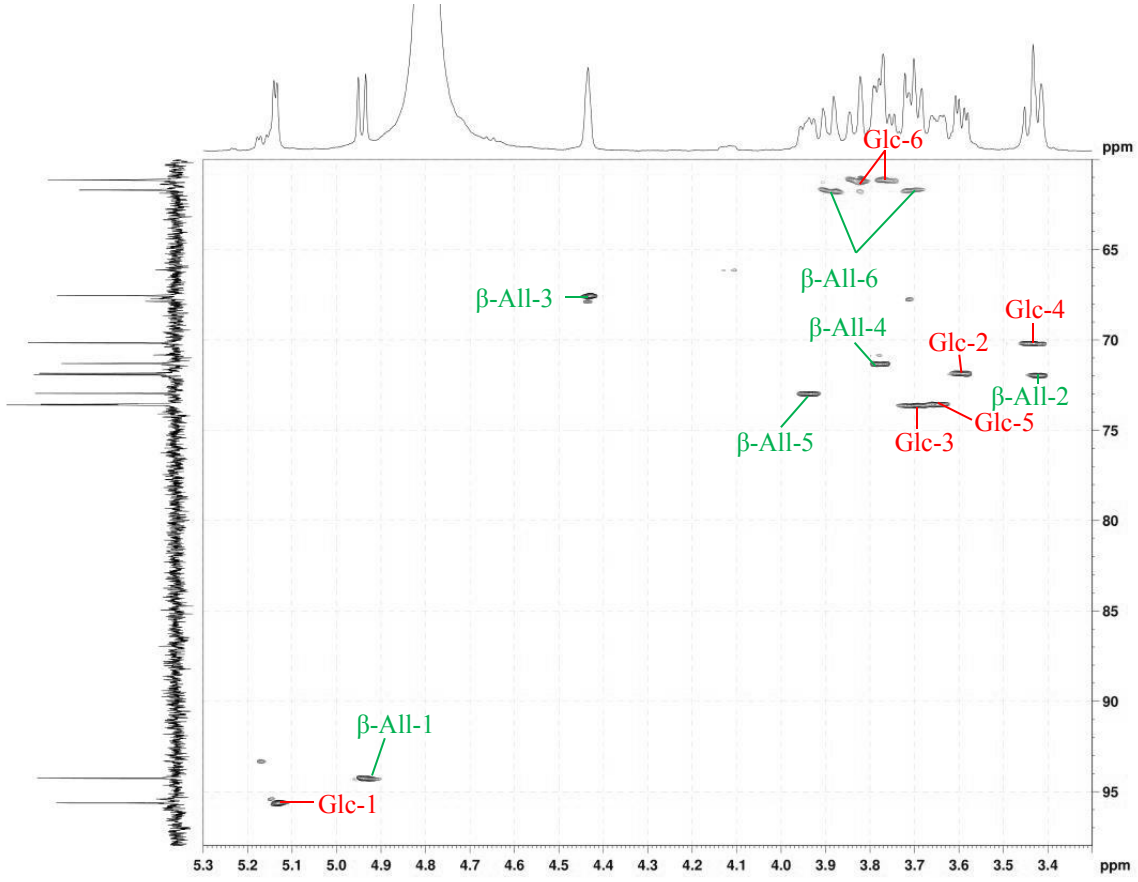

Fig. 25. HSQC-spectrum of synthesized product from All and β-Glc1*P*.

Each number shown after the residue indicates the number of carbon and proton.

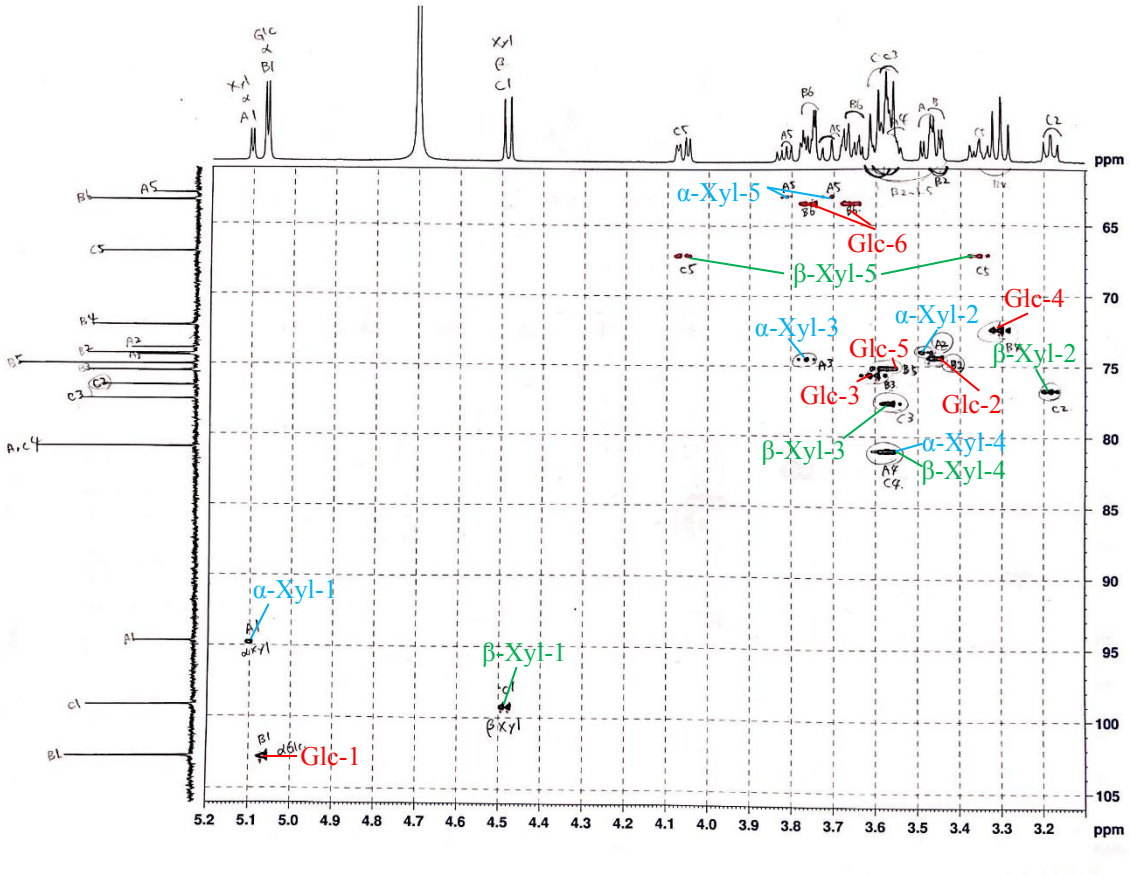

Fig. 26. HSQC-spectrum of synthesized product from Xyl and β-Glc1*P*.

Each number shown after the residue indicates the number of carbon and proton.

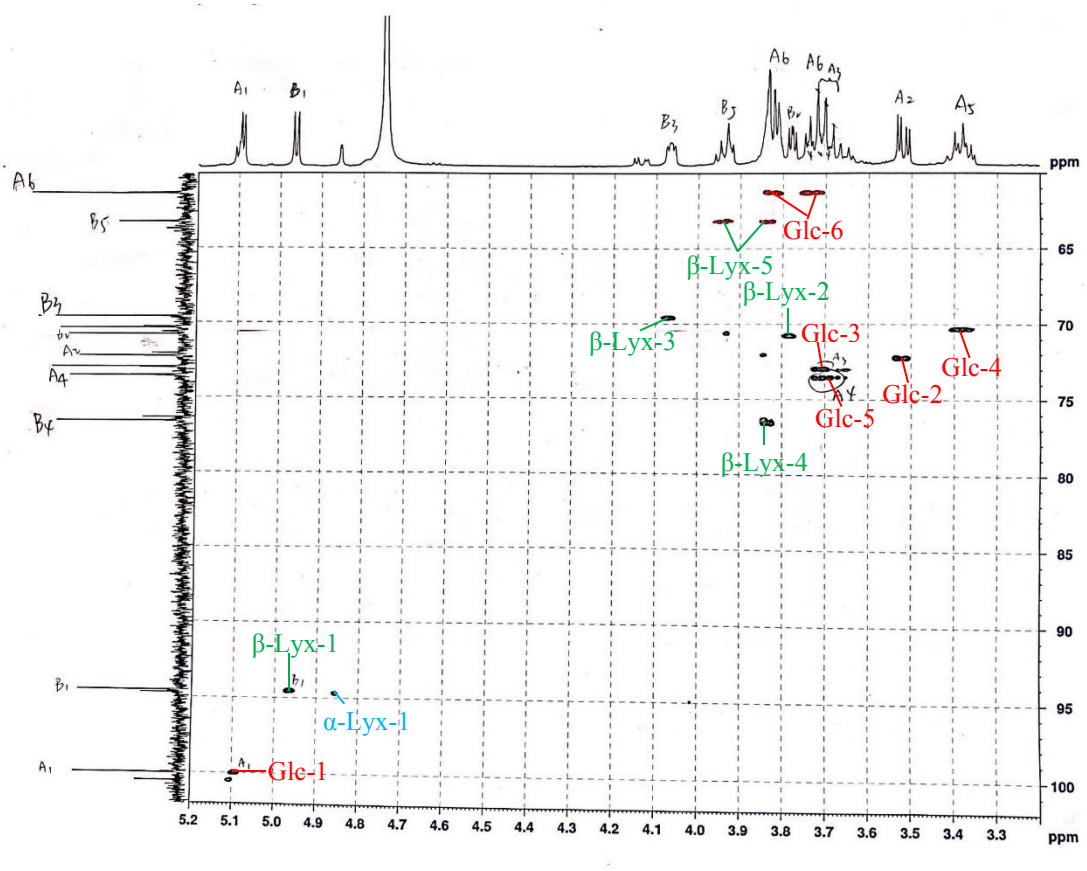

Fig. 27. HSQC-spectrum of synthesized product from Lyx and β-Glc1*P*.

Each number shown after the residue indicates the number of carbon and proton.

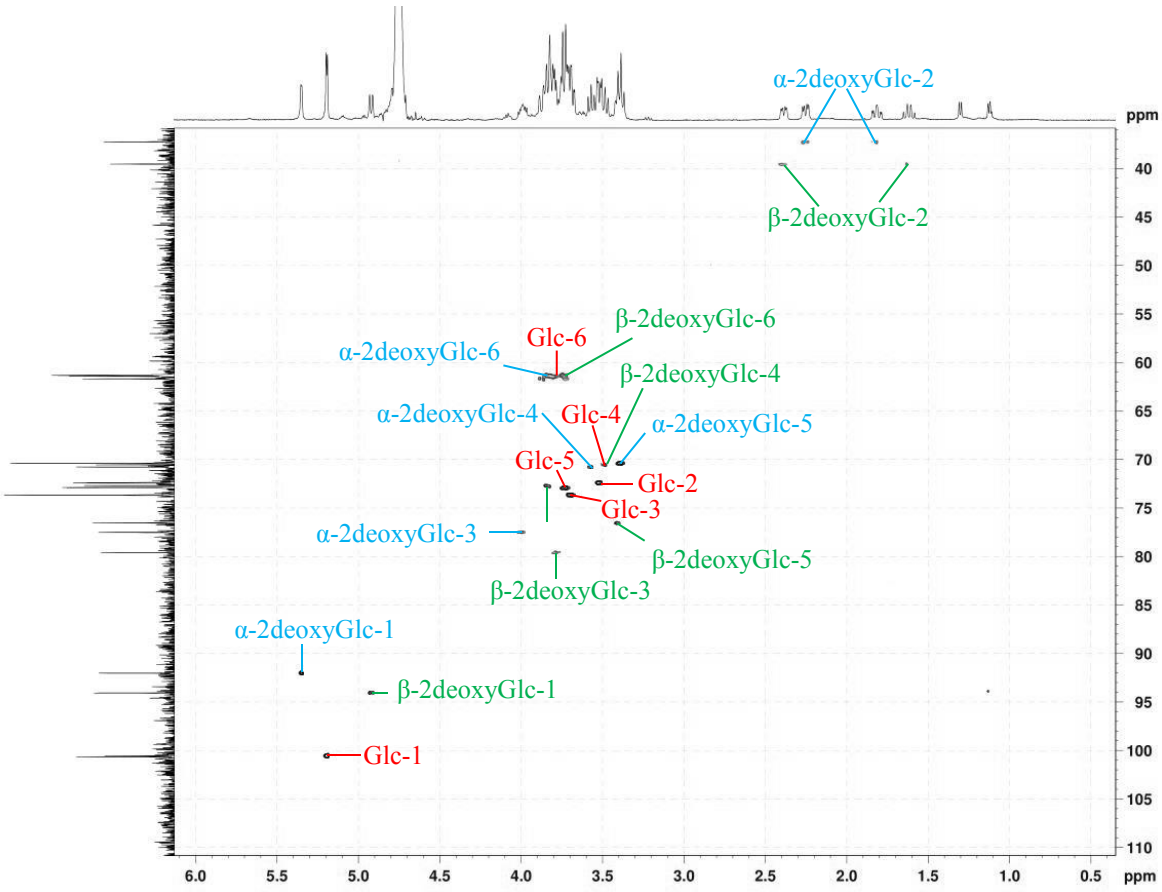

Fig. 28. HSQC-spectrum of synthesized product from 2-deoxyGlc and β-Glc1*P*.

Each number shown after the residue indicates the number of carbon and proton.

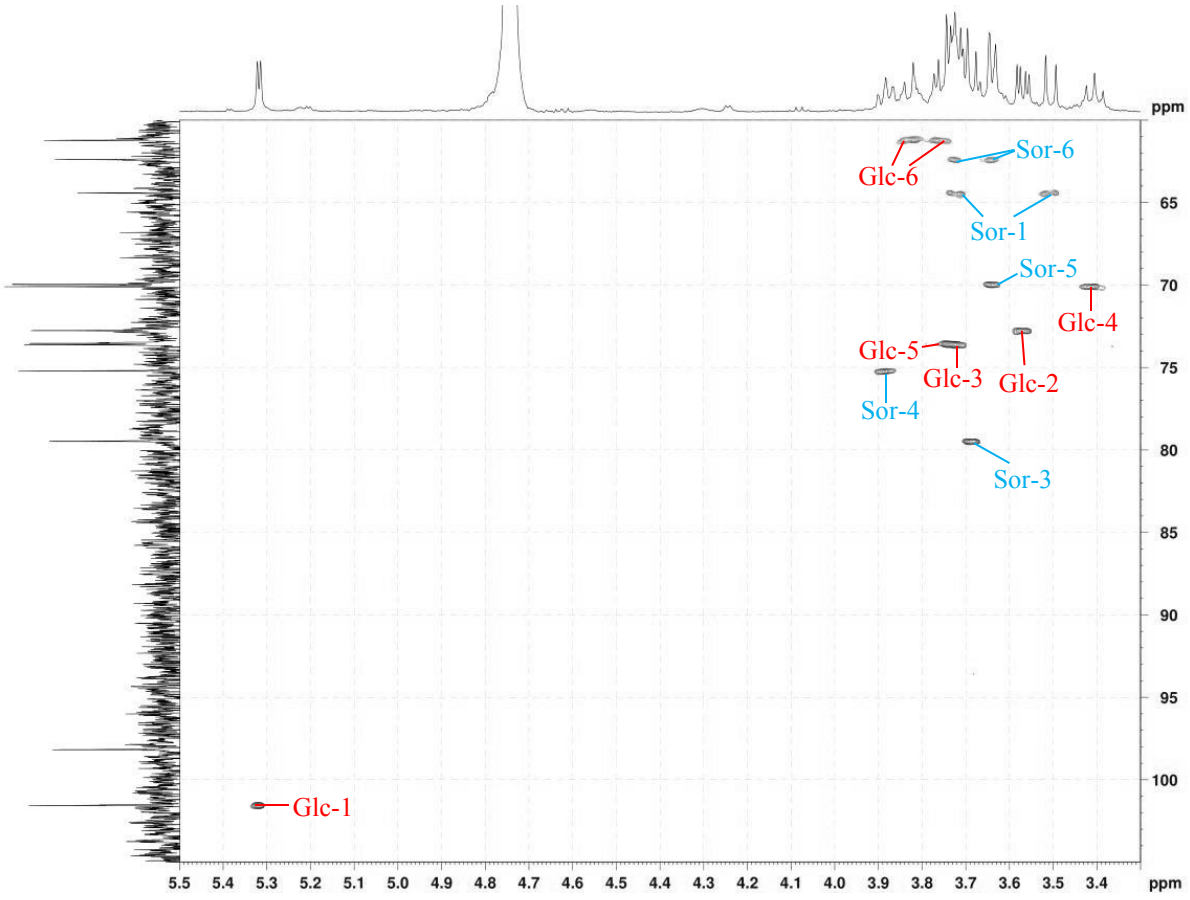

Fig. 29. HSQC-spectrum of synthesized product from Sor and β-Glc1*P*.

Each number shown after the residue indicates the number of carbon and proton.

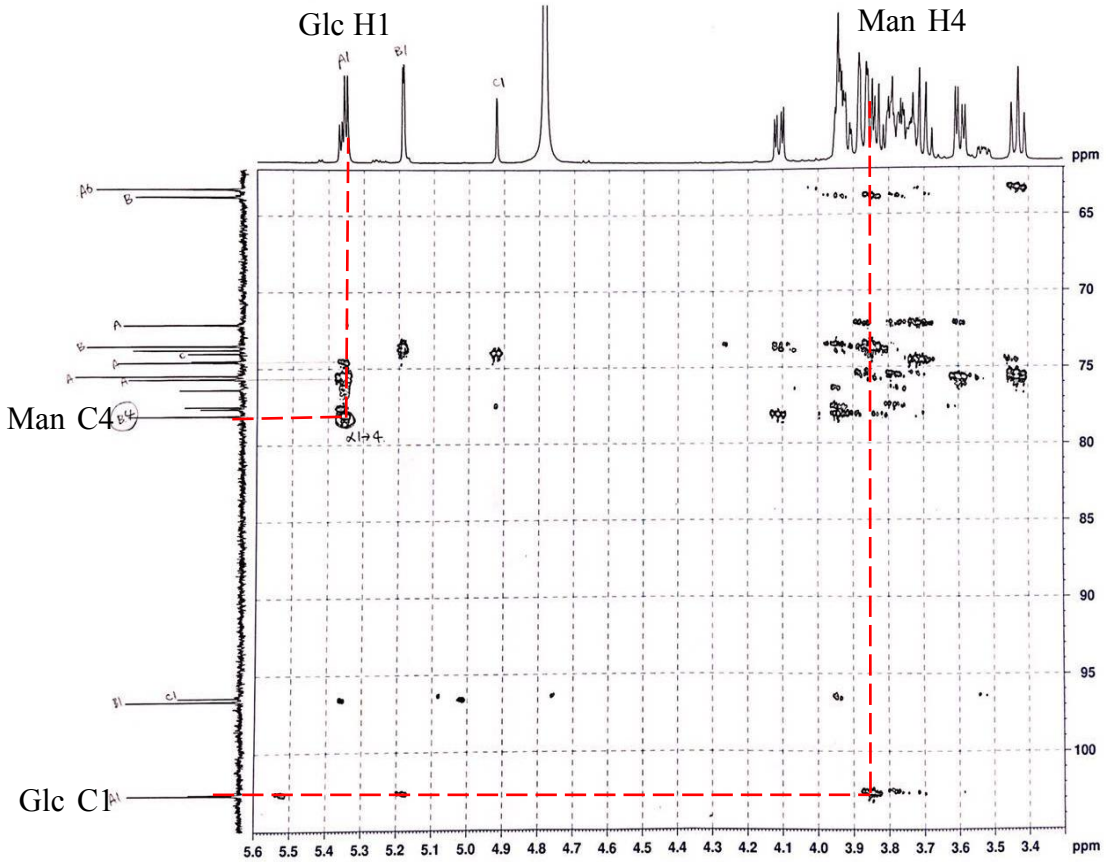

Fig. 30. HMBC spectrum of synthesized product from Man and β-Glc1*P*.

Dotted lines indicate correlations between Glc H1 and Man C4, and between Man H4 and Glc C1.

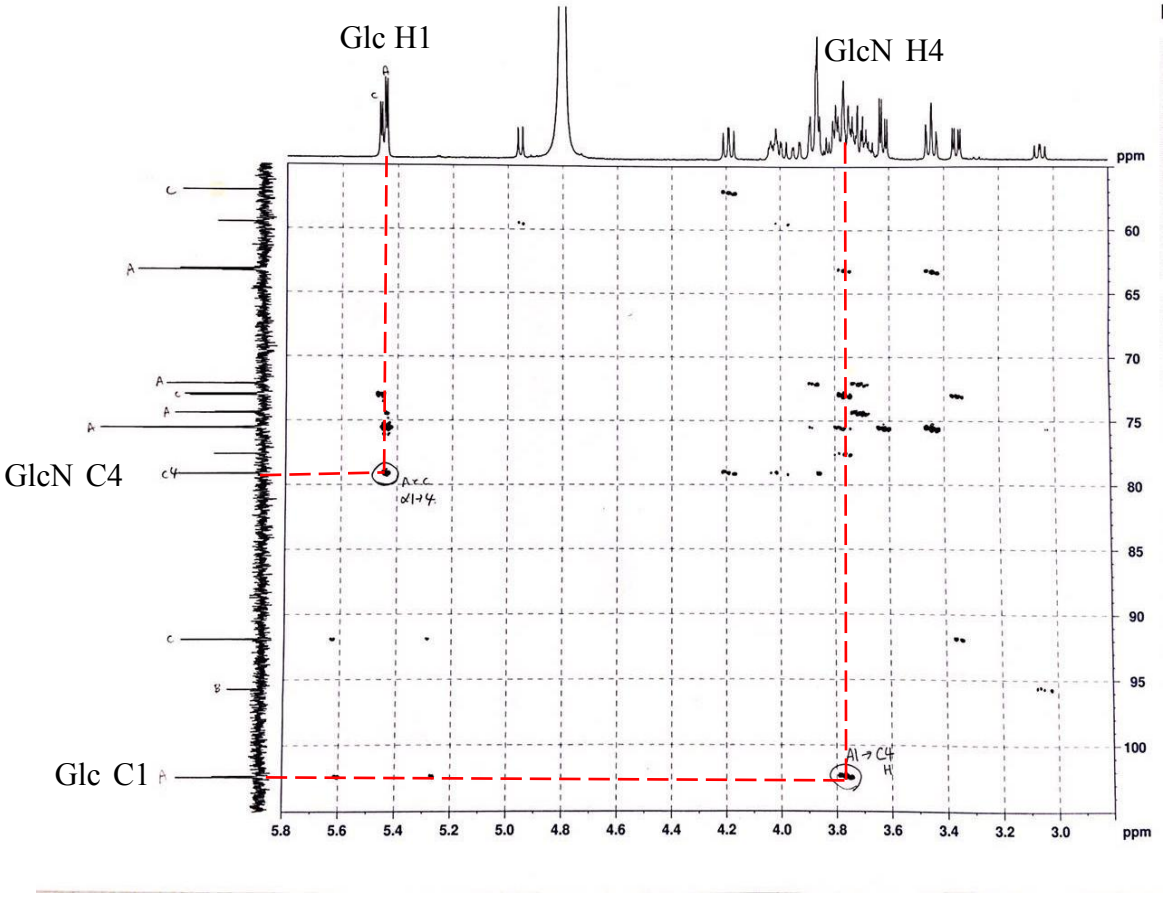

Fig. 31. HMBC spectrum of synthesized product from GlcN and β-Glc1*P*.

Dotted lines indicate correlations between Glc H1 and GlcN C4, and between GlcN H4 and Glc C1.

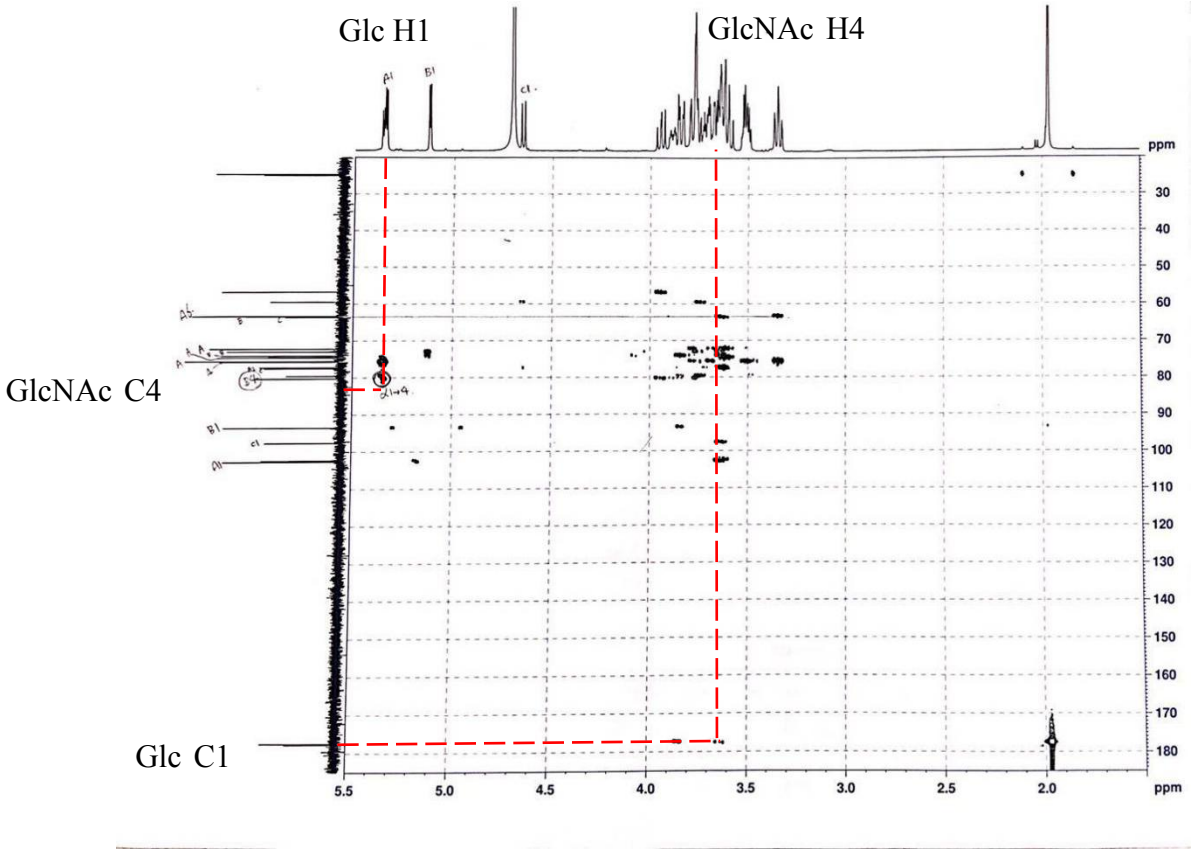

Fig. 32. HMBC spectrum of synthesized product from GlcNAc and β-Glc1*P*.
Dotted lines indicate correlations between Glc H1 and GlcNAc C4, and between GlcNAc H4 and Glc C1.

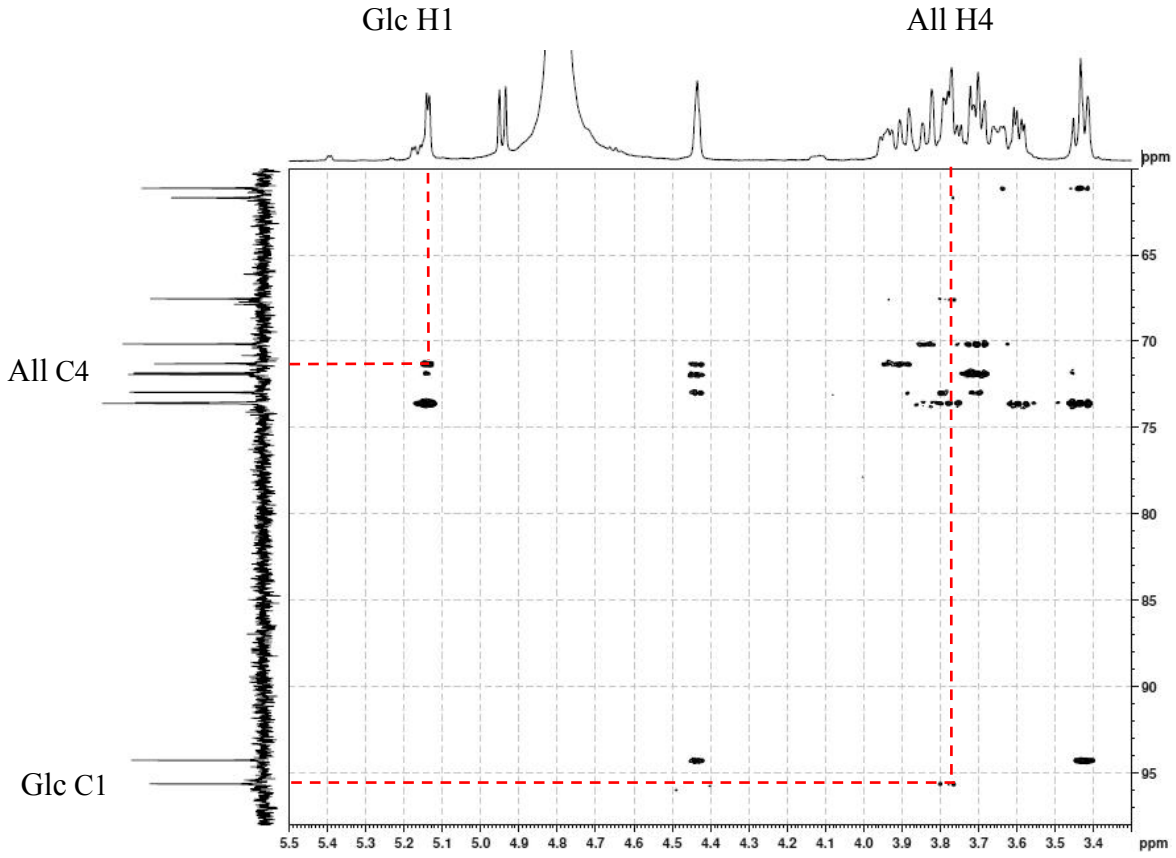

Fig. 33. HMBC analysis of synthesized product from All and β-Glc1*P*.

Dotted lines indicate correlations between Glc H1 and All C4, and between All H4 and Glc C1.

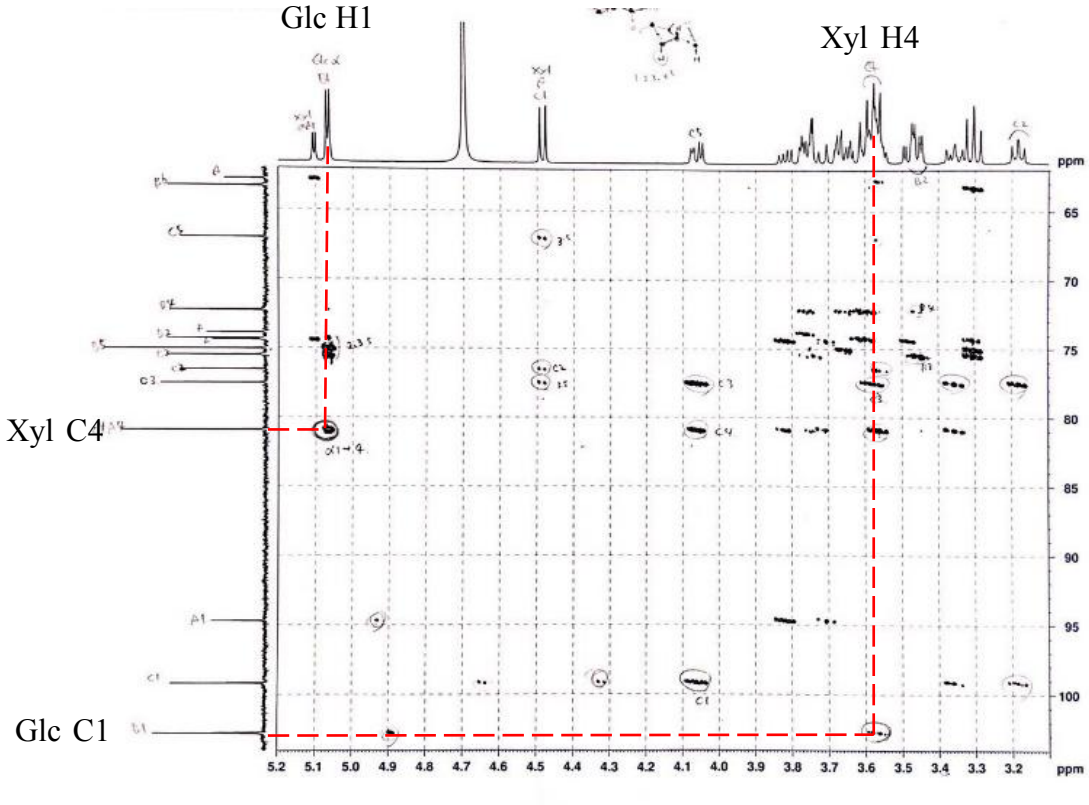

Fig. 34. HMBC spectrum of synthesized product from Xyl and β-Glc1*P*.

Dotted lines indicate correlations between Glc H1 and Xyl C4, and between Xyl H4 and Glc C1.

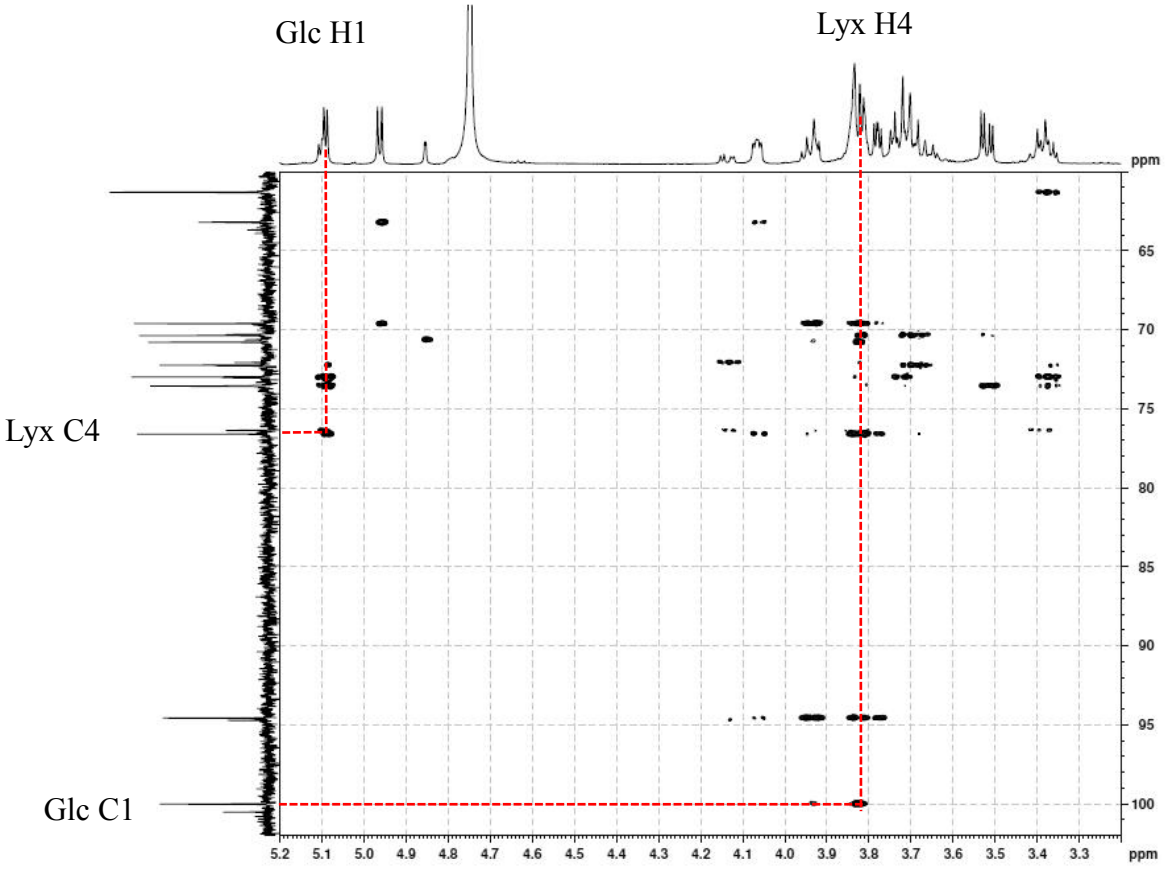

Fig. 35. HMBC spectrum of synthesized product from Lyx and β-Glc1*P*.

Dotted lines indicate correlations between Glc H1 and Lyx C4, and between Lyx H4 and Glc C1.

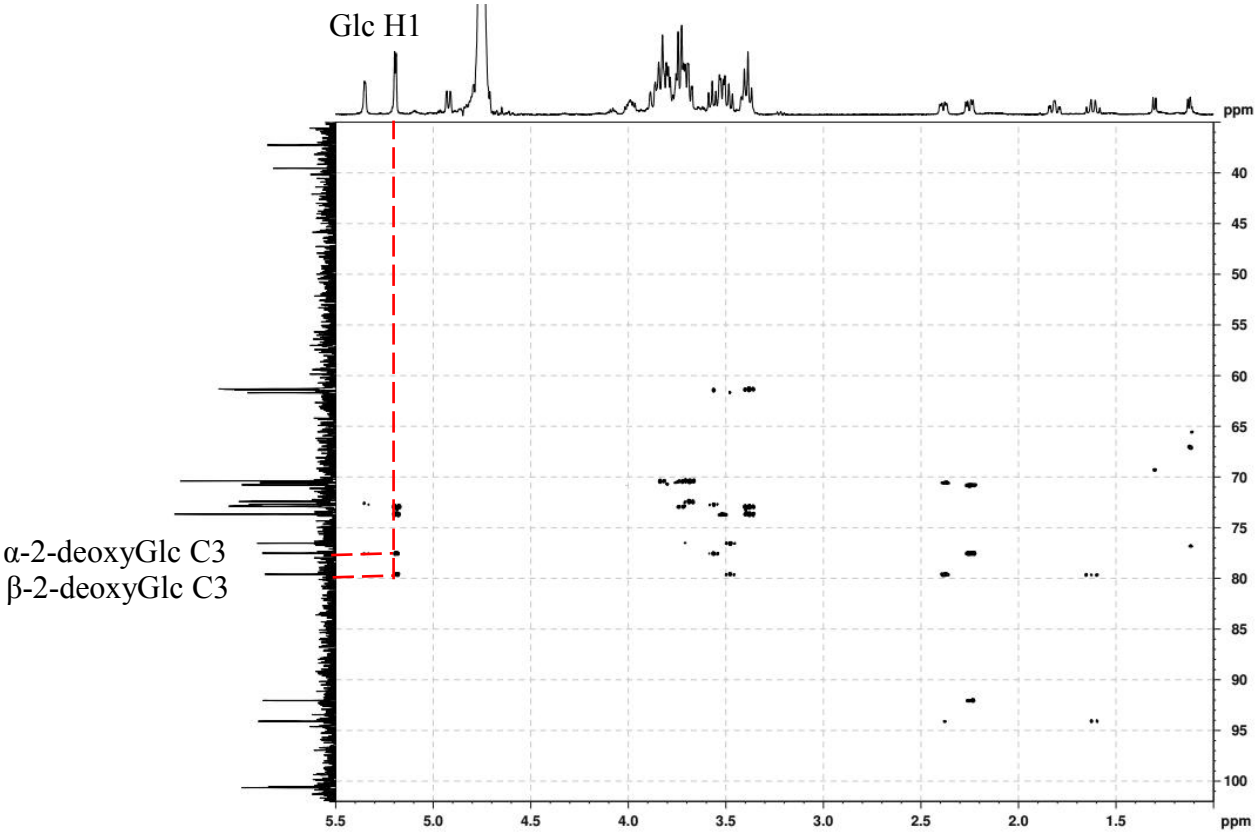

Fig. 36. HMBC spectrum of synthesized product from 2-deoxyGlc and β-Glc1*P*.

Dotted lines indicate correlations between Glc H1 and α(β)-2-deoxyGlc C3.

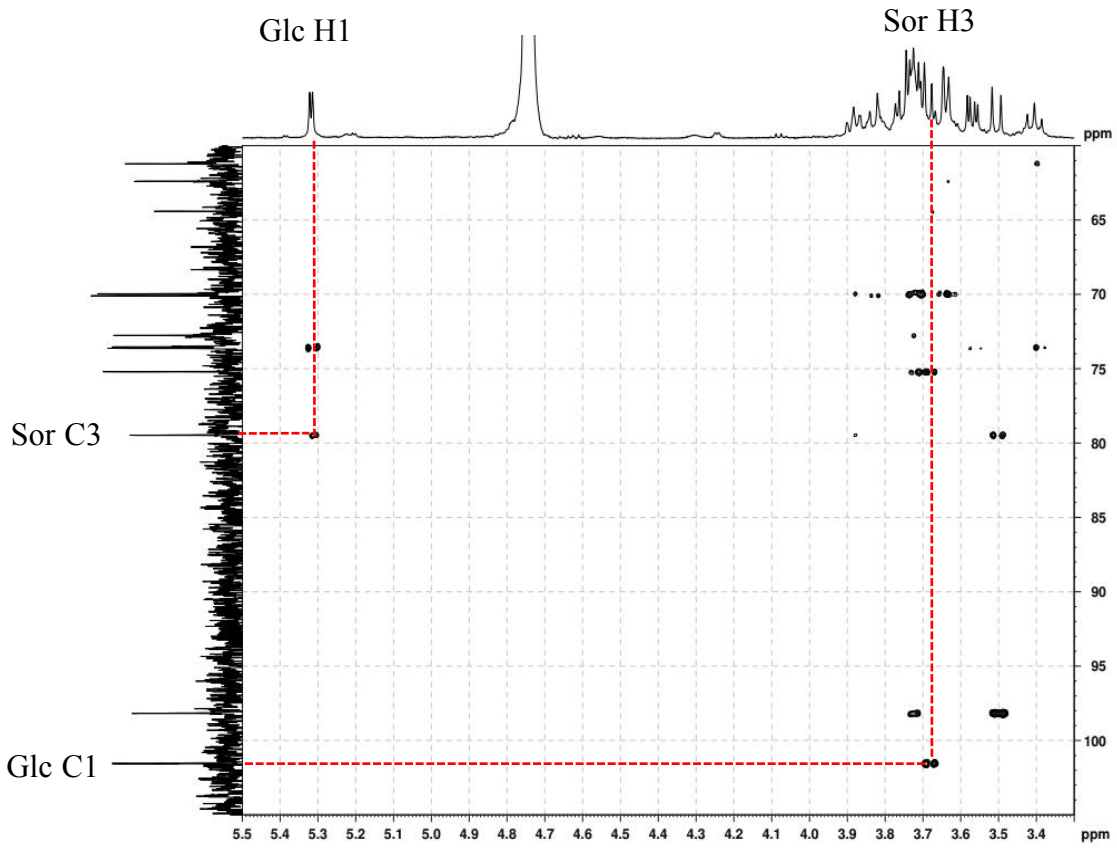

Fig. 37. HMBC spectrum of synthesized product from Sor and β-Glc1*P*.

Dotted lines indicate correlations between Glc H1 and Sor C3, and between Sor H3 and Glc C1.

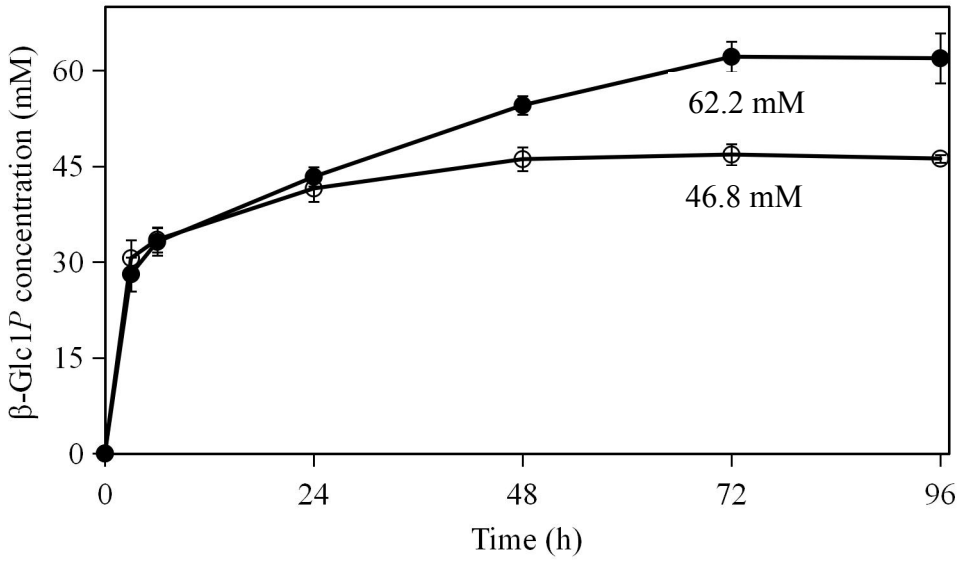

Fig. 38. Preparation of β-Glc1*P* from 0.1 M Mal and 0.4 M Pi catalyzed by MalE.

The produced concentrations of β-Glc1*P* in the presence of bakery yeast (closed circle) and absence of bakery yeast (opened circle) are shown. Values are mean ± standard deviation for three independent determinations.

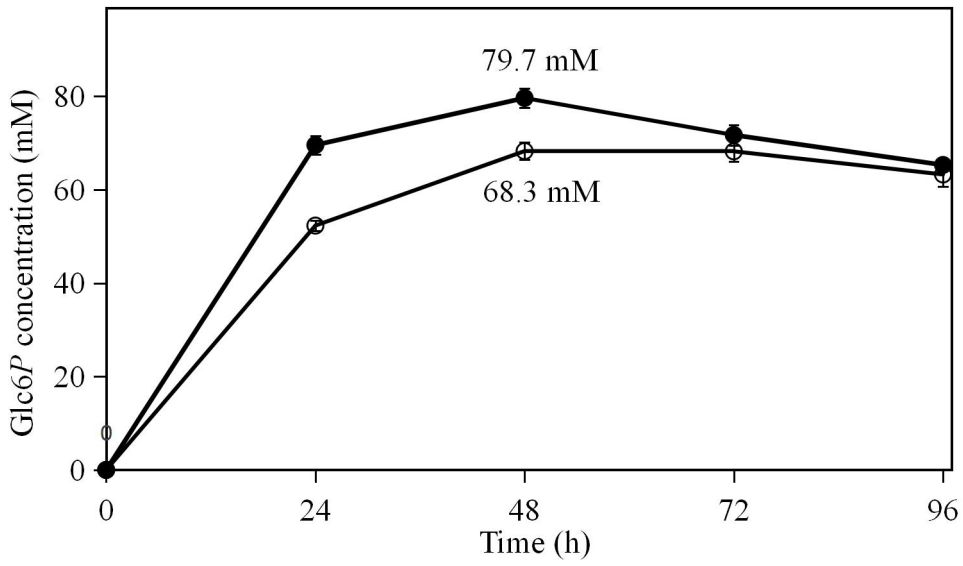

Fig. 39. Preparation Glc6*P* from 0.1 M Mal and 0.1 Pi by MalE and β-PGM.
The produced concentration of Glc6*P* in the presence of bakery yeast (closed circle) and absence of bakery yeast (opened circle) are shown. Values are mean ± standard deviation for three independent determinations.

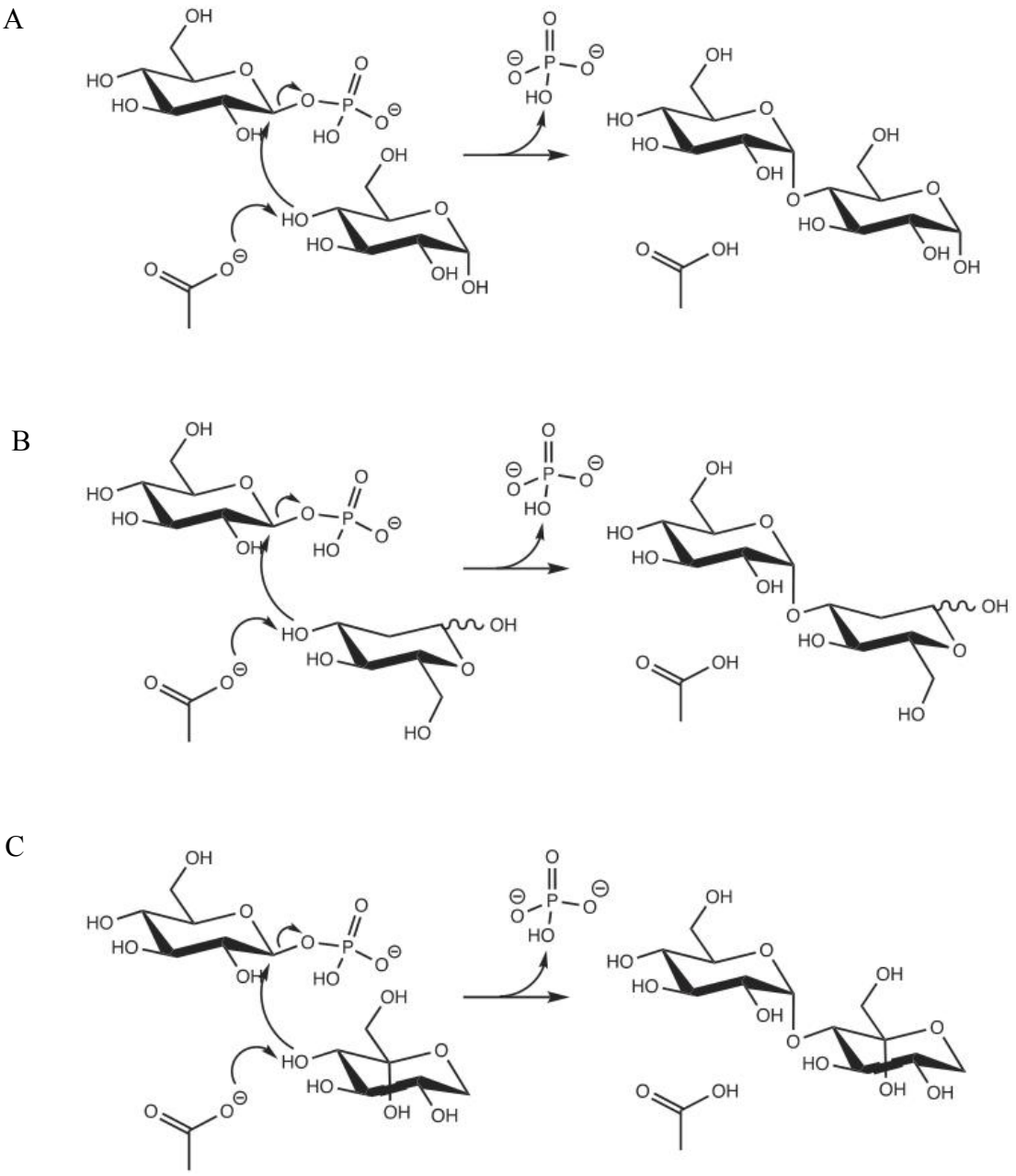

Fig. 40. Possible reaction mechanisms of reverse phosphorolysis.

Possible reaction mechanisms of reverse phosphorolysis with α-Glc (A), 2-deoxyGlc (B), and α-Sor (C) are shown.

CHAPTER IV. General discussion

Bacteria can utilize α-(1→4)-glucans such as polysaccharides, starch, glycogen, and amylose as carbon sources by hydrolyzing them into maltodextrin or Mal. Mal and maltodextrin metabolism has been widely investigated in both Gram-negative bacteria, such as *E. coli*, and Gram-positive bacteria, including *Bacillus subtilis*, *Lactococcus casei* and *Lactococcus lactis*, and these studies showed various metabolic pathways [25, 32, 33, 40, 77-79]. In some bacteria, Mal is transported by ABC transporter and degraded into Glc and Glc1*P* by MP. Previously, it is reported that the MP gene (*malE*) of *Bacillus* sp. AHU 2001 was downstream of the gene encoding GH31 α-glucosidase BspAG31A [49]. In this study, the recombinant MalE was characterized, and the enzyme was used to synthesize several oligosaccharides and two sugar phosphates.

In order to understand substrate binding mechanism, MalE was modelled using the crystal structure of LbMP [16] as template (Fig. 12A). The model suggested that His415 and Glu417 were predicted to form hydrogen bonds with 5-O and 1-O of the superimposed Glc in subsite +1, respectively. Tyr351 and Lys595 were predicted to interact with 3-O of the superimposed Glc in subsite +1. Furthermore, Met406 was predicted to interact with the 6-C of Glc in subsite +1 through a hydrophobic interaction. In reverse phosphorolysis, MalE can utilize several 2-C derivatives of Glc, including GlcN, GlcNAc, and Man. Even though only $k_{cat(app)}/K_{m(app)}$ value of GlcN was as high as that of Glc and $k_{cat(app)}/K_{m(app)}$ value of GlcNAc, and Man were at least 15-fold lower than that of Glc, this indicated that the equatorial 2-hydroxy group or amino group are required for good acceptors. Meanwhile, α-Glc*p*-(1→2)-D-Glc*p* (Koj) can be used as the sole disaccharide acceptor. GlcNAc and Koj as acceptors suggested that MalE can use various equatorial bulky chemical group of Glc at the 2-C position. This predicted that MalE may have an open space near the 2-O of Glc residue in subsite +1 (Fig. 12C). Also, 2-hydroxy group of the Glc

residue in subsite +1 might be possibly exposed to solvent. When 2-deoxyGlc was binding with MalE in subsite +1, Tyr351 and Lys595 might interact with 4-O of the 2-deoxyGlc, and the hydroxymethylene group of 2-deoxyGlc could be accommodated in the space near 2-C position of Glc. Thus, 3-OH group serves as the nucleophile, formed α-(1→3)-glucosidic linkage with Glc moiety at subsite −1. When Sor was situated in subsite +1 of MalE, Tyr351 and Lys595 interacted with 3-O, while His415 and Met406 interacted with 5-O and 6-C, respectively. 3-C might be located at position to 4-C of Glc, producing α-(1→3)-glucoside with β-Glc1*P* through reverse phosphorolysis. The amino acid residues mentioned above may play a key role in binding with substrate.

Oligosaccharides are well known to contribute to digestive health [80]. One of oligosaccharides, fructooligosaccharide (FOS), cannot be digested by the enzymes of the small intestine. It is fermented in the large intestine to selectively stimulate the growth of beneficial bacteria that are part of the commensal gut microbiota and produce short-chain fatty acids, mainly acetate, propionate, and butyrate [81, 82]. Due to its capacity of promoting a good balance of intestinal microbiota and decrease gastrointestinal infections, FOS containing these beneficial physiologic functions has been widely used for the food ingredient in commercial [83, 84]. There has been reported that *B. animalis* propagates significantly better on α-Glc*p*-(1→4)-D-GlcN, α-Glc*p*-(1→4)-D-GlcNA, α-Glc*p*-(1→4)-D-Xyl and α-Glc*p*-(1→4)-L-Fuc than on FOS [45]. Meanwhile, these four α-(1→4)-glucosides showed no significant differences with FOS on growth of *B. longum* [45]. In this study, the digestion rates of oligosaccharides produced by MalE, including that α-Glc*p*-(1→4)-D-GlcN, α-Glc*p*-(1→4)-D-GlcNAc, and α-Glc*p*-(1→4)-D-Xyl, showed high digestive tolerance compared to Mal, indicating that they could reach to large intestine and play a role in prebiotics in human. Even though there is no report to show that α-(1→3)-glucoside have an ability as prebiotics, α-Glc*p*-(1→3)-D-2-deoxyGlc*p* and α-Glc*p*-(1→3)-L-Sor*p* exhibited higher tolerance against the α-glucosidase than the α-(1→4)-glucosides, they might also be candidates for prebiotic oligosaccharides. However, many *in vitro* studies on prebiotic utilization have been carried out using

pure cultures of bacteria, but the growth effects may not necessarily be replicated in the gut, where many different carbon sources are potentially available for the bacteria. As it is unlikely that all of the Bifidobacteria have distinct health-promoting properties, simply measuring changes in their overall numbers does not actually prove too much. To date, glucooligosaccharides present some important physicochemical and physiological properties beneficial to the health, especially on prebiotics. The future work with the synthesized unnatural glucosides used as prebiotics needs to focus more on *in vivo* studies, including animal studies and human investigations, potential role of dietary manipulation for allergy prevention, the immune modulating effects of prebiotics and to ascertain whether they are long lasting.

In this study, the enzymatic functions of MalE and evaluated the oligosaccharides and sugar phosphates synthesized by this enzyme were demonstrated. Although the substrate binding mechanism was discussed based on the predicted MalE structure, the structure of complex of MP and Mal, which is experimentally determined through X-ray crystallography, is required to clarify the structural-function relationship of this typical GH65 enzyme. Obtaining the structure of complex of MP binding to Mal would be helpful for understanding structure-function relationship of MP as well as other GH65 enzymes with corresponding substrate.

REFERENCES

[1] O'Neill EC, Field RA. Enzymatic synthesis using glycoside phosphorylases. Carbohydrate Research. 2015;403:23-37.

[2] Pergolizzi G, Kuhaudomlarp S, Kalita E, Field RA. Glycan phosphorylases in multi-enzyme synthetic processes. Protein and Peptide Letters. 2017;24:696-709.

[3] Kuhaudomlarp S, Walpole S, Stevenson CEM, Nepogodiev SA, Lawson DM, Angulo J, Field RA. Unravelling the specificity of laminaribiose phosphorylase from *Paenibacillus* sp. YM-1 towards donor substrates glucose/mannose 1-phosphate by using X-ray crystallography and saturation transfer difference NMR spectroscopy. ChemBioChem. 2019;20:181-192.

[4] Puchart V. Glycoside phosphorylases: structure, catalytic properties and biotechnological potential. Biotechnology Advances. 2015;33:261-276.

[5] Lombard V, Golaconda Ramulu H, Drula E, Coutinho PM, Henrissat B. The carbohydrate-active enzymes database (CAZy) in 2013. Nucleic Acids Research. 2013;42:D490-495.

[6] Luley-Goedl C, Nidetzky B. Carbohydrate synthesis by disaccharide phosphorylases: reactions, catalytic mechanisms and application in the glycosciences. Biotechnology Journal. 2010;5:1324-1338.

[7] Hiraishi M, Igarashi K, Kimura S, Wada M, Kitaoka M, Samejima M. Synthesis of highly ordered cellulose II in vitro using cellodextrin phosphorylase. Carbohydrate Research. 2009;344:2468-2473.

[8] Yataka Y, Sawada T, Serizawa T. Multidimensional self-assembled structures of alkylated cellulose oligomers synthesized via in vitro enzymatic reactions. Langmuir. 2016;32:10120-10125.

[9] Nohara T, Sawada T, Tanaka H, Serizawa T. Enzymatic synthesis and protein adsorption properties of crystalline nanoribbons composed of cellulose oligomer derivatives with primary amino groups. Journal of Biomaterials Science. 2017;28:925-938.

[10] Nohara T, Sawada T, Tanaka H, Serizawa T. Enzymatic synthesis of oligo (ethylene glycol)-bearing cellulose oligomers for in situ formation of hydrogels with crystalline

nanoribbon network structures. Langmuir. 2016;32:12520-12526.

[11] Goedl C, Sawangwan T, Mueller M, Schwarz A, Nidetzky B. A high-yielding biocatalytic process for the production of 2-*O*-(α-D-glucopyranosyl)-*sn*-glycerol, a natural osmolyte and useful moisturizing ingredient. Angewandte Chemie International Edition. 2008;47:10086-10089.

[12] Nishimoto M, Kitaoka M. Practical preparation of lacto-*N*-biose I, a candidate for the bifidus factor in human milk. Bioscience, Biotechnology, and Biochemistry. 2007;71:2101-2104.

[13] Beerens K, De Winter K, Van de Walle D, Grootaert C, Kamiloglu S, Miclotte L, Van de Wiele T, Van Camp J, Dewettinck K, Desmet T. Biocatalytic synthesis of the rare sugar kojibiose: Process scale-up and application testing. Journal of Agricultural and Food Chemistry. 2017;65:6030-6041.

[14] Nihira T, Saito Y, Ohtsubo Ki, Nakai H, Kitaoka M. 2-*O*-α-D-glucosylglycerol phosphorylase from *Bacillus selenitireducens* MLS10 possessing hydrolytic activity on β-D-glucose 1-phosphate. PLOS ONE. 2014;9:e86548.

[15] Nihira T, Nishimoto M, Nakai H, Ki O, Kitaoka M. Characterization of two phosphorylases for α-1,3-oligoglucans from *Clostridium phytofermentans*. Journal of Applied Glycoscience. 2014;61:59-66.

[16] Egloff MP, Uppenberg J, Haalck L, van Tilbeurgh H. Crystal structure of maltose phosphorylase from *Lactobacillus brevis*: unexpected evolutionary relationship with glucoamylases. Structure. 2001;9:689-697.

[17] Okada S, Yamamoto T, Watanabe H, Nishimoto T, Chaen H, Fukuda S, Wakagi T, Fushinobu S. Structural and mutational analysis of substrate recognition in kojibiose phosphorylase. The FEBS Journal. 2014;281:778-786.

[18] Touhara KK, Nihira T, Kitaoka M, Nakai H, Fushinobu S. Structural basis for reversible phosphorolysis and hydrolysis reactions of 2-*O*-α-glucosylglycerol phosphorylase. Journal of Biological Chemistry. 2014;289:18067-18075.

[19] Van Hoorebeke A, Stout J, Van der Meeren R, Kyndt J, Van Beeumen J, Savvides SN. Crystallization and X-ray diffraction studies of inverting trehalose phosphorylase from *Thermoanaerobacter* sp. Acta Crystallographica Section F: Structural Biology and Crystallization Communications. 2010;66:442-447.

[20] Aleshin A, Golubev A, Firsov LM, Honzatko RB. Crystal structure of glucoamylase from *Aspergillus awamori* var. X100 to 2.2-A resolution. Journal of Biological Chemistry. 1992;267:19291-19298.

[21] Mizuno M, Tonozuka T, Suzuki S, Uotsu-Tomita R, Kamitori S, Nishikawa A, Sakano Y. Structural insights into substrate specificity and function of glucodextranase. Journal of Biological Chemistry. 2004;279:10575-81053.

[22] Nihira T, Saito Y, Kitaoka M, Otsubo K, Nakai H. Identification of *Bacillus selenitireducens* MLS10 maltose phosphorylase possessing synthetic ability for branched α-D-glucosyl trisaccharides. Carbohydrate Research. 2012;360:25-30.

[23] Inoue Y, Ishii K, Tomita T, Fukui F. Purification and characterization of maltose phosphorylase from *Bacillus* sp. RK-1. Bioscience, Biotechnology, and Biochemistry. 2001;65:2644-2649.

[24] Inoue Y, Yasutake N, Oshima Y, Yamamoto Y, Tomita T, Miyoshi S, Yatake T. Cloning of the maltose phosphorylase gene from *Bacillus* sp. strain RK-1 and Efficient Production of the cloned gene and the trehalose phosphorylase gene from *Bacillus stearothermophilus* RK-1 in *Bacillus subtilis*. Bioscience, Biotechnology, and Biochemistry. 2002;66:2594-2599.

[25] Schonert S, Seitz S, Krafft H, Feuerbaum EA, Andernach I, Witz G, Dahl MK. Maltose and maltodextrin utilization by *Bacillus subtilis*. Journal of Bacteriology. 2006;188:3911-3922.

[26] Mokhtari A, Blancato VS, Repizo GD, Henry C, Pikis A, Bourand A, de Fátima Álvarez M, Immel S, Mechakra-Maza A, Hartke A, Thompson J, Magni C, Deutscher J. E nterococcus faecalis utilizes maltose by connecting two incompatible metabolic routes via a novel maltose 6'-phosphate phosphatase (MapP). Molecular Microbiology. 2013;88:234-253.

[27] Kino K, Shimizu Y, Kuratsu S, Kirimura K. Enzymatic synthesis of α-anomer-selective D-glucosides using maltose phosphorylase. Bioscience, Biotechnology, and Biochemistry. 2007;71:1598-1600.

[28] Nakai H, Baumann MJ, Petersen BO, Westphal Y, Schols H, Dilokpimol A, Hachem MA, Lahtinen SJ, Duus JØ, Svensson B. The maltodextrin transport system and metabolism in *Lactobacillus acidophilus* NCFM and production of novel α-glucosides

through reverse phosphorolysis by maltose phosphorylase. The FEBS Journal. 2009;276:7353-7365.

[29] Kamogawa A, Yokobayashi K, Fukui T. Properties of maltose phosphorylase from *Lactobacillus brevis*. Agricultural and Biological Chemistry. 1973;37:2813-2819.

[30] Ehrmann MA, Vogel RF. Maltose metabolism of *Lactobacillus sanfranciscensis*: cloning and heterologous expression of the key enzymes, maltose phosphorylase and phosphoglucomutase. FEMS Microbiology Letters. 1998;169:81-86.

[31] Wood BJ, Rainbow C. The maltophosphorylase of beer *lactobacilli*. Biochemical Journal. 1961;78:204.

[32] Monedero V, Yebra MJ, Poncet S, Deutscher J. Maltose transport in *Lactobacillus casei* and its regulation by inducer exclusion. Research in Microbiology. 2008;159:94-102.

[33] Andersson U, Rådström P. Physiological function of the maltose operon regulator, MalR, in *Lactococcus lactis*. BMC Microbiology. 2002;2:28.

[34] Fitting C, Doudoroff M. Phosphorolysis of maltose by enzyme preparations from *Neisseria meningitidis*. Journal of Biological Chemistry. 1952;199:153-163.

[35] Selinger Z, Schramm M. Enzymatic synthesis of the maltose analogues, glucosyl glucosamine, glucosyl *N*-acetyl-glucosamine and glucosyl 2-deoxyglucose by an extract of *Neisseria perflava*. Journal of Biological Chemistry. 1961;236:2183-2185.

[36] Yoshida M, Nakamura N, Horikoshi K. Production and application of maltose phosphorylase and trehalose phosphorylase by a strain of *Plesiomonas*. Journal of Applied Glycoscience. 1995;42:19-25.

[37] Aisaka K, Masuda T, Chikamune T. Properties of maltose phosphorylase from *Propionibacterium freudenreichii*. Journal of Fermentation and Bioengineering. 1996;82:171-173.

[38] Martin S, Russell J. Transport and phosphorylation of disaccharides by the ruminal bacterium *Streptococcus bovis*. Applied and Environmental Microbiology. 1987;53:2388-2393.

[39] Hidaka Y, Hatada Y, Akita M, Yoshida M, Nakamura N, Takada M, Nakakuki T, Ito S, Horikoshi K. Maltose phosphorylase from a deep-sea *Paenibacillus* sp.: Enzymatic properties and nucleotide and amino-acid sequences. Enzyme and Microbial Technology.

2005;37:185-194.
[40] Nilsson U, Rådström P. Genetic localization and regulation of the maltose phosphorylase gene, malP, in *Lactococcus lactis*. Microbiology. 2001;147:1565-1573.
[41] Kamogawa A, Yokobayashi K, Fukui T. An enzymatic method for the determination of maltose in the presence of other oligosaccharides. Analytical Biochemistry. 1974;57:303-305.
[42] Huwel S, Haalck L, Conrath N, Spener F. Maltose phosphorylase from *Lactobacillus brevis*: purification, characterization, and application in a biosensor for *ortho*-phosphate. Enzyme and Microbial Technology. 1997;21:413-420.
[43] Nakai H, Petersen BO, Westphal Y, Dilokpimol A, Abou Hachem M, Duus JO, Schols HA, Svensson B. Rational engineering of *Lactobacillus acidophilus* NCFM maltose phosphorylase into either trehalose or kojibiose dual specificity phosphorylase. Protein Engineering, Design & Selection. 2010;23:781-787.
[44] Nakai H, Dilokpimol A, Abou Hachem M, Svensson B. Efficient one-pot enzymatic synthesis of α-(1→4)-glucosidic disaccharides through a coupled reaction catalysed by *Lactobacillus acidophilus* NCFM maltose phosphorylase. Carbohydrate Research. 2010;345:1061-1064.
[45] Vigsnaes LK, Nakai H, Hemmingsen L, Andersen JM, Lahtinen SJ, Rasmussen LE, Hachem MA, Petersen BO, Duus JO, Meyer AS, Licht TR, Svensson B. *In vitro* growth of four individual human gut bacteria on oligosaccharides produced by chemoenzymatic synthesis. Food Function. 2013;4:784-793.
[46] Tsumuraya Y, Brewer CF, Hehre EJ. Substrate-induced activation of maltose phosphorylase: interaction with the anomeric hydroxyl group of α-maltose and α-D-glucose controls the enzyme's glucosyltransferase activity. Archives of Biochemistry and Biophysics. 1990;281:58-65.
[47] Yoshida M, Nakamura N, Horikoshi K. Production of trehalose by a dual enzyme system of immobilized maltose phosphorylase and trehalose phosphorylase. Enzyme and Microbial Technology. 1998;22:71-75.
[48] Nihira T, Miyajima F, Chiku K, Nishimoto M, Kitaoka M, Ohtsubo K, Nakai H. One Pot Enzymatic Production of Nigerose from Common Sugar Resources Employing Nigerose Phosphorylase. Journal of Applied Glycoscience. 2014;61:75-80.

[49] Saburi W, Okuyama M, Kumagai Y, Kimura A, Mori H. Biochemical properties and substrate recognition mechanism of GH31 α-glucosidase from *Bacillus* sp. AHU 2001 with broad substrate specificity. Biochimie. 2015;108:140-148.
[50] Le Breton Y, Pichereau V, Sauvageot N, Auffray Y, Rince A. Maltose utilization in *Enterococcus faecalis*. Journal of Applied Microbiology. 2005;98:806-813.
[51] Ho SN, Hunt HD, Horton RM, Pullen JK, Pease LR. Site-directed mutagenesis by overlap extension using the polymerase chain reaction. Gene. 1989;77:51-59.
[52] Bradford MM. A rapid and sensitive method for the quantitation of microgram quantities of protein utilizing the principle of protein-dye binding. Analytical Biochemistry. 1976;72:248-254.
[53] Aitken A, Learmonth MP. Protein determination by UV absorption. The Protein Protocols Handbook; 2009. 3-6.
[54] Moore S, Stein WH. Photometric nin-hydrin method for use in the ehromatography of amino acids. Journal of Biological Chemistry. 1948;176:367-388.
[55] Laemmli UK. Cleavage of structural proteins during the assembly of the head of bacteriophage T4. Nature. 1970;227:680.
[56] Shirokane Y, Ichikawa K, Suzuki M. A novel enzymic determination of maltose. Carbohydrate Research. 2000;329:699-702.
[57] Hokse H. Purification of α-D-glucose-1-phosphate. Starch-Stärke. 1983;35:101-102.
[58] Miwa I. Mutarotase effect on colorimetric determination of blood glucosinolate with β-D-glucose oxidase. Clinica Chimica Acta. 1972;37:538-540.
[59] Cleland WW. The kinetics of enzyme-catalyzed reactions with two or more substrates or products. Biochimica et Biophysica Acta. 1963;67:104-137.
[60] Lowry OH, Lopez JA. The determination of inorganic phosphate in the presence of labile phosphate esters. Journal of Biological Chemistry. 1946;162:421-428.
[61] Kim YK, Kitaoka M, Krishnareddy M, Mori Y, Hayashi K. Kinetic studies of a recombinant cellobiose phosphorylase (CBP) of the *Clostridium thermocellum* YM4 strain expressed in *Escherichia coli*. Journal of Biochemistry. 2002;132:197-203.
[62] Christian E, Watkins M, Prohaska T, Nidetzky B. Fungal trehalose phosphorylase: kinetic mechanism, pH-dependence of the reaction and some structural properties of the enzyme from *Schizophyllum commune*. Biochemical Journal. 2001;356:757-767.

[63] Kelley LA, Mezulis S, Yates CM, Wass MN, Sternberg MJ. The Phyre2 web portal for protein modeling, prediction and analysis. Nature Protocols. 2015;10:845.

[64] Larkin MA, Blackshields G, Brown N, Chenna R, McGettigan PA, McWilliam H, Valentin F, Wallace IM, Wilm A, Lopez R, Thompson JD, Gibson TJ, Higgins DG. Clustal W and Clustal X version 2.0. Bioinformatics. 2007;23:2947-2948.

[65] Levy H, Daouk G. Simultaneous analysis of NAD-and NADP-linked activities of dual nucleotide-specific dehydrogenases. Application to Leuconostoc mesenteroides glucose-6-phosphate dehydrogenase. Journal of Biological Chemistry. 1979;254:4843-4847.

[66] Van der Borght J, Desmet T, Soetaert W. Enzymatic production of β-D-glucose-1-phosphate from trehalose. Biotechnology Journal. 2010;5:986-993.

[67] Abdel-Banat BM, Hoshida H, Ano A, Nonklang S, Akada R. High-temperature fermentation: how can processes for ethanol production at high temperatures become superior to the traditional process using mesophilic yeast? Applied Microbiology and Biotechnology. 2010;85:861-867.

[68] Pampulha ME, Loureiro-Dias MC. Combined effect of acetic acid, pH and ethanol on intracellular pH of fermenting yeast. Applied Microbiology and Biotechnology. 1989;31:547-550.

[69] Sutton D, Lampen J. Localization of sucrose and maltose fermenting systems in *Saccharomyces cerevisiae*. Biochimica et Biophysica Acta. 1962;56:303-312.

[70] Kitaoka M, Hayashi K. Carbohydrate-processing phosphorolytic enzymes. Trends in Glycoscience and Glycotechnology. 2002;14:35-50.

[71] Ben-Zvi R, Schramm M. A phosphoglucomutase specific for β-glucose 1-phosphate. Journal of Biological Chemistry. 1961;236:2186-2189.

[72] Sjöberg A, Hahn-Hägerdal B. β-Glucose-1-phosphate, a possible mediator for polysaccharide formation in maltose-assimilating *Lactococcus lactis*. Applied Microbiology and Biotechnology. 1989;55:1549-1554.

[73] Marechal LR, Oliver G, Veiga LA, de Ruiz Holgado AA. Partial purification and some properties of β-phosphoglucomutase from *Lactobacillus brevis*. Archives of Biochemistry and Biophysics. 1984;228:592-599.

[74] Belocopitow E, Marechal LR. Metabolism of Trehalose in *Euglena gracilis*.

European Journal of Biochemistry. 1974;46:631-637.

[75] Pollak A, Baughn RL, Whitesides GM. Large-scale enzymic synthesis with cofactor regeneration: glucose 6-phosphate. Journal of the American Chemical Society. 1977;99:2366-2367.

[76] Neuberg C, Lustig H, Rothenberg M. Fructose-1, 6-diphosphoric acid and fructose-6-monophosphoric acid. Archive of Biochemistry. 1943;3:33-44.

[77] Boos W, Shuman H. Maltose/maltodextrin system of *Escherichia coli*: transport, metabolism, and regulation. Microbiology and Molecular Biology Reviews. 1998;62:204-229.

[78] Dippel R, Boos W. The maltodextrin system of *Escherichia coli*: metabolism and transport. Journal of Bacteriology. 2005;187:8322-8331.

[79] Kamionka A, Dahl MK. *Bacillus subtilis* contains a cyclodextrin-binding protein which is part of a putative ABC-transporter. FEMS Microbiology Letters. 2001;204:555-560.

[80] Sangwan V, Tomar S, Singh R, Singh A, Ali B. Galactooligosaccharides: novel components of designer foods. Journal of Food Science. 2011;76:R103-111.

[81] Yun JW. Fructooligosaccharides—occurrence, preparation, and application. Enzyme and Microbial Technology. 1996;19:107-117.

[82] Wang Y, Zeng T, Wang S, Wang W, Wang Q, Yu HX. Fructo-oligosaccharides enhance the mineral absorption and counteract the adverse effects of phytic acid in mice. Nutrition. 2010;26:305-311.

[83] Roberfroid M. Prebiotics: the concept revisited. The Journal of Nutrition. 2007;137:830S-837S.

[84] Dominguez AL, Rodrigues LR, Lima NM, Teixeira JA. An overview of the recent developments on fructooligosaccharide production and applications. Food and Bioprocess Technology. 2014;7:324-337.

ACKNOWLEDGEMENTS

Firstly, I would like to extend my heartfelt gratitude and greatest appreciation to my supervisor, Professor Haruhide Mori. His conscientious academic spirit and modest, open-minded personality always inspire me both in academic study and daily life. Meanwhile, I am much obliged to Lecturer Wataru Saburi, for his patient guidance, valuable suggestions and constant encouragement on my research. They gave me a mount of advice during the whole process of my working and writing, which made my doctoral student's career going smoothly.

Three years has passed so fast, let me tear myself away from all the Biochemistry mates. Thanks everyone for helping me a lot, not only taught me many professional knowledge but also brought me integrating into Japanese society and culture. These three years has become one of the most valuable memories keep in my mind.

Furthermore, I would like to express my sincere gratitude to Prof. Hirokazu Matsui, Mr. Nishigai and Mrs. Shao. Without their assistants, I could not fulfill my dream of studying in Hokkaido University. As seniors, they provided me kind suggestions as always on my study and everyday life, that made me warm and lost homesickness.

Last but not least, I would like to express my special thanks to my families, whose care and support motivate me to move on and make me want to be a better man.

In particular, I would like to present this thesis to my father. He gave me biggest support for studying in Japan. Even though he left me eternal during I studied in Japan, I still remember what he enlightened me, encouraged me, and guided me all the time. Now I've finished my study in Japan, as he expected before I came. I am willing to offer this thesis that is embodied what I've studied in these three years, for showing my highest respect and love to him.

Gao Yu